CRITICAL EVALUATION AND THERMODYNAMIC OPTIMIZATION OF THE IRON-RARE-EARTH SYSTEMS

BIKRAM KONAR

DEPARTMENT OF MINING AND MATERIALS ENGINEERING

McGILL UNIVERSITY, MONTREAL

AUGUST 2011

A thesis submitted to McGill University in partial fulfillment of the requirements of the degree of Master of Science

Acknowledgements

I would like to express my sincere gratitude towards my supervisor Prof. In-Ho Jung, whose continuous guidance and financial assistance was indispensible throughout my study.

I am very grateful to my mother, father and sister who constantly encouraged me in fulfillment of my thesis.

I would like to thank Dr. Marie Aline VAN-Ende and Dr. Pierre Hudon, for their helpful advice during the course of my study. I am grateful to all my research group mates in "High-temperature Thermochemistry Group" for their constructive comments.

I would like to acknowledge the financial assistance provided by KITECH for my research work.

I am also thankful to my friends, Manas, Sriraman, Kiran, Kinnor, Chiradeep, Adarsh, Jing, Sarah and Amrita for their enthusiastic support throughout my study at McGill University.

Résumé

Les terres rares, en vertu de leurs propriétés magnétiques, électroniques et chimiques uniques, gagnent en importance dans les industries électroniques, des centrales, des télécommunications et des technologies vertes. Les aimants de terres rares possèdent des propriétés très supérieures par rapport aux aimants traditionnels. Ils disposent d'une puissance et d'une longévité plus élevées, et d'une meilleure usinabilité à haute température. Le déséquilibre entre la demande et l'approvisionnement en terres rares a accru l'importance du recyclage et de l'extraction des terres rares à partir des aimants permanents usagés. Cependant, le manque de données thermodynamiques sur les systèmes de terre rare a rendu difficile la conception de procédés efficaces de recyclage et d'extraction. À cet égard, les calculs thermodynamiques peuvent servir d'outil rentable en termes de temps et d'argent afin de concevoir un procédé de recyclage des aimants permanents usagés. L'aimant permanent de terre rare le plus commun est l'aimant au néodyme ($Nd_2Fe_{14}B$). Divers éléments tels que Dy, Tb, Pr, Cu, Co, Ni, etc. sont également ajoutés pour améliorer ses propriétés magnétiques et mécaniques.

Afin d'effectuer des calculs thermodynamiques fiables pour le procédé de recyclage des terres rares, des bases de données thermodynamiques précises pour les terres rares et leurs alliages sont requises. Les bases de données thermodynamiques peuvent être développées en utilisant la méthode dite CALPHAD. Le développement de bases de données basé sur la méthode CALPHAD consiste essentiellement en l'évaluation critique et en l'optimisation de toutes les données thermodynamiques et de diagramme de phase disponibles. En conséquence, un ensemble de fonctions thermodynamiques cohérentes pouvant reproduire tous les données thermodynamiques et de diagramme de phase fiables est obtenu pour toutes les phases dans un système donné. La base de données contenant les fonctions optimisées d'énergie libre de Gibbs peut être utilisée pour calculer des réactions chimiques complexes pour n'importe quels procédés à haute température. Typiquement, une routine de minimisation de l'énergie libre de Gibbs, telle que présente dans le logiciel FactSage, peut être utilisée pour obtenir l'équilibre thermodynamique précis dans un système comprenant de multiples composants.

Dans le cadre du développement d'une base de données thermodynamiques pour le recyclage des aimants permanents et la conception d'alliages de magnésium, toutes les données thermodynamiques et de diagramme de phase dans la littérature pour les quatorze systèmes binaires Fe-terre rare incluant Fe-La, Fe-Ce, Fe-Pr, Fe-Nd, Fe-Sm, Fe-Gd, Fe-Tb, Fe-Dy, Fe-Ho, Fe-Er, Fe-Tm, Fe-Lu, Fe-Sc et Fe-Y sont évaluées de manière critique et optimisées pour obtenir les paramètres du modèle thermodynamique.

Les paramètres du modèle peuvent ensuite être utilisés pour calculer les diagrammes de phases et les énergies libres de Gibbs de toutes les phases en fonction de la température et de la composition. Cette base de données peut être incorporée à la base de données thermodynamiques présente dans le logiciel FactSage afin de calculer des réactions chimiques complexes et des diagrammes de phase pour le procédé de recyclage des aimants de terres rares.

ABSTRACT

Rare-Earth elements by virtue of its typical magnetic, electronic and chemical properties are gaining importance in power, electronics, telecommunications and sustainable green technology related industries. The Magnets from RE-alloys are more powerful than conventional magnets which have more longevity and high temperature workability. The dis-equilibrium in the Rare-Earth element supply and demand has increased the importance of recycling and extraction of REE's from used permanent Magnets. However, lack of the thermodynamic data on RE alloys has made it difficult to design an effective extraction and recycling process. In this regard, Computational Thermodynamic calculations can serve as a cost effective and less time consuming tool to design a waste magnet recycling process. The most common RE permanent magnet is Nd magnet ($Nd_2Fe_{14}B$). Various elements such as Dy, Tb, Pr, Cu, Co, Ni, etc. are also added to increase its magnetic and mechanical properties.

In order to perform reliable thermodynamic calculations for the RE recycling process, accurate thermodynamic database for RE and related alloys are required. The thermodynamic database can be developed using the so-called CALPHAD method. The database development based on the CALPHAD method is essentially the critical evaluation and optimization of all available thermodynamic and phase diagram data. As a results, one set of self-consistent thermodynamic functions for all phases in the given system can be obtained, which can reproduce all reliable thermodynamic and phase diagram data. The database containing the optimized Gibbs energy functions can be used to calculate complex chemical reactions for any high temperature processes. Typically a Gibbs energy minimization routine, such as in FactSage software, can be used to obtain the accurate thermodynamic equilibrium in multicomponent systems.

As part of a large thermodynamic database development for permanent magnet recycling and Mg alloy design, all thermodynamic and phase diagram data in the literature for the fourteen Fe-RE binary systems: Fe-La, Fe-Ce, Fe-Pr, Fe-Nd, Fe-Sm, Fe-Gd, Fe-Tb, Fe-Dy, Fe-Ho, Fe-Er, Fe-Tm, Fe-Lu, Fe-Sc and Fe-Y are critically evaluated and optimized to obtain thermodynamic model parameters. The model parameters can be used to calculate phase diagrams and Gibbs energies of all phases as functions of temperature and composition. This database can be incorporated with the present thermodynamic database in FactSage software to perform complex chemical reactions and phase diagram calculations for RE magnet recycling process.

TABLE OF CONTENTS

Acknowledgements

Résumé i

Abstract iii

Table of contents vi

List of figures viii

List of tables xiii

List of symbols xiv

1. **Introduction** 1

2. **CALPHAD thermodynamic modeling**

2.1 CALPHAD 4

2.2 Thermodynamic modeling 6

2.3 Modified Quasichemical Model (MQM) 8

2.4 Compound energy formalism [13] for solid solution 10

2.5 Stoichiometric intermetallic phases 11

2.6 Prediction of Enthalpy using theoretical calculations 12

2.6.1. Miedema's model and calculations 13

2.7 Procedure of critical evaluation/optimization of system 15

2.8 References 17

3. **Thermodynamic modeling of Fe-RE binary systems**

3.1. The Fe-La (Iron-Lanthanum) System 19

3.1.1. Phase diagram data 19

3.1.2. Thermodynamic data 20

3.1.3. Reference 21

3.2. The Fe-Ce (Iron-Cerium) system 25

3.2.1. Phase diagram data 25

3.2.2. Thermodynamic Data 26

3.2.3. Magnetic Data 26

3.2.4. References 28

3.3. The Fe-Pr (Iron-Praseodymium) system 33

3.3.1. Phase diagram data 33

3.3.2. Thermodynamic Data 34

3.3.3. Magnetic Data 35

3.3.4. References 37

3.4. The Fe-Nd (Iron-Neodymium) system 41

3.4.1. Phase diagram data 41

3.4.2. Thermodynamic Data 41

3.4.3. Magnetic Data 42

3.4.4. References 43

3.5. The Fe-Sm (Iron-Samarium) system 48

3.5.1. Phase diagram data 48

3.5.2. Thermodynamic Data 48

3.5.3. Magnetic Data 49

3.5.4. References 51

3.6. The Fe-Gd (Iron-Gadolinium) system 54

3.6.1. Phase diagram data 54

3.6.2. Thermodynamic Data 55

3.6.3. Magnetic Data 56

3.6.4. References 58

3.7. The Fe-Tb (Iron-Terbium) system 63

3.7.1. Phase diagram data 63

3.7.2. Thermodynamic Data 64

3.7.3. Magnetic Data 64

3.7.4. References 67

3.8. The Fe-Dy (Iron-Dysprosium) system 70

3.8.1. Phase diagram data 70

3.8.2. Thermodynamic Data 70

3.8.3. Magnetic Data 71

3.8.4. References 73

3.9. The Fe-Ho (Iron Holmium) system 76

3.9.1. Phase diagram data 76

3.9.2. Thermodynamic Data 76

3.9.3. Magnetic Data 76

3.9.4. References 78

3.10. The Fe-Er (Iron-Erbium) system 80

3.10.1. Phase diagram data 80

3.10.2. Thermodynamic Data 80

3.10.3. Magnetic Data 81

3.10.4. References 82

3.11. The Fe-Tm(Iron-Thulium) system 85

3.11.1. Phase diagram data 85

3.11.2. Thermodynamic Data 85

3.11.3. Magnetic Data 85

3.11.4. References 87

3.12. The Fe-Lu (Iron-Lutetium) System 88

3.12.1. Phase diagram data 89

3.12.2. Thermodynamic Data 89

3.12.3. Magnetic Data 89

3.12.4. References 91

3.13. The Fe-Y (Iron-Yttrium) System 94

3.13.1. Phase diagram data 94

3.13.2. Thermodynamic Data 94

3.13.3. Magnetic Data 95

3.13.4. References 97

3.14. The Fe-Sc (Iron-Scandium) System 102

3.14.1. Phase diagram data 102

3.14.2. Thermodynamic Data 102

3.14.3. Magnetic Data 103

3.14.4. References 104

4. Discussion and systematic Analysis 107

5.Summary 113

LIST OF FIGURES

Fig 3.1.1. The optimized Fe-La system.

Fig. 3.1.2. Iron-rich side of the Fe-La phase diagram.

Fig. 3.1.3. Lanthanum-rich side of the Fe-La phase diagram.

Fig. 3.1.3. Lanthanum-rich side of the Fe-La phase diagram.

Fig.3.1.4. Enthalpy of mixing of Fe-La alloy at 1923K and 1723K

Fig 3.2.1. The optimized Fe-Ce system

Fig. 3.2.2. Low temperature heat capacity of $CeFe_2$

Fig. 3.2.3. Low temperature heat capacity of Ce_2Fe_{17}

Fig. 3.2.4. Iron-rich side of the Fe-Ce phase diagram.

Fig. 3.2.5. Enthalpy of mixing of Fe-Ce alloy at 1900K

Fig. 3.2.6. Activity of Ce and Fe in liquid at 1500 K.

Fig 3.3.1. The optimized Fe-Pr system.

Fig. 3.3.2. Low temperature heat capacity of Pr_2Fe_{17}.

Fig. 3.3.3. Temperature dependence of activity measured on an alloy of 21.8 at. % Pr.

Fig. 3.3.4. Activity of praseodymium Pr-Fe alloys.

Fig. 3.4.1. The optimized Fe-Nd system.

Fig. 3.4.2. Optimized Fe-rich corner of the Fe-Nd phase diagram.

Fig. 3.4.3. Evolution of the Gibbs Energy of formation of Nd_2Fe_{17} with temperature.

Fig. 3.4.4. Evolution of the Gibbs Energy of formation of Nd_5Fe_{17} with temperature.

Fig. 3.4.5. Calculated evolution of the chemical potential of Nd with temperature, compared with measured values.

Fig. 3.5.1. The optimized Fe-Sm system.

Fig. 3.5.2. Low temperature heat capacity of Sm_2Fe_{17}.

Fig. 3.5.3. Enthalpy of mixing of Fe-Sm alloy at 1829K.

Fig. 3.6.1. The optimized Fe-Gd system.

Fig. 3.6.2. Low temperature heat capacity of $GdFe_2$.

Fig. 3.6.4 Formation Enthalpies of Fe-Gd compounds.

Fig. 3.6.5. Iron-rich side of the Fe-Gd phase diagram.

Fig. 3.6.6. Gadolinium-rich side of the Fe-Gd phase diagram.

Fig 3.7.1. The optimized Fe-Tb system.

Fig.3.7.2. Low temperature heat capacity of $TbFe_2$.

Fig. 3.7.3. Formation Enthalpies of Fe-Tb compounds

Fig. 3.8.1. The optimized Fe-Dy phase diagram.

Fig. 3.8.2. Low temperature heat capacity of $DyFe_2$.

Fig. 3.8.3 Formation Enthalpies of Fe-Dy compounds.

Fig. 3.9.1. The optimized Fe-Ho phase diagram.

Fig. 3.9.2. Low temperature heat capacity value for $HoFe_2$.

Fig 3.10.1 The optimized Fe-Er system.

Fig. 3.10.2. Low temperature heat capacity value for $ErFe_2$.

Fig. 3.10.3. Formation Enthalpies of Fe-Er compound.

Fig 3.11.1. The optimized Fe-Tm system.

Fig.3.11.2. Low temperature heat capacity value for $TmFe_2$.

Fig 3.12.1.The optimized Fe-Lu system**.**

Fig.3.12.2. Low temperature heat capacity value for $LuFe_2$.

Fig. 3.12.3. Low temperature heat capacity value for Lu_2Fe_{17}.

Fig 3.13.1. The optimized Fe-Y system.

Fig 3.13.2. The solubility of Y in Fe(FCC) reported by Domagala et al.

Fig 3.13.3. The solubility of Fe in Y(HCP) reported by Domagala et al.

Fig.3.13.4. Enthalpy of mixing of Fe-Y at 1850K.

Fig.3.13.5. Gibbs energy of formation at 973K.

Fig.3.13.6. Enthalpy of formation at 973K.

Fig.3.13.7. Entropy of formation at 973K.

Fig.3.13.8. Low temperature heat capacity value for Y_2Fe_{17}.

Fig 3.14.1 The optimized Fe-Sc system.

Fig 3.14.2. Enthalpy of mixing of Fe-Sc alloy at 1873K.

Fig. 3.14.3. Iron-rich side of the Fe-Sc phase diagram.

Fig. 4.1 Calculated curve of enthalpy of formation for stable intermetallic compounds at 298K in the heavy-Fe-RE(RE is Gd,Tb,Dy,Ho,Er,Lu,Tm) systems.

Fig. 4.2. Calculated curve of enthalpy of formation for stable intermetallic compounds at 298K in the light-Fe-RE(RE is Ce,Pr,Sm) systems.

Fig. 4.3. Calculated curve of entropy of formation for stable intermetallic compounds at 298K in the heavy-Fe-RE(RE is Gd,Tb,Dy,Ho,Er,Lu,Tm) systems.

Fig. 4.4. Calculated curve of entropy of formation for stable intermetallic compounds at 298K in the heavy-Fe-RE(RE is Ce, Pr, Sm) systems.

Fig. 4.5. Calculated curve of enthalpy of mixing of Fe and RE in liquid heavy-RE(RE is Gd,Tb,Dy,Ho,Er,Lu,Tm)-Fe- at 1973K.

Fig. 4.6. Calculated curve of enthalpy of mixing of Fe and RE in liquid light-RE(RE is La,Ce,Pr, Nd, Sm)-Fe- at 1973K.

Fig. 4.7. Calculated curve of entropy of mixing of Fe and RE in liquid heavy-RE(RE is Gd,Tb,Dy,Ho,Er,Lu,Tm)-Fe- at 1973K.

Fig. 4.8. Calculated curve of entropy of mixing of Fe and RE in liquid liquid-RE(RE is La,Ce,Pr,Sm)-Fe- at 1973K.

LIST OF TABLES

Table 3.1.1. Optimized thermodynamic data of the La-Fe system.

Table 3.2.1. Optimized thermodynamic data of the Ce-Fe system.

Table 3.3.1. Optimized thermodynamic data of the Pr-Fe system.

Table 3.4.1. Optimized thermodynamic data of the Nd- Fe system.

Table 3.5.1. Optimized thermodynamic data of the Sm-Fe system.

Table 3.6.1. Optimized thermodynamic data of the Gd-Fe system.

Table 3.7.1. Optimized thermodynamic data of the Tb-Fe system.

Table 3.8.1. Optimized thermodynamic data of the Dy-Fe system.

Table 3.9.1. Optimized thermodynamic data of the Ho-Fe system.

Table 3.10.1. Optimized thermodynamic data of the Er-Fe system.

Table 3.11.1. Optimized thermodynamic data of the Tm-Fe system.

Table 3.12.1. Optimized thermodynamic data of the Lu-Fe system.

Table 3.13.1. Optimized thermodynamic data of the Y-Fe system.

Table 3.14.1. Optimized thermodynamic data of the Sc-Fe system.

Table 4.1. Summary of stable compounds in Fe-RE systems

LIST OF SYMBOLS

C_p	Molar heat capacity (J/mol·K)
G^0_i	Standard Gibbs energy of *i*
G^m	Gibbs energy of solution
G^E	Excess Gibbs energy in solution
g^E	Molar excess Gibbs energy in solution
g^0_i	Molar Gibbs energy of *i*
Δg_{ij}	Gibbs energy change for the formation of two moles of *i-j* pairs
H^0_i	Standard enthalpy of *i*
ΔH	Molar enthalpy of mixing
ΔH_T	enthalpy of formation of the compound from elements
n_{ij}	Number of moles of *i-j* bonds in one mole of solution
q^{ij}_{AB}	Excess interaction parameter between A and B
S^0_i	Standard entropy of component *i*
ΔS_T	entropy of formation of the compound from elements
ΔS^{conf}	Molar configurational entropy of solution
$S^{non\text{-}conf}$	Molar non-configurational entropy of solution
n_i	Number of moles of component *i*
T	Absolute temperature (K)
at. %	Atomic percent
wt. %	Weight percent

y_i	Site fraction of component *i*
Y_i	Coordination-equivalent fractions
X_i	Mole fraction of component *i* in solution
X_{ij}	Pair fraction of *i-j* pairs
Z_i	Coordination number of *i*
Z^i_{ii}	The values of Z_i when all the nearest neighbors of an *i* are *i*'s
Z^i_{ij}	The values of Z_i when all the nearest neighbors of an *i* are *j*'s
n_{WS}	electron density
ϕ	work functions

Chapter 1: Introduction

Rare Earth elements (REEs) are a group of seventeen elements (including Scandium, Yttrium and the lanthanide series) that exhibit same characteristic chemical and physical properties. These properties make them valuable to the electronic, appliance, green technology, weapon and medical device manufacturing industries. Compounds of REE with other metals (like Co, Fe, Ni etc.) have unique properties of luminescence, thermal and electrical conductivity, magnetism and ability to act as catalysts and polishing compounds.

They are not only indispensable for some electronic gadgets of today, like computers, music systems, mobile devices, televisions and MRI machines, but also holds a key to more greener technology of the future. They contribute to the development of more efficient and environment friendly version of everyday products such as cars and light bulbs. REE compounds revolutionized the magnet industry by making them smaller and more powerful with increased longevity, and high temperature workability, which are used in motors and generators that power electronics, telecommunications, electric automobiles and turbines. The ability of REE alloys to store hydrogen makes them an important component in the hybrid car batteries.

The typical alloying behavior of the rare earth metals or more specifically the lanthanide elements (except Yttrium and Scandium) have some typical, specific characteristics that can be attributed to their electronic configuration. The normal electronic configuration of the lanthanides in the metallic state is $4f^{n}(5d,6s)^{3}$, that is a trivalent electronic state, with the exception of Ytterbium (Yb) and Europium (Eu) which have divalent electronic state $4f^{n+1}(5d,6s)^{2}$. Due to the trivalent electronic states of the rare earth metals, the group of elements can be categorized as a family where they show similar or periodic physical and chemical behavior. Looking more closely as we move across the lanthanide series with increasing atomic number we can see minute variation in their chemical and elemental properties. This small variation of the elemental property such as electronic configuration and atomic dimensions influences the constitutive property of the elements.

The REEs are traditionally divided into light (lanthanum through samarium) and heavy elements (europium through lutetium, with yttrium), the latter being more economically important. The global market of the rare earth elements is monopolized by China. It accounts for 50 per cent of world's rare earth element deposits, however 95 to 97 percent of the global supply. In 2010, the de facto supplier of these elements, China announced drastic cuts in REE exports, which caused serious concerns for the manufacturing industries all around the world. In the face of underdeveloped mining operations and mine explorations of REEs in the rest of the world. The mineral extraction and processing of rare earths also involves significant environmental risks by spreading radioactive material and toxic chemicals, and acidification of soil which almost nullifying the benefits accrued by their 'green' technological applications. Thus, recycling of rare earth metals from permanent magnet scraps becomes inevitable to keep the balance between supply and demand. Since the recycling process of the magnet materials has not been well established yet, fundamental research on the thermodynamic behavior of rare earth magnet materials and on the chemical reactions between the magnet materials and the solvent medium are critical to understand and improve the rare earth recycling process.

In order to aid the aforesaid objective, Computational Thermodynamics serve as a powerful instrument. Computational thermochemistry based on the CALPHAD method is a modern tool that helps to obtain quantitative data to guide the development and optimization of materials processing. To design an efficient recycling process for Rare Earth alloys, a thermodynamic database containing model parameters, which describes the thermodynamic properties of the involved phases as a function of temperature and composition must be developed. Such thermodynamic database along with a Gibbs energy minimizing software like FACTSAGE (FactSage 6.2) will help us in processing the useful phases and suggest the process variables, which is otherwise obtained by trial and error experiments money and time.

As part of large thermodynamic database development for the RE containing alloy system, the present work focus on the critical evaluation and optimization of the Iron-Rare Earth systems whose intermediate compounds show interesting magnetic and absorption properties.

In this work, thermodynamic modeling of the binary systems including Fe-La, Fe-Ce, Fe-Pr, Fe-Nd, Fe-Sm, Fe-Gd, Fe-Tb, Fe-Dy, Fe-Ho, Fe-Er, Fe-Tm, Fe-Lu, Fe-Y and Fe-Sc have been carried out. Due to insufficient experimental data, the Fe-Yb, Fe-Eu and Fe-Pm(promethium being radioactive) systems were neither critically evaluated or modeled. All available thermodynamic and phase diagram data for these Fe-RE systems were collected and critically assessed for their reliability. The Gibbs energies of all phases were represented by appropriate model equations. The parameters of these models were obtained by an optimization procedure using the FactSage (FactSage 6.2) software. A systematic study to evaluate thermodynamic properties of compounds which are not known based on the other systems and the similarity between Fe-RE systems. The thermodynamic property database prepared in this work can be integrated with other binary and multi-component systems to provide a complete multi-component database for REE recycling process design and other applications.

Chapter 2: CALPHAD thermodynamic modeling

2.1 CALPHAD

Calphad is an acronym for the CALculation of PHAse Diagrams, better described as "The computer coupling of Phase Diagrams and Thermochemistry".

For more than 30 years, several research groups around the globe have been collaborating to develop methods and techniques to produce data, which provide thermodynamically consistent description of different phases and help, predict phase diagrams of several material system. This commune of scientist is known as CALPHAD (CALculation of PHAse Diagrams) and the methodology followed by these researchers is better known as "The CALPHAD approach".

Under the CALPHAD approach, several kinds of thermodynamic information such as phase diagram data, enthalpy data, and Gibb's energy data are critically evaluated and optimized simultaneously. The usage of a proper model is crucial as it will make the optimization reproduce experimental data more successfully and increases its predictive ability in the higher order system. Optimization is deemed successful which can reflect the thermo-chemical properties of a phase with a minimum number of adjustable parameters. Over the years various parametric models are developed which enables thermodynamic modeling of solutions like liquids, solid solutions, intermetallic compounds, oxides, order-disorder transformation and several others.

The correlation between thermodynamics and phase equilibria was established more than a century ago by J.W. Gibbs. Van Laar[1] in 1908 described the relation between the thermodynamic properties and the equilibrium phase diagram for a binary system. Wagner[2] in 1952 elaborated some features of equilibrium phase diagram and the interdependence of Gibbs energy, enthalpy and entropy values. Meijering[3] produced a summary of earlier work on phase diagram construction using the thermo-chemical data.

In the early days phase diagram were drawn by common tangent construction to the hand calculated Gibbs Energy curves. Kubachewski and Chart[4] summarized this approach for phase diagram calculation.

The wider applicability of thermodynamic phase diagram calculation technique was attained when Kaufman[5] illustrated the importance and use of the concept of "lattice stabilities" while calculating phase diagrams. The differences in Gibbs energy of different stable and metastable lattice structure of an element with respect to temperature, lattice stability, made the calculation of the equilibrium boundaries between different phases of a system more accurate.

Hillert[6] proposed that phase equilibrium calculations can be more realistic by the synergy of experimental phase diagram data and thermodynamic data using various computer techniques, thus the assessed thermodynamic properties can be more universally applicable. During this time the computer calculation of phase diagram was at rudimentary stage. Kaufman's group in US, Ansara's group (led by I. Ansara) in University of Grenoble, France, Hillert's group (led by M. Hillert) in Royal Institute of Technology, Stockholm, Sweden and Kubachewski's group (led by O. Kubachewski) in National Physical Laboratory, Teddington, UK were engaged in computer calculation of phase diagrams.

The inaugural CALPHAD meet was organized by Larry Kaufmann in 1973 at ManLabs in Boston. Discussions on various topics were reported, including reevaluation of the lattice stabilities of metals, high temperature specific heat of liquids and influence on Gibbs free energy, binary phase diagram calculation by several techniques, ternary phase diagram calculations by various interaction models, magnetic effect on Gibbs free energy and proposal for universal thermo-chemical notation. Later in 1979, in conjunction with the CALPHAD conference a CALPHAD journal was published. Since then this journal serves as the primary literature source for articles representing detailed thermodynamic formalisms and assessed parameters of many alloys, slag, oxides and many aqueous systems.

The publication of optimized phase diagram data phase diagram data by least square optimization method by inputting different type of data by Lukas et al.[7] replaced the previous rigorous hand calculation procedure in order to establish consistency between experimental thermodynamic properties and phase boundary values. In present times a

number of computer software packages combined with thermodynamic property databases are commercially available for calculating multi-component phase diagrams and phase equilibria. The most prominent of these packages include FactSage [8], MTDATA [9], Thermo-Calc [10].

2.2 Thermodynamic modeling

Thermodynamic models are required to adequately represent the thermodynamic properties of materials. Complex solutions require sophisticated and refined models for the proper representation of their thermochemical properties. A good model should be able to represent the thermodynamic properties with just a small numbers of adjustable parameters. For this, the model should be based on the structure of the solution to adequately represent the configurational entropy of the solution. Also these models have high predictive capability in higher-order systems. Hence, models should be developed which can describe the configurational entropy of the solutions without the addition of large arbitrary model parameters.

General equations:

The standard Gibbs energy of a pure component *i* can be written as:

$$G_i^0 = H_i^0 - TS_i^0 \tag{2.1}$$

where G_i^0, H_i^0 and S_i^0 are respectively the standard Gibbs energy. Enthalpy and entropy of species I, and T is the absolute temperature.

When two components A and B are mixed then the energy of the solution depends on the interaction between A and B atoms or molecules. The Gibbs energy of a solution in which there is no interaction between A and B is an ideal solution for which:

$$G^m = g_A^0 n_A + g_B^0 n_B - T\Delta S^{conf} \tag{2.2}$$

where G^m is the molar Gibbs energy of the solution, g_i^0 is the molar Gibbs energy of component i, and ΔS^{conf} is the configurational entropy obtained by random mixing of n_A

moles of A and n_B moles of B on the same sublattice and X_i is the mole fraction of species i.

$$\Delta S^{conf} = -R(n_A ln\, X_A + n_B ln\, X_B) \quad (2.3)$$

However in reality, atoms of the component present in a solution have interaction among them. Such interactions can be called g^E, the molar excess Gibbs energy of the solution. In this casethe energy of the solution can be stated by:

$$G^m = g_A^0 n_A + g_B^0 n_B - T\Delta S^{conf} + (n_A + n_B) g^E \quad (2.4)$$

g^E is often expanded as a polynomial in the mole fractions as:

$$g^E = \sum q_{AB}^{ij} X_A^i X_B^j \quad (2.5)$$

where the excess interaction parameters $q_{AB}^{ij} (= a + bT + cT^2 \ldots\ldots)$ may be temperature dependent.

In many cases, the thermodynamic property of a binary solution can be well described with the expression in Eq. (2.5). For binary system often don't deviate a lot from ideality, however when Gibbs energy expression from a lower order system is used to predict the thermodynamic properties of a higher-order system many inconsistencies arise. Even sometimes in a binary system a larger number of interaction parameters are required in this simple polynomial based model in order to reproduce all thermodynamic experimental data available for the system.

To adequately represent the thermodynamic properties of liquid phase, Pelton et al. [11] and Pelton and Chartrand[12] developed the Modified Quasichemical Model (MQM). They modified the classical quasichemical model by improving the configurational entropy term of the model. MQM has been applied only to metallic alloys but to liquid slag, sulphides, and salts. The utility of the MQM over a random-mixing model can be better realized with these solutions which show more ordering than metallic solutions, and where the configurational entropy terms become more important.

2.3 Modified Quasichemical Model (MQM) for liquid solution

In the present work the MQM was used to model liquid solution in all binary systems. Recently, the model has been described in detail by Pelton et al.[11]. A brief summary is presented here.

In the MQM in the pair approximation, the following pair exchange reaction between atoms A and B on neighboring lattice sites is considered:

$$(A\text{-}A) + (B\text{-}B) = 2(A\text{-}B) \; ; \quad \Delta g_{AB} \tag{2.6}$$

Let n_A and n_B be the number of moles of A and B, n_{ij} be the number of moles of (i-j) pairs, and Z_A and Z_B be the coordination numbers of A and B. The pair fractions, mole fractions, and "coordination-equivalent" fractions are defined respectively as:

$$X_{ij} = n_{ij}/(n_{AA} + n_{BB} + n_{AB}) \tag{2.7}$$

$$X_A = n_A/(n_A + n_B) = 1 - X_B \tag{2.8}$$

$$Y_A = Z_A n_A/(Z_A n_A + Z_B n_B) = Z_A X_A/(Z_A X_A + Z_B X_B) = 1 - Y_B \tag{2.9}$$

The following equations may be written:

$$Z_A X_A = 2n_{AA} + n_{AB} \tag{2.10}$$

$$Z_B X_B = 2n_{BB} + n_{AB} \tag{2.11}$$

The Gibbs energy of the solution is given by:

$$G^m = (n_A \; g_A^o + n_B \; g_B^o) - T\Delta S^{config} + (n_{AB}/2)\Delta g_{AB}$$

$$= (n_A \; g_A^o + n_B \; g_B^o) - T\Delta S^{config} + g^E \tag{2.12}$$

where g_A^o and g_B^o are the molar Gibbs energies of the pure components and ΔS^{config} is the configurational entropy of mixing given by randomly distributing the *(A-A), (B-B)* and *(A-B)* pairs in the one-dimensional Ising approximation:

$$\Delta S^{config} = -R(n_A ln\, X_A + n_B ln\, X_B)$$

$$-R[n_{AA}\, ln(\, X_{AA}/Y_A^2) + n_{BB} ln(\, X_{BB}/Y_{BB}^2) + n_{AB} ln\, (X_{AB}/2Y_A Y_B)] \qquad (2.13)$$

Δg_{AB} is expanded in terms of the pair fractions:

$$\Delta g_{AB} = \Delta g_{AB}^o + \sum_{i\geq 1} g_{AB}^{i0} X_{AA}^i + \sum_{j\geq 1} g_{AB}^{0j} X_{BB}^j \qquad (2.14)$$

where Δg_{AB}^o, g_{AB}^{i0} and g_{AB}^{0j} are the parameters of the model which may be functions of temperature.

The equilibrium pair distribution is calculated by setting

$$(\partial G/\partial n_{AB})_{n_A, n_B} = 0 \qquad (2.15)$$

This gives the "equilibrium constant" for the quasichemical reaction of (Eq. 1):

$$\frac{X_{AB}^2}{X_{AA} X_{AB}} = 4exp\left(-\frac{\Delta g_{AB}}{RT}\right) \qquad (2.16)$$

As Δg_{AB} becomes progressively more negative, the reaction (Eq. 2.1) is shifted progressively to the right, and the calculated enthalpy and configurational entropy of mixing assume, respectively, the negative "V" and "m" shapes characteristic of SRO(short range ordering).

The composition of maximum SRO is determined by the ratio of the coordination numbersZ_A/Z_B, as given by the following equations:

$$\frac{1}{Z_A} = \frac{1}{Z_{AA}^A}\left(\frac{2n_{AA}}{2n_{AA}+n_{AB}}\right) + \frac{1}{Z_{AB}^A}\left(\frac{n_{AB}}{2n_{AA}+n_{AB}}\right) \qquad (2.17)$$

$$\frac{1}{Z_B} = \frac{1}{Z_{BB}^B}\left(\frac{2n_{BB}}{2n_{BB}+n_{AB}}\right) + \frac{1}{Z_{BA}^B}\left(\frac{n_{AB}}{2n_{BB}+n_{AB}}\right) \quad (2.18)$$

where Z_{AA}^A and Z_{AB}^A are the values of Z_A respectively when all the nearest neighbors of an A are A's and when all nearest neighbors of an A are B's, and where Z_{BB}^B and Z_{BA}^B are defined similarly. Note that Z_{AB}^A and Z_{BA}^B represent the same quantity and can be used interchangeably.

Although the model is sensitive to the ratio of the coordination number, it is less sensitive to their absolute values. The use of the one-dimensional Ising model in Eq. 2.13 introduces a mathematical approximation into the model which we have found, by experience, can be partially compensated by selecting values of Z_A and Z_B which are smaller than the actual values.

2.4 Compound energy formalism [13] for solid solution

The solid solution appearing in a binary system is usually treated with a random-mixing single-sublattice model. As the name suggests, this model assumes the random mixing of the atoms, one randomly replacing the other by substitution on lattice sites. The Gibbs energy of such a solution in which atoms A and B replace each other on lattice sites is given as:

$$G^m = (x_A g_A^o + x_B g_B^o) + RT[x_A ln x_A + x_B ln x_B] + g^E \quad (2.19)$$

where g_i^o and x_i are the Gibbs energy and mole fraction of *i* component in the system and g^E is the excess Gibbs energy to produce the interactions between atoms. Typically g^E is expressed by the Redlich-Kister formula:

$$g^E = \sum_i (X_A X_B L_{AB}^i (X_B - X_A)^i \quad (2.20)$$

Excess parameters L_{AB}^i are the model parameters of the model.

2.5 Stoichiometric intermetallic phases

If the thermodynamic properties of the solid intermetallic phase are unknown, typically Newman Kopp rule was used in the present study. That is, the Gibbs energy function for any stoichiometric phase A_xB_y per mole of atoms is represented as:

$$g^{A_xB_y}(T) = \frac{x}{x+y} g_A^o + \frac{y}{x+y} g_B^o + \Delta H_T - T\Delta S_T \quad (2.21)$$

where ΔH_T and ΔS_T are the enthalpy and entropy of formation of the compound from A and B elements respectively. This can be model parameter to reproduce the phase diagram and available thermodynamic property data. If the entropy at 298 K of intermetallic phase is available from its low temperature heat capacity data, the ΔS_T can be fixed. ΔH_T can be fixed based on the enthalpy of formation at 298 K. Of course, if the high temperature heat capacity is known, ΔH_T and ΔS_T parameters can be in function of temperature.

In FACTSAGE [8] the magnetic contribution (G_{mag}) of a metal or its alloys are considered to calculate the Gibbs free energy. Where G_{mag} can be defined as,

$G_{mag} = RTln(\beta + 1)g(\tau)$ where $\tau = \frac{T}{T_c}$ where T_c is the critical temperature for magnetic ordering, i.e. the Curie temperature(T_c) for ferromagnetic ordering and Neel temperature(T_N) for anti-ferromagnetic ordering. β is the magnetic moment. β is a quantity related to the total magnetic entropy and is set equal to the Bohr magnetic moment per mole.

$$g(\tau) = \frac{1}{D}\left\{1 - \left[\frac{79\tau^{-1}}{140\,p} + \frac{474}{497}(p^{-1} - 1)\left(\frac{\tau^3}{6} + \frac{\tau^9}{135} + \frac{\tau^{15}}{600}\right)\right]\right\} \text{ when } \tau \leq 1 \quad (2.22)$$

$$g(\tau) = \frac{1}{D}\left\{\left[\frac{\tau^{-5}}{10} + \frac{\tau^{-15}}{315} + \frac{\tau^{-25}}{1500}\right]\right\} \text{ when } \tau \geq 1 \quad (2.23)$$

where $D = \frac{518}{1125} + \frac{11692}{15975}(p^{-1} - 1)$, p is dependent on the structure of the intermetallic phase. p=0.4 for b.c.c. structure and p=0.28 for the others

2.6 Prediction of Enthalpy using theoretical calculations

The enthalpy of formation is one of the important thermodynamic properties of a metallic compound that determine the stability of the compound, therefore experimentation primarily by drop solution calorimetry is done to determine the formation enthalpies. Due to the lack of availability of experimental data several computational techniques are employed to get a reasonable estimate for the formation enthalpy of the compounds. Theoretical methods can be broadly classified into the following four types:

- First principle calculations, within the density-functional theory framework.
- Statistical mechanics based approaches, using atomistic simulation techniques like molecular dynamics.
- Solution thermodynamics, with experimentation and extrapolation, for example CALPHAD method
- Semi empirical methods like Miedema's model.

Each of the above methods has some advantages and disadvantages. Highly accurate values can be predicted from the first principle calculations although crystal structure information is essential and the computation is cost intensive. Atomistic simulations alongwith statistical mechanics can also be used, however this requires knowledge of several physical properties and intricate models which may not be universally applied and also requires complex computation. The CALPHAD as explained will be the basis of our current study. Though this approach predicts a phase diagram fairly fast, it is limited by the availability of experimental data. Unreliable and inconsistent database often predict something which is completely erroneous.

Amongst the semi-empirical approaches, Miedema's approach is the most commonly used theoretical calculation technique for the enthalpy of formation of compounds. Miedema proposed a semi-empirical model for calculation of enthalpies of formation and mixing enthalpies in solid and liquid binary metal systems. The semi-empirical nature of this formalism comes from the element specific constants involved in the calculations are derived from the physical properties of the elements and are subsequently adjusted to

give the best possible fit for the experimental data available. The process of parameter adjustment to reproduce the experimental data enables the model to predict the enthalpy of formation for the compounds in binary alloy systems.

2.6.1. Miedema's model and calculations

The principle and application of this model was elaborated by Boer et al. [14]. The model considers that the alloys are made up of cellular atoms of the constituent elements, each with a defined volume. When these atomic cells are brought into contact they will form an alloy. However this will lead to difference in electron density n_{WS} at the boundaries of the two metal atoms causing a repulsive contribution. Electron transfer into higher energy levels in the system is required to eliminate the electron density in homogeneity giving a positive contribution to the enthalpy estimation. This contribution was found to be proportional to the squared difference in the cube root of the electron densities, $n_{WS}^{1/3}$ of the constituent elements in the bulk metal state. The value of n_{WS} has been derived for the transition metal system from the experimental Bulk modulus and molar volume data. For non-transition metals, the superposition of the charge densities if free atoms placed in the respective lattice points yields an acceptable approximation for n_{WS} [14].

The electronic charge and chemical potential difference ($\Delta\phi^*$) provides the negative contribution to the enthalpies of formation and mixing aiding stabilization of the systems with respect to the constituent elements. This electronegativity term originally derived from the work functions(ϕ) of the pure metals and later adjusted (ϕ^*) to reproduce the experimental data for enthalpies of formation for the compound. This contribution is proportional to the square of the difference of electronegativity term ($\Delta\phi^{*2}$) of the constituent elements of the binary system. Thus the formulation for the interfacial enthalpy of formation between neighbouring atoms is proportional to:

$$\Delta H^{interface} \propto -P(\Delta\phi^*)^2 + Q(\Delta n_{WS}^{1/3})^2 - R_m \qquad (2.24)$$

with

$\Delta H^{interface}$: Enthalpy effect at the interface between dissimilar atomic cells.

P, Q: Constants for specific combination of metals, tabulated in Boer et al. [14].

$\Delta\phi^*$: Difference of Miedema electronegativities of the constituents (adjusted with experimental data).

Δn_{WS} : Difference of electron densities at the Wigner Seitz cell boundary of the constituents. This is derived from physical properties and electronic structure calculations.

R_m This term expresses the hybridization term, which accounts for the extra stabilizing interaction of the p-electrons of the main group metal to the d-orbitals of the transition metal component. Experimental analysis shows that within a group of elements R can be considered to be constant.

Later Zhang et al. [16] prescribed some correction factors in order to have better prediction of the enthalpy of formation of the compounds. They suggested that the atomic size difference would reduce the contact surface area between the dissimilar atoms of the compound lowering the package density of the crystalline lattice. They proposed an equation of formation enthalpy

$$\Delta H_f^0 = f(c).\frac{S(c).V_B^{2/3}}{(n_{WS}^{-1/3})_{av}}\left\{-P(\Delta\phi^*)^2 + Q(\Delta n_{WS}^{1/3})^2\right\} \quad (2.25)$$

where *f(c)* is a function of alloy composition , which takes into account the chemical short range-ordering(CSRO) effect in the formation enthalpy of an ordered intermetallic compound on .

$$f(c) = \gamma c_A^s c_B^s[1 + 8(c_A^s c_B^s)^2] \quad (2.26)$$

Where the CSRO(γ) is 8 for the intermetallic compound and is constant for the compound. The pre-factor S(c) is aimed to accommodate the effect of size difference of atoms on the contact surface and the bonding energy. S(c) is expressed as,

$$S(c) = 1 - c_B^2\left|V_A^{2/3} - V_B^{2/3}\right|/(c_A^s V_A^{2/3} - c_B^s V_B^{2/3}) \; . \quad (2.27)$$

$\left|V_A^{2/3} - V_B^{2/3}\right|$ is an absolute value and is positive..

Sun et al.[15] restated the equations for formation enthalpy of the binary alloy system for both ordered and disordered alloys.

$$f_{AB} = 2pV_A^{2/3}V_B^{2/3}\frac{(q/p)(\Delta n_{WS}^{1/3})^2-(\Delta\phi)^2-a(r/p)}{(\Delta n_{WS}^{1/3})_A^{-1}+(\Delta n_{WS}^{1/3})_B^{-1}} \quad (2.28)$$

For disordered alloys

$$\Delta H_{AB} = f_{AB}\frac{x_A[1+\mu_A x_B(\phi_A-\phi_B)]\times x_B[1+\mu_B x_A(\phi_B-\phi_A)]}{x_A V_A^{2/3}[1+\mu_A x_B(\phi_A-\phi_B)]+x_B V_B^{2/3}[1+\mu_B x_A(\phi_B-\phi_A)]} \quad (2.29)$$

For ordered alloys

$$(\Delta H_{AB})_{order} = \Delta H_{AB}\times\left[1+\gamma\times\frac{V_A^{2/3}V_B^{2/3}\Delta H_{AB}}{f_{AB}\times(x_A V_A^{2/3}[1+\mu_A x_B(\phi_A-\phi_B)]+x_B V_B^{2/3}[1+\mu_B x_A(\phi_B-\phi_A)]}\right] \quad (2.30)$$

In this study we calculated the formation enthalpy of the compounds by using Miedema Calculator as available in http://zrftum.wordpress.com/ which basically uses the Eq. 2.29. We used MATLAB and Maple to calculate the equation proposed by Sun et al. [15] tried to evaluate the enthalpy of formation of liquid which can be termed as disordered alloy and that of the compounds which are the ordered alloys for some of the binary phases where experimental data was unavailable and the predictions were coherent to the periodic trend of these alloys. During the present work we also found out that the original Miedema's equation cannot be directly used to predict the enthalpy of formation of compounds or that of liquid, as it require some correction factors for the decrease in molar volume in the elements in the lanthanide series.

2.7 Procedure of critical evaluation/optimization of system

The objective of the present work was to critically evaluate and develop the thermodynamic database for Iron-Rare-Earth based alloys. In this regard, fifteen binary systems were critically evaluated and optimized:

All the calculations and optimizations in the present work were performed with the FactSage thermochemical software (FactSage, 2009). The critical evaluation and optimization were carried out with the following procedure:

i) The binary systems to be optimized during the present work were identified:

ii) Collection of data in the literature for the system:

All the data in the literature on the thermodynamic properties of the chosen systems were collected. These data were phase diagram data, thermodynamic properties like enthalpy of mixing in a solution phase or enthalpy of formation for compounds, activity of constituents in a solution, etc.

iii) Choosing appropriate thermodynamic model for given phases:

As stated in Chapter 2.2, an adequate model representing the Gibbs energy functions for a phase is required. This is very important since a good physical model based on the structure of the phase increases the accuracy of predictions of solution properties in multi-component systems. In the present work, the Modified Quasichemical Model (MQM) capable of taking into account short range ordering was chosen.

iv) Critical evaluation of collected experimental data:

The experimental data reported in the literature from each other beyond the stated experimental error range. The simultaneous optimization of various thermodynamic data which includes the phase diagram data and the thermodynamic properties of the phases removed the inconsistency amongst the thermodynamic data.

v) Optimization of model parameters for the system:

After evaluation of the experimental data, optimization was performed on the basis of selected reliable data to obtain the values of the model parameters. Even though FactSage has an optimization software, the Optisage module in FactSage, in present work, the optimized parameters are obtained by trial and error method.

vi) Back-calculation of all thermodynamic data and phase diagram:

One satisfactory model parameters were obtained; all the thermodynamic data and experimental data were back-calculated for comparison with the optimized values.

2.8 References

1. Van Laar,J.J., *Melting-point and freezing –point curves in binary systems, when the solid phase is a mixture(amorphous solid solution or mixed crystals) or both components.* Second part, 1908, Z. Phys. Chem. 63 216-21

2. Wagner C, Thermodynamics of Alloys, Addison-Wesley, 1952, Reading, MA.

3. Meijering J.L., Physical Chemistry of Metallic Solutions and Intermetallic Compounds, 1959, 2(5A), HMSO , London.

4. Kubaschwski O, T.G. Chart, *Theoretical approaches to calculation of phase diagrams*, J. Inst. Metals,1965, 93, 329-333.

5. Kaufman L., Bernstein H., *Computer calculation of Phase Diagrams*, 1970, Academic Press, New York.

6. Hillert, M., Phase Transformations, ASM, 1968, Cleveland, OH.

7. Lukas H., Fries S.G., Sundman B., Computational Thermodynamics: The CALPHAD Method, 2007, Cambridge Univ. Press.

8. Bale, C.W., Belisle, E.,Chartrand, P., Degeterov, S.A., Eriksson, G., Hack, K., Jung, I.-H, Kang Y.-B, Mahfoud,R.B., Melancon, J., Pelton, A.D., Robelin, C., Petersen, S., Calphad 33(2009), 2009, 295-311.

9. Davies, R.H., Dinsdale, A.T., Gisby, J.A., Robinson, J.A.J., Martin, S.M., *MTDATA- and phase equilibrium software* from the National Physical Laboratory, 2002.

10. Andersson, J.O. , Helander, T., Hoglund, L Shi P., Sundman, B.,*Thermo-Calc & DICTRA, computational tools for materials science*.

11.Pelton, A., Degterov, S., Eriksson, G., Robelin, C. & Dessureault, Y., *The modified quasichemical model I—Binary solutions*. Metallurgical and Materials Transactions B, 2000*,* 31**,** 651-659.

12. Pelton, A. D. & Chartrand, P*., The modified quasi-chemical model: Part II. Multicomponent solutions*, Metallurgical and Materials Transactions A: Physical Metallurgy and Materials Science, 2001. ,32**,** 1355-1360.

13. Hillert, M.. *The compound energy formalism. J. Alloys Compd*., 2001, 320**,** 161-176.

14. De Boer, F.R., R. Boom, W.C.M. Mattens, A.R. Miedema And A.K. Niessen, *Cohesion in Metals*,Transition Metal Alloys, 1988., Amsterdam, North Holland.

15. Sun, S. P., Yi, D. Q., Liu, H. Q., Zang, B. & Jiang, Y. *Calculation of glass forming ranges in Al-Ni RE (Ce, La, Y) ternary alloys and their sub-binaries based on Miedema's model.* Journal of Alloys and Compounds, 2010*.,* 506**,** 377-387.

16. Zhang, R. F. & Liu, B. X*., Proposed model for calculating the standard formation enthalpy of binary transition-metal systems*. Applied Physics Letters, 2002, 81**,** 1219-1221.

Chapter 3. Thermodynamic modeling of Fe-RE binary systems

3.1. The Fe-La (Iron-Lanthanum) System

Gschneider [1] reviewed the Iron-Lanthanum system and suggested a diagram which shows a eutectic reaction and an unusual flattened liquidus region on the Fe-rich side. This finding was later confirmed by Kepka et al.[2]. The system has a eutectic reaction. Savitsij et al.[3] proposed two compounds in their phase diagram, $LaFe_5$ and $LaFe_2$ peritectically melting at 1350 and 1100^oC, respectively, quite analogous to the Iron Cerium system, which was later withdrawn in their next assessment Savitski et al.[4]. Independent research by two other groups of Richerd [5] and Daane [6] and Wallace et al. [7] confirmed that there are compounds existing in this binary system. The non existence of the $LaFe_5$ was confirmed by Ning et al. [8] where a prediction was made for some new intermetallic compounds between transition metals and rare earth metals. The hydrogen absorption capacities of Fe_xLa alloys as done by Guidotti [9] changed very little when x was increased from 0 to 5, and it behaved similar to that of pure La as a binary system would have behave without any intermetallic compounds. Povoden [10] reported that the solubility of La in γ-Fe_{ss} is not significantly higher than solubility of La in α-Fe_{ss} at 930^oC.

3.1.1. Phase diagram data

A reduction of the transition temperature of α-$Fe_{ss}$$\rightarrow$ γ-Fe_{ss} for La saturated Fe is 6 ^oC. The γ-Fe_{ss} $\rightarrow$$\delta$-$Fe_{ss}$ transition temperature is increased by 12 ^oC as compared to polymorphic phases of pure Fe Zhang et al. [11]. In the phase diagram proposed by Richerd [5] the γ-Fe_{ss} and δ-Fe_{ss} was not reported. The maximum solubility of La in α-Fe_{ss} is lesser than 0.1at. % at 1053K and less than 0.2 at. % at approximately 1160 K [2, 12]. Richerd [5] used microscopic and microprobe analysis of Iron with varying amount of Lanthanum impurities found the maximum solubility of La in α-Fe_{ss} between 0.34 and 0.36 at. % at 930^oC. Savitskii [3] reported larger solubility of La in α-Fe_{ss} and γ-Fe_{ss} , however in there subsequent publication on the same system the used the solubility values from Daane[12]. The maximum solubility of Fe in β-La_{ss} is reported to be lesser

than 0.25 at.% at around 780 ^{o}C [1, 13, 14]. Richerd[5] determined the solubility of Fe in β-La_{ss} to be 0.25at. % at the solidus temperature of 880 ^{o}C.

Richerd[5] investigated the system in the La-rich side and found an eutectic point at 91.5 at. % La (96.4% wt. % La) and 780 ± 5 ^{o}C. Haefling et al.[6] assumed the anomalous liquidus to be "real" and is not due to formation of two immiscible liquids. Richerd[5] did not carry out any experiment in the iron rich side to comment on the weird flattening. Kepka and Skala[2] confirmed the findings.

3.1.2. Thermodynamic data

Berezutskii et al.[15] And Esin et al.[16] determined the enthalpies of mixing of Fe-La liquid from 0-35 at.% at 1450^{o}C and from 60 to 100 at.% Fe at 1650^{o}C respectively by using solution calorimetry. The liquidus of La shows unusual flattening.Similar phenomena has also been referred in Ce-Mn[17, 18] and La-Mn[19] system. Although no explanation has been provided for the flattening by Haefling [20] and Srenl'nikova[17] discount any chance of a miscibility gap. Iandelli [18] and Rolla et al.[19] support a miscibility gap. Kubachewski[21] suggested that with respect to the small difference in the value of Gibbs energy and the possible influence of impurities, grain boundary and strain energies arriving to a definite conclusion is impossible. Previous assessment by Zhang[11] also suggests that miscibility gap is the only thermodynamically acceptable in such a binary phase diagram. The phase diagram proposed by Povoden[10] do not show any miscibility gap.

Table 3.1.1. Optimized thermodynamic data of the La-Fe system.

Liquid phase (Quasichemical model parameters)
Coordination numbers: $Z^{Fe}_{FeFe} = Z^{\mathrm{La}}_{\mathrm{LaLa}} = Z^{\mathrm{La}}_{LaFe} = Z^{\mathrm{Fe}}_{\mathrm{FeLa}} = 6$
$\Delta g_{FeLa} = 6270 - 3762X_{FeFe} - 1045X_{LaLa}$

Solid Solution (parameters of the Compound Energy Formalism with two-sublattice approach) $(Fe, La)_1^I(Va)_1^{II}$	
FCC	${}^0L_{Fe,La} = 56430+0.6061T$
BCC	${}^0L_{Fe,La} = 56430+0.6061T$
HCP	${}^0L_{Fe,La} = 250800$

3.1.3. Reference

1. Gschneidner, K.A., Jr., *Binary Alloy Systems*. Rare Earth Alloys1961, NewYork: Van Nostrand.
2. Kepka, M., J.Skala, *Effect of Rare-Earth Elements on Prop- erties of Steels.* Hutník (Prague), 1972. **22**(v): p. 12–17
3. Savitsij, E.M., *Rare Metals and Alloys.* Dom Tekhniki,Moscow, 1959.
4. Savitskii, E.M., *Rare-Earth Metals,.* Metalloved. Term. Obrab. Met. Trans., 1961. **9**.
5. Richerd, J., *Lanthanum and Cerium in Pure Iron.* Mem. Sci. Rev. Metall, 1962. **59**(78): p. 539-548.
6. Haefling, J.F. and A.H. Daane, *Iron-Lanthanum System.* Inst. At. Res.
7. Wallace, W.E., K.A. Gschneidner, Jr., Editor.
8. Ning, Y.-T., et al., *The prediction and synthesis of some new intermetallic compounds between transition metals and rare earth metals.* Journal of the Less Common Metals, 1989. **147**(2): p. 167-173.
9. Guidotti, R.A., G.B. Atkinson, and M.M. Wong, *Hydrogen absorption by rare earth-transition metal alloys.* Journal of the Less Common Metals, 1977. **52**(1): p. 13-28.
10. Povoden-Karadeniz, E., et al., *Thermodynamic Assessment of the La-Fe-O System.* Journal of Phase Equilibria and Diffusion, 2009. **30**(4): p. 351-366.
11. Zhang, W. and C. Li, *The Fe-La (Iron-Lanthanum) System.* Journal of Phase Equilibria, 1997. **18**(3): p. 301-304.
12. Spedding, F.H. and A.H. Daane., ed. *The Rare Earths*. 1961, John Wiley & Sons: New York.
13. Van Diepen, A.M. and F.K. Lotgering, *Mössbauer effect in $LaFe_{12}O_{19}$.* Journal of Physics and Chemistry of Solids, 1974. **35**(12): p. 1641-1643.

14. Nassau, K., L.V. Cherry, and W.E. Wallace, *Intermetallic compounds between lanthanons and transition metals of the first long period. I. Preparation, existence and structural studies.* Phys. Chem. Solids, 1960. **16**,p. 123-30.
15. Berezutskii, V., N. Usenko, and M. Ivanov, *Thermochemistry of binary alloys of lanthanum with 3d-Transition Metals.* Powder Metallurgy and Metal Ceramics, 2006. **45**(5): p. 266-271.
16. Esin, Y.O., A.F. Ermakov, M.G. Valishev, G.M. Ryss, P.V. Geld, and E.S. Levin, *Enthalpy of Formation of Liquid Binary Alloys of Iron with Lanthanum and Cerium.* Zh. Fiz. Khim., 1981. **55**(7): p. 1665-1669.
17. Strel'nikova, M.S.M.a.I.A., Trans. Inst. Met. Akad. Nauk SSSR 1957. **2**: p. 135–138.
18. Iandelli, A., Lincei-Rend. Sc. fis. mat. e nat., 1952. **13**: p. 265–268.
19. Rolla, L. and A. Iandelli, *Beiträge zur Kenntnis der Metalle der seltenen Erden und ihrer Legierungen. Die Legierungen des Lanthans mit Mangan.* Berichte der deutschen chemischen Gesellschaft (A and B Series), 1942. **75**(12): p. 2091-2095.
20. Haefling, J. F. , A.H.Daanes, *Iron-Lanthanum System.*
21. Kubaschewski, O., *Iron-Lanthanum,Iron-Binary Phase Dia-grams*1982, New York: Springer-Verlag.

Figures

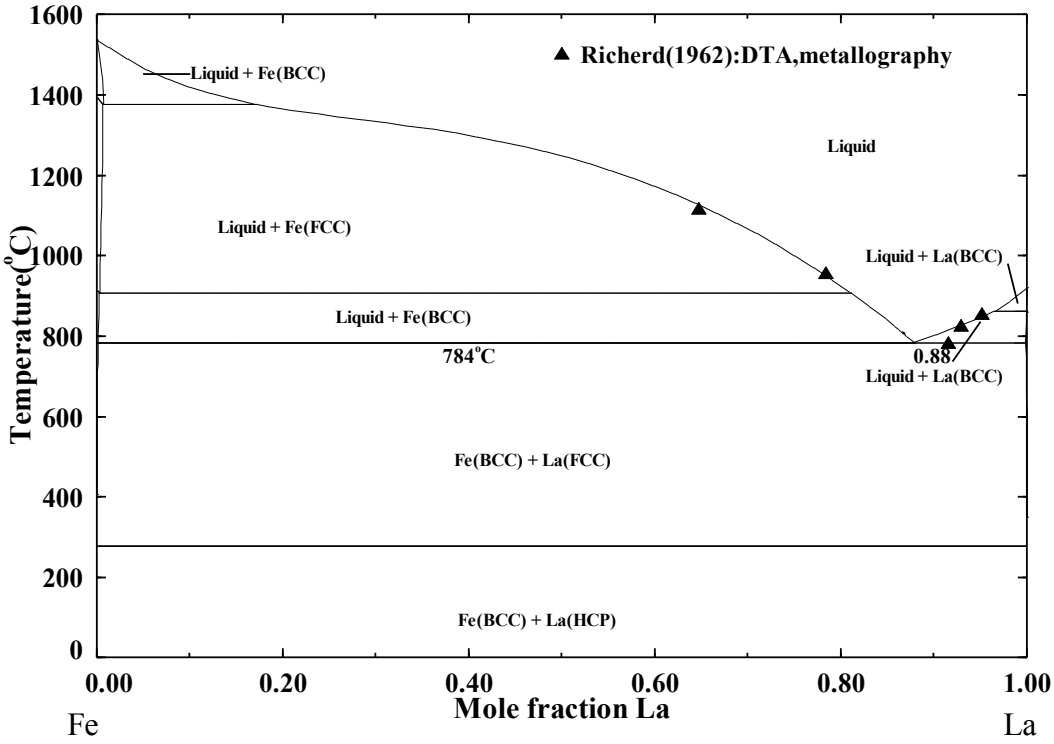

Fig 3.1.1. The optimized Fe-La system.

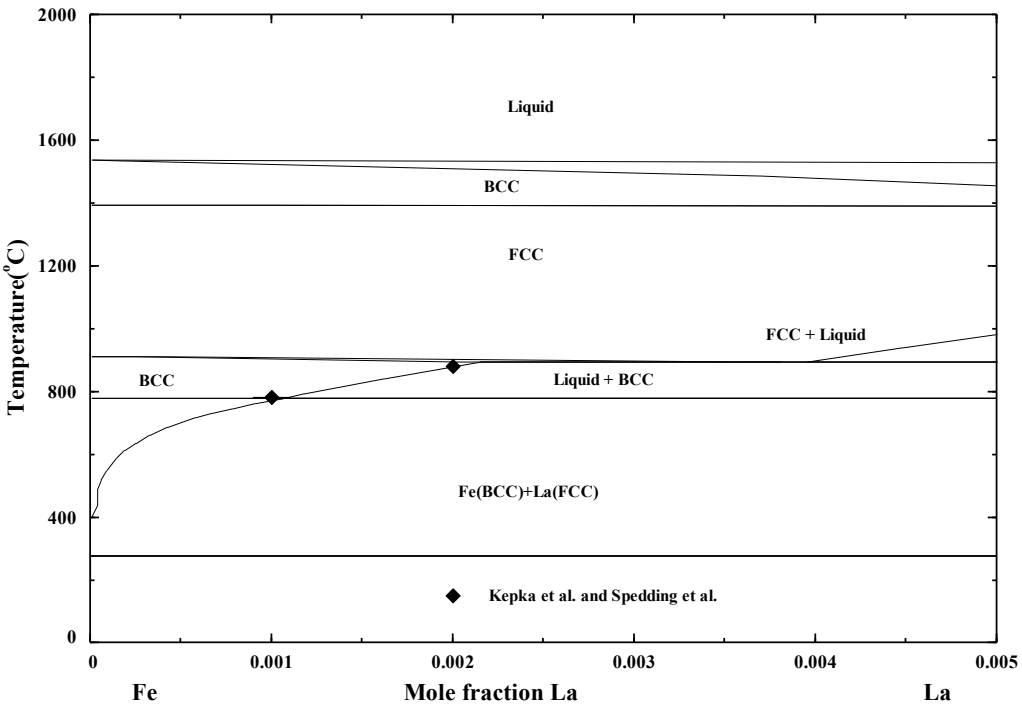

Fig. 3.1.2. Iron-rich side of the Fe-La phase diagram.

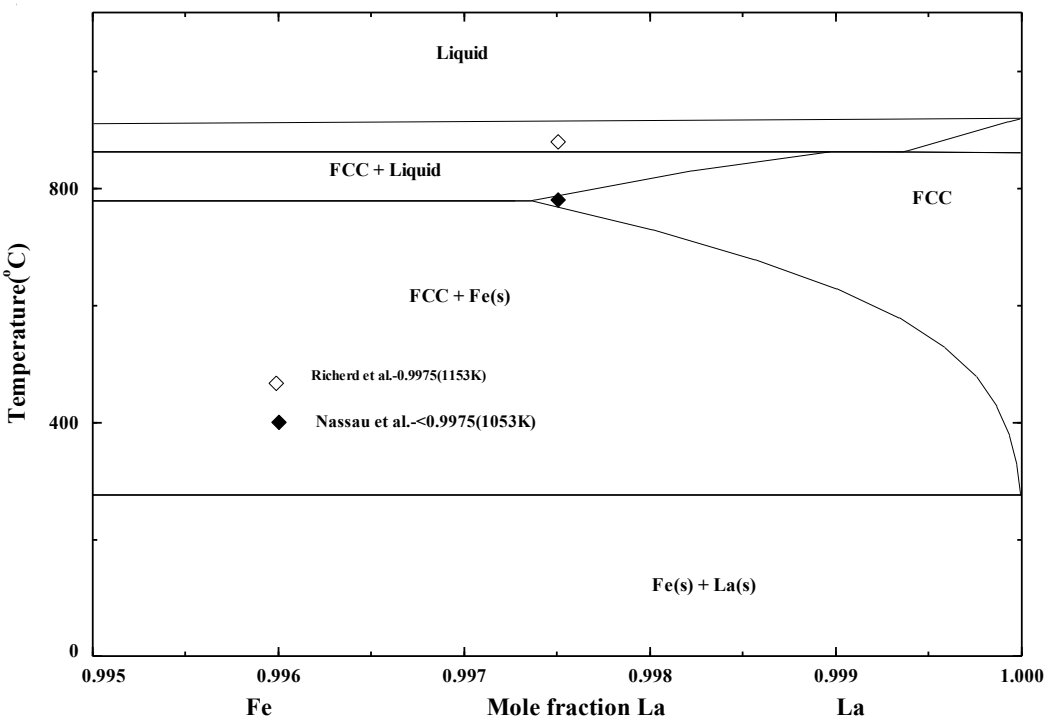

Fig. 3.1.3. Lanthanum-rich side of the Fe-La phase diagram.

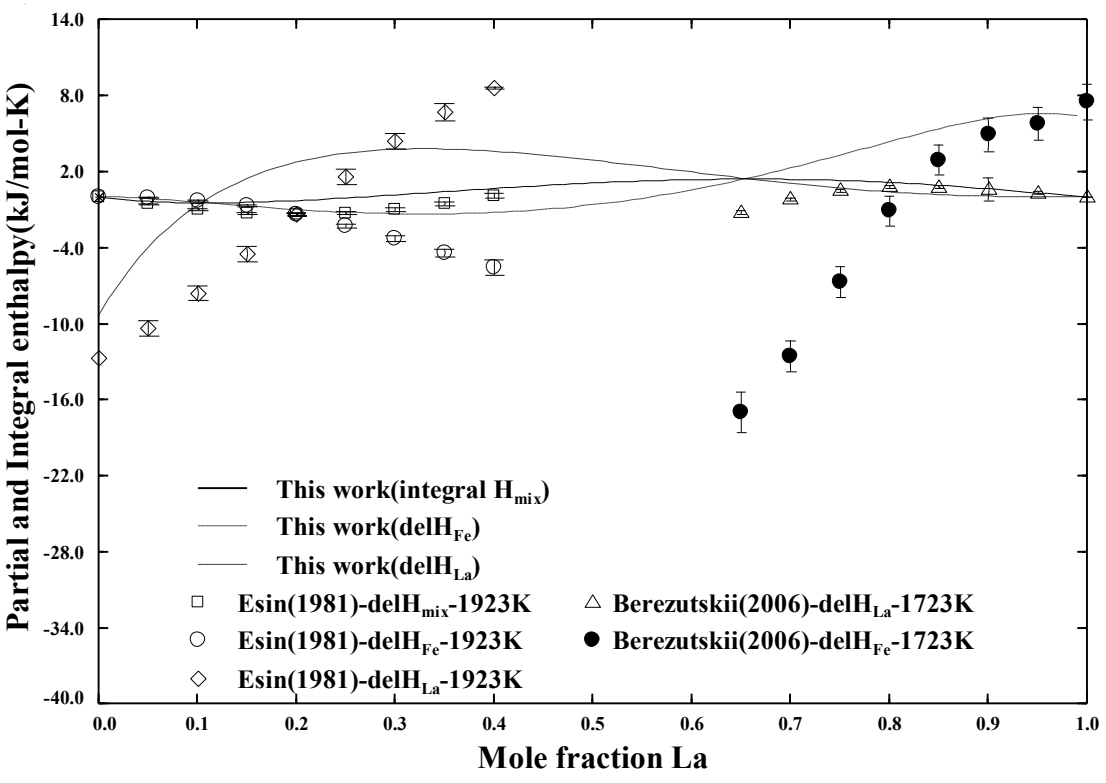

Fig.3.1.4. Enthalpy of mixing of Fe-La alloy at 1923K and 1723K

3.2. The Fe-Ce (Iron-Cerium) system

The Fe-Ce system was assessed Zhang [1], Su et al. [2], by Marazza et al. [3] and Okamoto[4]. The Fe-Ce phase diagram in Massalski [5] was redrawn from the original form of Zhang's phase diagram [1]. Due to phase rule violation, the enlarged Ce-rich portion of the diagram presented by Massalski [5] was deleted by Zhang [1]. Su et al. [2] assessed the Ce-Fe system by thermodynamic modeling.

3.2.1. Phase diagram data

The Cerium-Iron system was first investigated by Vogel [6] who reported presence of $CeFe_2$ and Ce_2Fe_5 . Vogel suggested the solubility of Ce in alpha and gamma iron (12 and 15 wt. % respectively), which was rather weird according to Jepson and Duwez[7] considering the quite dissimilar atomic radius of Ce and Fe. They presented a modified phase diagram which suggested solubility of cerium in iron to be 0.4 wt. % at 815-1015 ^oC instead of 12 wt. % and the Iron rich phase suggested by Vogel to be corresponding to $CeFe_5$ instead of Ce_2Fe_5 with the help of X-ray diffraction techniques. Some other researchers [8, 9] also reported the presence of $CeFe_2$ and $CeFe_5$ as the intermetallic phases. Later other researchers reported the presence of only two intermetallic stable phases cubic $CeFe_2$ and $CeFe_7$ with $MgCu_2$ crystal structure [10]. Johnson [11] and Buschow at al. [12] reported that there are only two compounds in this binary system which are $CeFe_2$ and Ce_2Fe_{17}. Ce_2Fe_{17} polymorphically transform from β-Ce_2Fe_{17} which is Th_2Fe_{17}-type rhombohedral to α-Ce_2Fe_{17} Th_2Ni_{17}-type hexagonal. Gschneidner [13] reported the binary phase diagram with two intermetallic compounds $CeFe_2$ and Ce_2Fe_{17}. With the help of thermal, microscopic and x-ray diffraction techniques Chuang et al.[14] investigated the phase diagram. The phase diagram of Chuang et al.[14] resembles to that suggested by Gschneidner[13].

This system have two compounds $CeFe_2$ and Ce_2Fe_{17} melting peritectically, and terminal solid phases α-Fe(bcc_A2), δ-Fe(bcc_A2), γ-Fe(fcc_A1), δ-Ce(bcc_A2), γ-Ce (fcc_A1) and β-Ce (dhcp). The solid solubility of cerium in (α-Fe) is 0.038 at.% at 900^oC, 0.035% at 850^oC[14] and 0.019 at. % at room temperature as suggested by Yan et al [15] and Zhang et al.[16]. The δ-Fe → γ-Fe transformation temperature increases by 5 ^oC (from

1394 ^{o}C) and that of γ-Fe → α-Fe increases by 10 ^{o}C (from 912 ^{o}C) when cerium is added.

3.2.2. Thermodynamic Data

The low temperature heat capacity was measured by Janssen [17] by Quantum design Magnetic Property Measurement System (MPMS) for the Ce_2Fe_{17} and by Haldar et al. [18] for the $CeFe_2$ by Physical Property Measurement System(PPMS) instruments. The S_{298} for Ce_2Fe_{17} and $CeFe_2$ are obtained by integrating the low temperature heat capacity values. No enthalpy of formation data for both compounds is experimentally determined. Esin[19] determined the mixing enthalpies of liquid in the Ce-Fe system in the composition range 0-35 at.% Ce at 1627^{o}C. Burylev [20] determined the activities of the binary system at 1227 ^{o}C by thermodynamic calculation rather than experimentation. Esin's data could not be reproduced as the Ce_2Fe_{17} phase could not be formed if liquid was made more stable in the iron rich side, with the obtained experimental entropy. The integral data reported by Esin[1] was well reproduced by the current optimization, but due to lack of experimental details we are not sure about the partial data reported by them. We used a couple of temperature dependence parameter for the excess gibbs energy for the liquid. As reported by Buschow[2] Ce2Fe17 have a polymorphic transformation, However we are not sure of the temperature and in this assessment such transformation is not considered, if the transformation can be introduced we can reproduce the S298 as reported by Janssen et al.[3]

3.2.3. Magnetic Data

Both the intermetallic phases of Cerium and Iron are magnetic in nature. The Curie temperatures of these phases are below room temperature 235K and 238K [21] for $CeFe_2$ and Ce_2Fe_{17} respectively. The S_{298} value for both these phases includes the magnetic contributionas they are derived from low temperature heat capacity (C_p) data.

Table 3.2.1. Optimized thermodynamic data of the Ce-Fe system.

Liquid phase (Quasichemical model parameters)
Coordination numbers: $Z^{Fe}_{FeFe} = Z^{\mathrm{Ce}}_{\mathrm{CeCe}} = Z^{\mathrm{Ce}}_{\mathrm{CeFe}} = Z^{\mathrm{Ce}}_{\mathrm{CeFe}} = 6$
$\Delta g_{FeCe} = -1337.6 + 6270X_{FeFe}$

Solid phases			
$\Delta H_f^{\circ}{}_{298}$ **(kJ mol^{-1})**			
Compound	**Optimized elements as reference**	**Experimental elements as reference**	**Reference**
$CeFe_2$	-13.4	-	-
Ce_2Fe_{17}	-19.8	-	-
S°_{298} **(J mol^{-1} K^{-1})**			
Compound	S°_{298} **Optimized**	S°_{298} **Experimental**	**Reference**
$CeFe_2$	122.96	122.960235	[22]
Ce_2Fe_{17}	627	679.6028	[23]
C_p **(J mol^{-1} K^{-1})**			
Compound	**Optimized**		**Reference**
$CeFe_2$			$C_p = C_p(Ce_{(hcp)}) + 2C_p(Fe_{(bcc)})+29.79$
298-1000 K	$74.402363+ 0.03101068T -273202T^{-2} +2.631762E-6T^2$		
1000-1811 K	$153.358443-0.034502894T -23372850T^{-2} +1.228891E-5T^2$		
1811-2000K	$198.329843--0.052092974T -23063414T^{-2} +1.1581786E-5T^2-4.132854E33E-33T^{-10}$		
Ce_2Fe_{17}			
298-1000K	$489.4109+0.17635688T -2557738T^{-2}+ 9.85983E-6T^2$		
1000-1811K	$647.32306-0.045329732T -48757034T^{-2} +2.9174126E-5T^2$		$C_p = 2C_p(Ce_{(hcp)}) + 17C_p(Fe_{(bcc)}) +5.007363$
1811-2000K	$1029.57996-0.104185948T -46126828T^{-2} +2.3163572E-5T^2-3.5129259E34T^{-10}$		
Solid Solution (parameters of the Compound Energy Formalism with two-sublattice approach) $(Fe, Ce)_1^{I}(Va)_1^{II}$			
FCC	${}^0L_{Fe,Ce} = -12540+41.8T$		
BCC	${}^0L_{Fe,Ce} = 50160$		

Compound	Magnetic moment	Curie Temperature(K)	References
$CeFe_2$	2.48	235	[21]
Ce_2Fe_{17}	29.7	238	[21]

3.2.4. References

1. Zhang, W., G.L., K. Han, *Monograph Series on Alloy Phase Diagrams:Phase Diagram of Binary Iron Alloys*1993, Ohio: ASM International, Metals Park.
2. Su, X. and J.-C. Tedenac, *Thermodynamic modeling of the ternary Ce-Fe-Sb system: Assessment of the Ce-Sb and Ce-Fe systems.* CALPHAD: Comput. Coupling Phase Diagrams Thermochem., 2006. **30**,p. 455-460.
3. Marazza, R., P. Riani, and G. Cacciamani, *Critical assessment of iron binary systems with light rare earths La, Ce, Pr, and Nd.* Inorg. Chim. Acta, 2008. **361**,p. 3800-3806.
4. Okamoto, H., *Ce-Fe (Cerium-Iron).* Journal of Phase Equilibria and Diffusion, 2008. **29**(1): p. 116-117.
5. Massalski, T.B., *Binary Alloy Phase Diagrams,*ASM International, 1990, **2.** 6. Vogel, R., *Über Cer-Eisenlegierungen.* Zeitschrift für anorganische und allgemeine Chemie, 1917. **99**(1): p. 25-49.
7. Jepson, J.O. and P. Dumez, *Partial phase diagram of the iron-cerium system.* Trans. Am. Soc. Met., 1954. **Preprint No. 2**,p. 13 pp.
8. Shunk, F.A., ed. *Constitution of Binary alloys*. 1969, McGraw-Hill: New York. 231.
9. Nassau, K., L.V. Cherry, and W.E. Wallace, *Intermetallic compounds between lanthanons and transition metals of the first long period , : I--Preparation, existence and structural studies.* Journal of Physics and Chemistry of Solids, 1960. **16**(1-2): p. 123-130.
10. Ray, A.E., *The crystal structure of $CeFe_7$, $PrFe_7$, $NdFe_7$, and $SmFe_7$.* Acta Crystallogr., 1966. **21**,p. 426-30.
11. Johnson, G., D.H.Wood, G.S. Smith and A.E. Ray, *Refinement of a Th_2Zn_{17} Structure.* Acta Crystallogr. Sect. B, 1968. **24**: p. 274-276.
12. Buschow, K.H.J. and J.S. van Wieringen, *Crystal structure and magnetic properties of cerium-iron compounds.* physica status solidi (b), 1970. **42**(1): p. 231-239.

13. Gschneidner, K.A., Jr., *Binary Alloy Systems*. Rare Earth Alloys1961, NewYork: Van Nostrand.
14. Chuang, Y.C., C.H. Wu, and Z.B. Shao, *Investigation of the cerium-iron binary system.* J. Less-Common Met., 1987. **136**,p. 147-53.
15. Yan, Y-X. and F.-Z. Zhang, *Determination of solid solubility of cerium in iron by means of electron probe micro-analyzer.* Xi You Jin Shu/Rare Metals, 1987. **6**(2): p. 131-136.
16. Zhang, F., L.Gu, W. Qu and Y.Y. Liu, Acta Metall.Sin., 1987. **23**.
17. Janssen, Y., et al., *Magnetic phase diagram of Ce_2Fe_{17}.* Phys. Rev. B: Condens. Matter Mater. Phys., 2007. **76**,p. 054420/1-054420/17.
18. Haldar, A., K.G. Suresh, and A.K. Nigam, *Magnetic and magnetocaloric properties of Ce1-xRxFe2 and Ce(Fe1-xMx)2 compounds.* J. Phys. D: Appl. Phys., 2010. **43**,p. 285004/1-285004/6.
19. Esin, Y.O., A.F.Ermakov., M.G. Valishev, G.M. Ryss, P.V. Geld, and E.S. Levin, *Enthalpy of Formation of Liquid Binary Alloys of Iron with Lanthanum and Cerium.* Zh. Fiz. Khim., 1981. **55**(7): p. 1665-1669.
20. Burylev, B.P. and L.P. Moisov, *Thermodynamic activities of components of the iron-cerium and iron-yttrium systems.* Izv. Vyssh. Uchebn. Zaved., Chern. Metall., 1988,p. 1-3.
21. Buschow, K.H.J., *Intermetallic compounds of rare earth and 3d transition metals.* Rep. Prog. Phys., 1977. **40**,p. 1179-256.
22. Mandal, K., A.Yan, P. Kerschl, A. Handstein, O. Gutfleisch and K.H. Muller, *The study of magnetocaloric effect in R_2Fe_{17} (R=Y, Pr) alloys.* Journal of Physics D:Applied Physics, 2004. **37**: p. 2628-2631.
23. Kreyssig, A., et al., *Crystallographic phase transition within the magnetically ordered state of Ce2Fe17.* Phys. Rev. B: Condens. Matter Mater. Phys., 2007. **76**,p. 054421/1-054421/8.

Figures

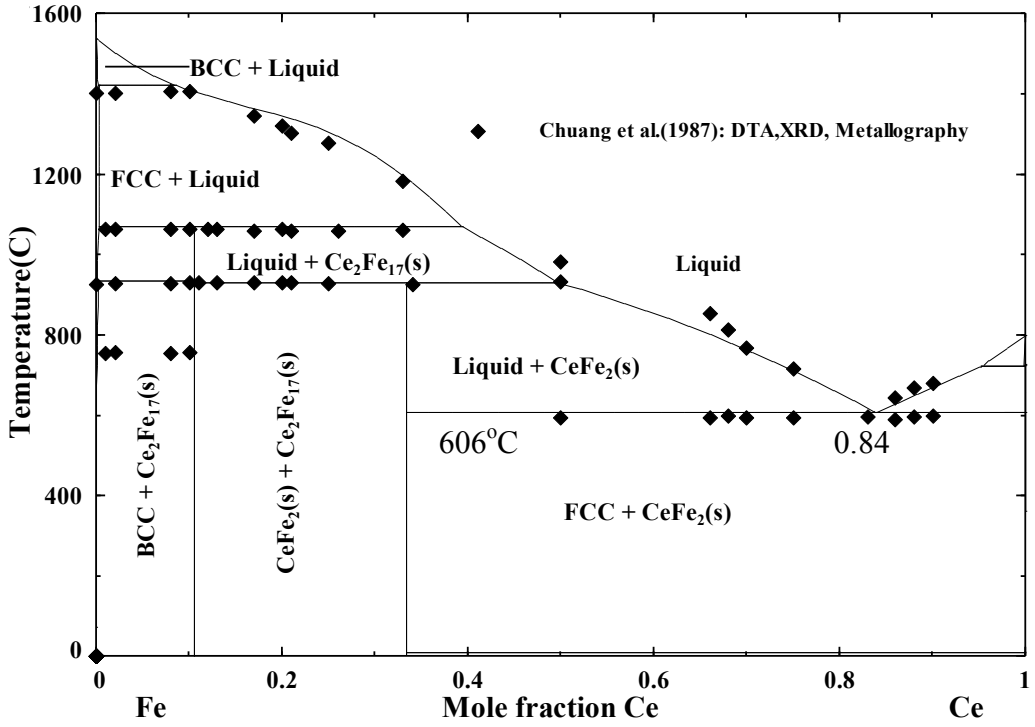

Fig 3.2.1. The optimized Fe-Ce system

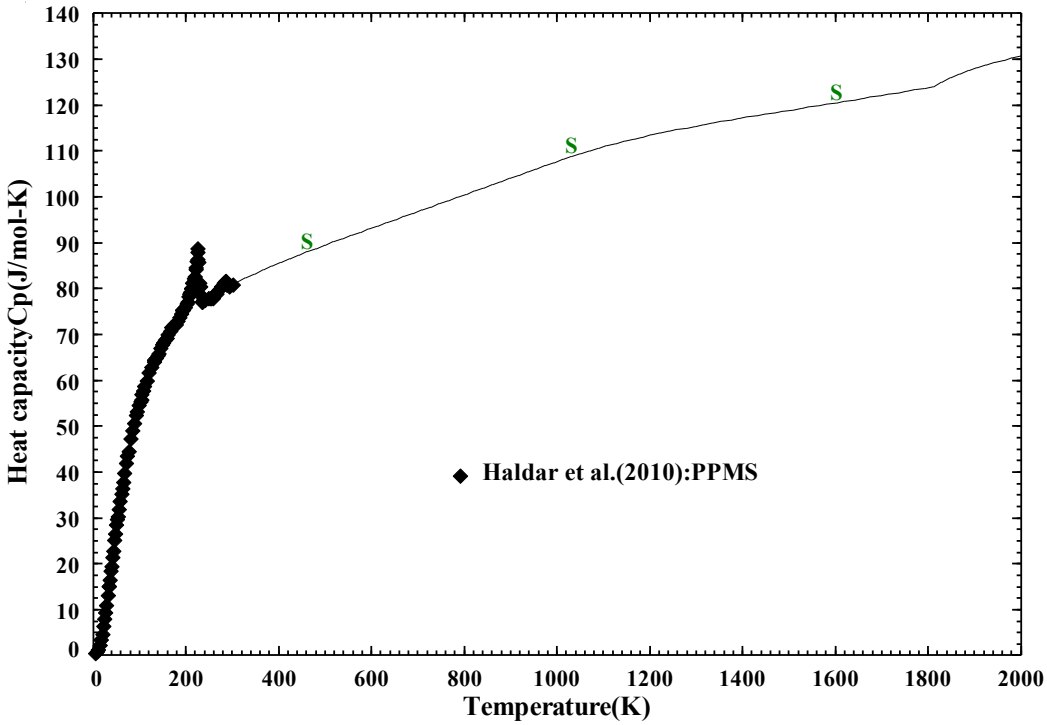

Fig. 3.2.2. Low temperature heat capacity of $CeFe_2$

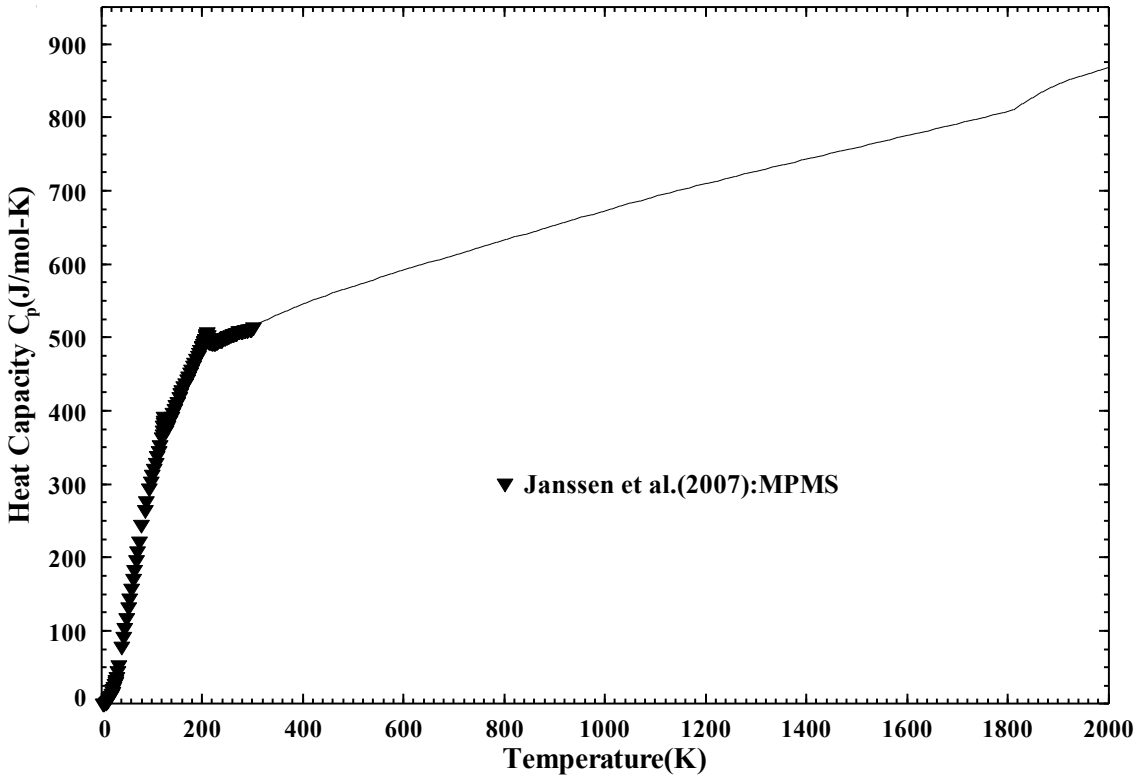

Fig. 3.2.3. Low temperature heat capacity of Ce_2Fe_{17}

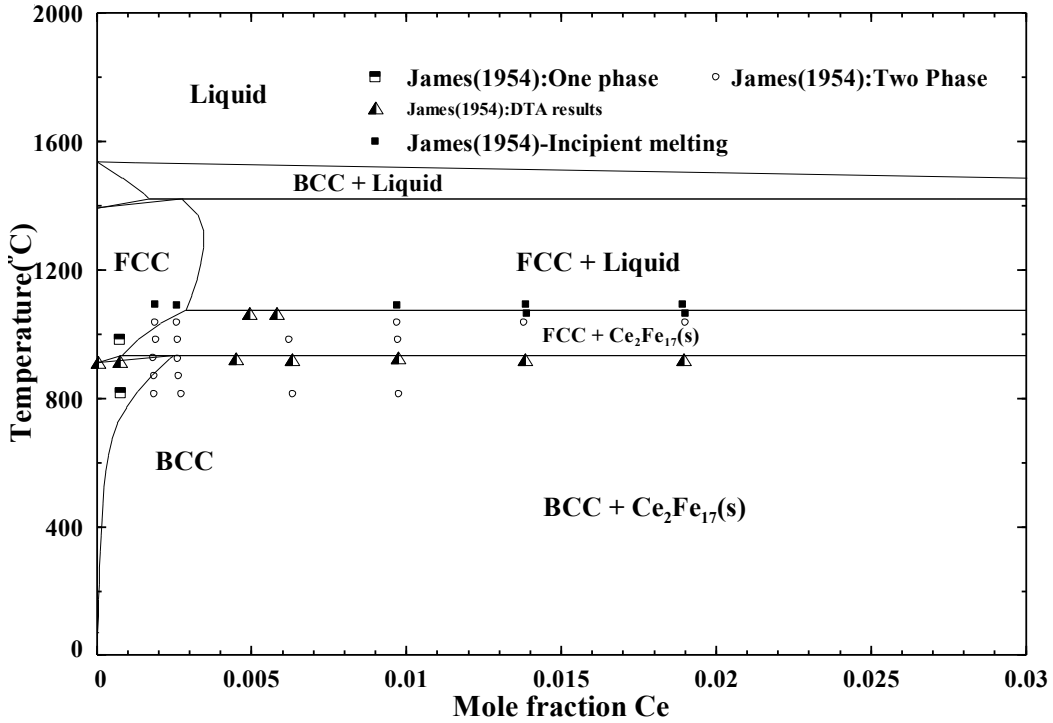

Fig. 3.2.4. Iron-rich side of the Fe-Ce phase diagram.

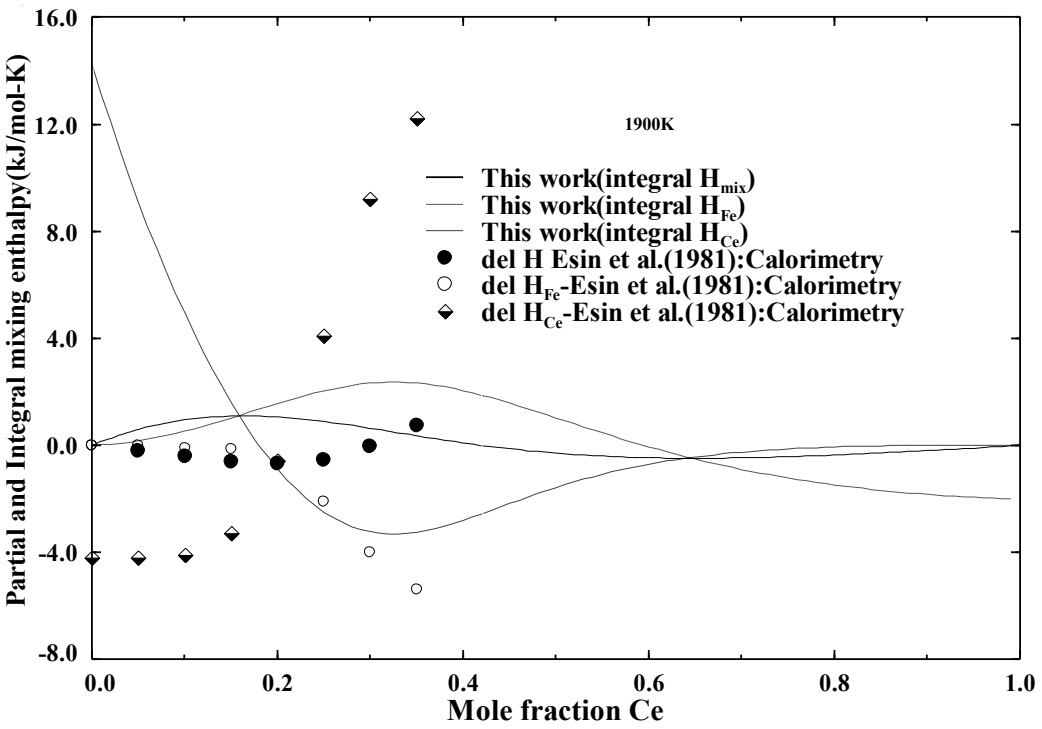

Fig. 3.2.5. Enthalpy of mixing of Fe-Ce alloy at 1900K

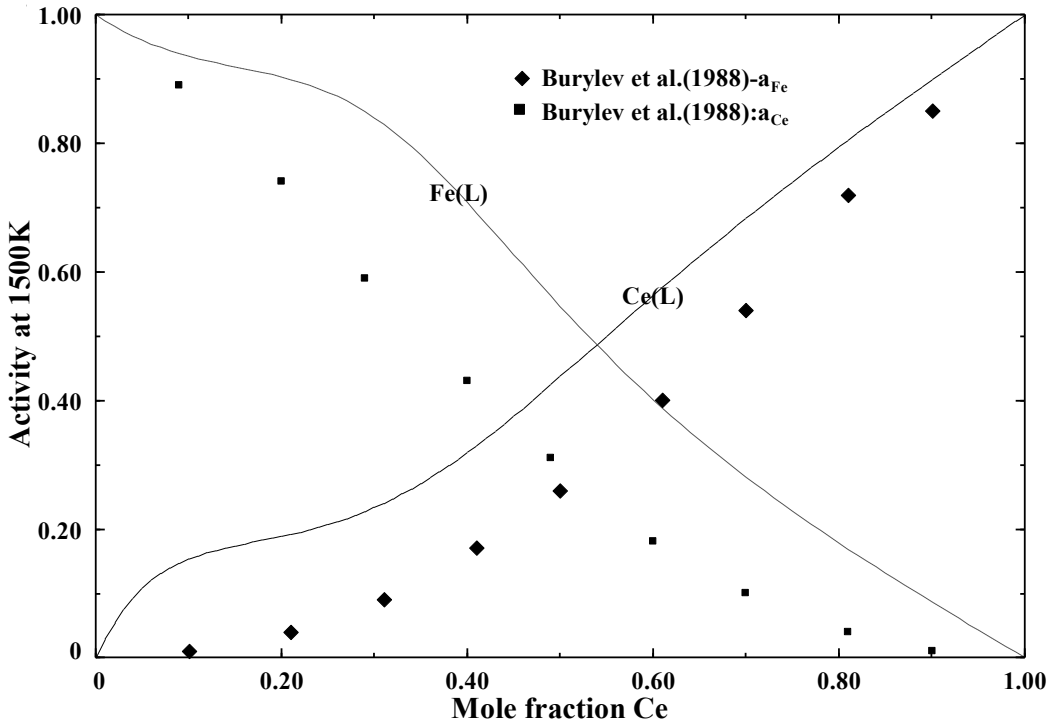

Fig. 3.2.6. Activity of Ce and Fe in liquid at 1500 K.

3.3. Fe-Pr (Iron-Praseodymium) system

The binary Fe-Pr phase diagram has been proposed by several researchers Ray, Zhuang et al., Burkhanov et al., Tian et al, and Bär et al.[1-5]. Ray, Zhuang et al., Tian et al.., [1, 2, 4] based their phase diagram on DTA and XRD analysis. Kubachewski[6] reported a phase diagram based primarily on Ray[1] with minute alterations. Ray[1] and Zhuang et al. [2] reported two stoichiometric phases Pr_2Fe_{17} and $PrFe_2$, whereas Tian et al. [4] in his phase diagram only exhibited one phase Pr_2Fe_{17}. The $PrFe_2$ phase also appeared in Kubaschewski [6] as an equilibrium phase. It was found that Fe_2Pr forms under high pressure as reported by Cannon et al. [7], Shimotomai et al. [8]. Kubaschewski[6] in his reported phase diagram had no $PrFe_2$ intermetallic phase.

3.3.1. Phase diagram data

The phase diagram of Zhuang et al. [2] seems to be thermodynamically improbable. Okamoto [9] suggested possible contamination during the experiments which has not been reported or else the phase diagram was in weight percentage composition scale instead of atomic percentage as is reported. Okamoto [9] stated the discrepancies which include erroneous melting point estimation of γ-Fe, and the slope of the liquidus seems to be too steep in comparison with the empirical trend. Bar et al. [5] did experiments and thermodynamic assessment, and presented a phase diagram which is very similar to those reported by Tian et al.[3], Okamoto[4] and Burkhanov et al.[9]. The solubility of Pr in Fe at 900^o C as suggested by Burkhanov et al [3] is 0.25 at. % . The α-Pr→β-Pr transformation temperature is 796^o C [10], 790^o C (Moffat) and 795^o C [4, 6, 11] which are very similar. The melting point of Pr was reported to be 918^{o}C by Kubaschewski[6] and Tian et al. [4], 917^{o}C by (Moffat) and 931^{o}C [10, 11]. As suggested by Bar et al. [5] the L+δ-Fe↔ γ-Fe and γ-Fe+$Fe_{17}Pr_2$↔α-Fe invariant reactions are at 1398^{o}C and 916^{o}C respectively. Bar et al. [5] also gave a L+β-Pr ↔ α-Pr peritectic reaction temperature is lower than the pure Pr polymorphic transformation point. Ray et al. [12] and Ray [13] mentioned a compound as $PrFe_7$, but later Kripyakevich et al. [14] and Weik et al. [15] found the intermetallic phase is Pr_2Fe_{17} with the rhombohedral Th_2Zn_{17} crystal structure. Single crystal and X-ray diffraction studies conducted by Johnson [16] confirmed existence of $Fe_{17}Pr_2$. The compound has a peritectic melting at 1165^{o}C [12], 1108^{o}C

(Moffat), 1310°C [2], 1102°C [4] and 1105°C [5]. The low temperature heat capacity data was reported by Mandal et al. [17] which were also considered to get the entropy of Pr_2Fe_{17} at 298K.

Although the $PrFe_2$ phase was reported by several researchers as discussed above, Cannon et al. [7] first mentioned that this is phase is formed at high pressure, Mansey et al.[18] reported that it is impossible to form this phase under their experimental conditions with normal atmospheric pressures. Shimotomai st al. [8] when casted the alloy at a stoichiometric ratio of $PrFe_2$ obtained an elemental Pr and compound Pr_2Fe_{17} without any detectable $PrFe_2$. In the same work they mentioned synthesizing the $PrFe_2$ (C15) phase at 55kbar. This phase can also be formed by quenching the melt at 7.7GPa pressure [19]. Tian et al. [4] heat treated at 600°C, no $PrFe_2$ phase was observed, and no peritectic reaction was detected by either magnetic or thermal analysis. Burkhanov et al. [3] annealed the Pr-Fe alloys at 400°C and 600°C, where in addition of αPr and Pr_2Fe_{17}, metastable $PrFe_2$ with (C14) and (C15) structure. He suggested that the metastable $PrFe_2$ go through a structural rearrangement to Pr_2Fe_{17} (Fe_2Pr (C14) [cubic-$MgCu_2$-type] → $PrFe_2$ (C15) [hexagonal-$MgZn_2$-type] → Pr_2Fe_{17} [$MgZn_2$-type].

3.3.2. Thermodynamic data

The experimental data of Gibbs energy of formation by Bar et al. [5] who did EMF experiments (galvanic cells using CaF_2 as a solid electrolyte) between 800 and 1200 K. He also measured activity of Praseodymium at various temperatures (650, 700, 750 and 800 °C) and the EMF change with temperature. The experimental data are all reproduced by our optimization and are shown in Fig.3.3.1. The optimized heat capacity of Pr_2Fe_{17} compound (obtained using the heat capacity functions of the elemental constituents Fe and Pr) was increased by 45.17 J $mol^{-1}K^{-1}$ in order to fit the experimental low temperature heat capacity data by Mandal et al. [17]. But on integration of data the S_{298} obtained could not be used for optimization, 30.842J/mol-atoms were used instead of 37.7J/mol atoms which was obtained by integration. As the Curie temperature of the Pr_2Fe_{17} is 283 K (below 298 K) the low temperature heat capacity data is integrated from 0K to 298.15 K and the magnetic contribution is taken into consideration in the S_{298} of the intermetallic phase.

Experimental data on liquid were not found in the literature. The thermodynamic optimization of the Fe-Pr system is performed using the Gibbs energy and activity data from Bar et al. [5]. The S_{298} was determined from Mandal et al.[17] low temperature heat capacity calculations. . The optimized values for the model parameters are listed in Table 3.3.1. The phase diagrams and other thermodynamic properties calculated with the optimized set of model parameters are shown in Figs. 3.3.1 to 3.3.4 and compared with experimental data. The calculated curves are in good agreement with the measured values. EMF variation with temperature data reported by Bar et al.[5] was converted to activity data and presented with assessed activity data in Fig. 3.3.3.

3.3.3. Magnetic Data

The Magnetic data for the four intermetallic phases were obtained from Buschow[20]. However the optimization was not influenced by magnetic contribution to the Gibbs energy.

Table 3.3.1. Optimized thermodynamic data of the Pr-Fe system.

Liquid phase (Quasichemical model parameters)			
Coordination numbers: $Z^{Fe}_{FeFe} = Z^{\mathrm{Pr}}_{\mathrm{PrPr}} = Z^{\mathrm{Pr}}_{\mathrm{Pr}Fe} = Z^{\mathrm{Pr}}_{\mathrm{FePr}} = 6$ $\Delta g_{FePr} = 1463 - 6.27T - (5434)X_{FeFe}$			
Solid phases			
$\Delta H_f°_{298}$ **(kJ mol^{-1})**			
Compound	**Optimized elements as reference**	**Experimental elements as reference**	**Reference**
Pr_2Fe_{17}	-23.4737	-	-
$S°_{298}$ **(J mol^{-1} K^{-1})**			
Compound	$S°_{298}$ **Optimized**	$S°_{298}$ **Experimental**	**Reference**
Pr_2Fe_{17}	620	717.207	[17]
C_p **(J mol^{-1} K^{-1})**			
Compound	**Optimized**		**Reference**
Pr_2Fe_{17}			
298-500K	537.5783 -0.14220032 T -4659746T^{-2}+ 0.00030822255T^2		C_p = $2C_p(Pr_{(hcp)})$ +17$C_p(Fe_{(bcc)})$) +88.352
500-800K	445.5249+0.16940072T -2630206T^{-2}+2.0764674E-5T^2		
800-1068K	537.5783 +0.66479768 T +43724994^{-2}-0.000181096242T^2		
1068-1204K	1611.9837214-1.071210344T -286337566T^{-2}+ 0.000377946978T^2		
1204-1811K	485.6825+0.14951568T -2630206T^{-2} +6.010554E-6T^2		
1811-3800K	867.9394-3.5129259E34T^{-10}		
Solid Solution (parameters of the Compound Energy Formalism with two-sublattice approach) $\mathbf{(Fe, Pr)^{I}_{1}(Va)^{II}_{1}}$			
FCC	$^0L_{Fe,Pr}$ = 44726		
BCC	$^0L_{Fe,Pr}$ = 41800		

Compound	**Magnetic moment**	**Curie Temperature(K)**	**References**
Pr_2Fe_{17}	30.6	283	**[20]**

3.3.4. References

1. Ray, A.E., *The Iron-Praseodymium Phase Diagram*, 1969, Air Force Materials Laboratory: Ohio. p. 13.
2. Zhuang, Y., H. Zhou, and J. Zheng, *Phase diagram of binary praseodymium-iron system.* Jinshu Xuebao, 1987. **23**, p. B42-B43.
3. Burkhanov, G.S., et al., *Equilibrium and metastable phases in Pr-Fe alloys.* Metally, 1994 p. 163-9.
4. Tian, J., Y. Huang, Liang J., *THE Pr-Fe-B TERNARY SYSTEM.* Sci. Sin., 1987. **30** (Ser. A(Engl. Ed.)): p. 607–619.
5. Bär,S., H.J. Schaller, *Zur Konstitution und Thermodynamik von Fe-Pr-Legierungen.* Z. Metallkd., 1995. **86** p. 388–394.
6. Kubaschewski, O., *IRON-Binary Phase Diagrams*1982, Berlin: Springer.
7. Cannon, J.F., D.L. Robertson, and H.T. Hall, *Synthesis of lanthanide-iron Laves phases at high pressures and temperatures.* Mater. Res. Bull., 1972. **7**, p. 5-11.
8. Shimotomai, M., H. Miyake, and M. Doyama, *Magnetic characteristics of Laves phase 1:2 praseodymium-iron compound.* J. Phys. F, 1980. **10**, p. 707-13.
9. Okamoto, H., *Phase Diagrams of Binary Iron Alloys*. J. Phase Equilib., ed. H. Okamoto1993, Materials Park, Ohio: Materials Information Society.
10. Hultgren, R.D., R.L. Orr, P.D. Anderson, K.K. Kelly, *Selected Values of Thermodynamic Properties of Metals and Alloys*1963: Wiley.
11. Massalski, T.B., *Binary Alloy Phase Diagrams,*ASM International, 1990, **2.**
12. Ray, A.E., K. Strnat, and D. Feldmann, *Preparation and thermomagnetic analysis of compounds of Ce, Pr, and Nd with Fe having the approximate composition RFe7.* Proc. Conf. Rare Earths Res., 3rd, Clearwater, Florida, 1964. **1963**, p. 443-57.
13. Ray, A.E., *The crystal structure of CeFe7, PrFe7, NdFe7, and SmFe7.* Acta Crystallogr., 1966. **21**,p. 426-30.
14. Kripyakevich, P.I. and D.P. Frankevich, *New compounds of the lanthanides with Mn and Fe, and their crystalline structures.* Kristallografiya, 1965. **10**, p. 560.

15. Weik, H., et al., *Investigations of the structure and magnetic behavior of peritectic Pr-Fe and Nd-Fe compounds of the type RFe7 by neutron diffraction.* Proc. Conf. Rare Earth Res., 4th, Phoenix, Ariz., 1965, p. 19-25.
16. Johnson, G., D.H. Wood, G.S. Smith and A.E. Ray, *Refinement of a Th_2Zn_{17} Structure.* Acta Crystallogr. Sect. B, 1968. **24**: p. 274-276.
17. Mandal, K., A. Yan, P. Kerschl, A. Handstein, O. Gutfleisch and K.H. Muller, *The study of magnetocaloric effect in R_2Fe_{17} (R=Y, Pr) alloys.* Journal of Physics D:Applied Physics, 2004. **37**: p. 2628-2631.
18. Mansey, R.C., G.V. Raynor, and I.R. Harris, *Rare-earth intermediate phases. V. The cubic Laves phases formed by rare-earth metals with iron and nickel.* J. Less-Common Metals, 1968. **14**, p. 329-36.
19. Tsvyashchenko, A.V. and S.V. Popova, *New phases melt quenched under high pressure in R-Fe systems (R = Pr, Sm, Dy, Tb, Ho, Er, Tm, Yb, Lu).* Journal of the Less Common Metals, 1985. **108**(1): p. 115-121.
20. Buschow, K.H.J., *Intermetallic compounds of rare earth and 3d transition metals.* Rep. Prog. Phys., 1977. **40**, p. 1179-256.

Figures

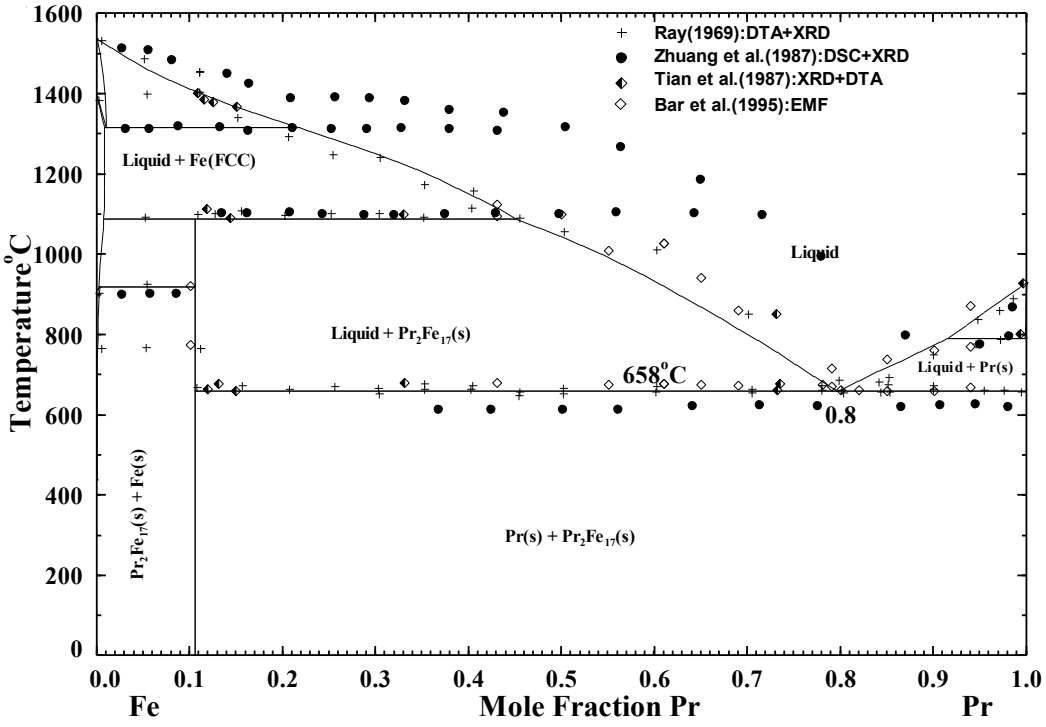

Fig 3.3.1. The optimized Fe-Pr system.

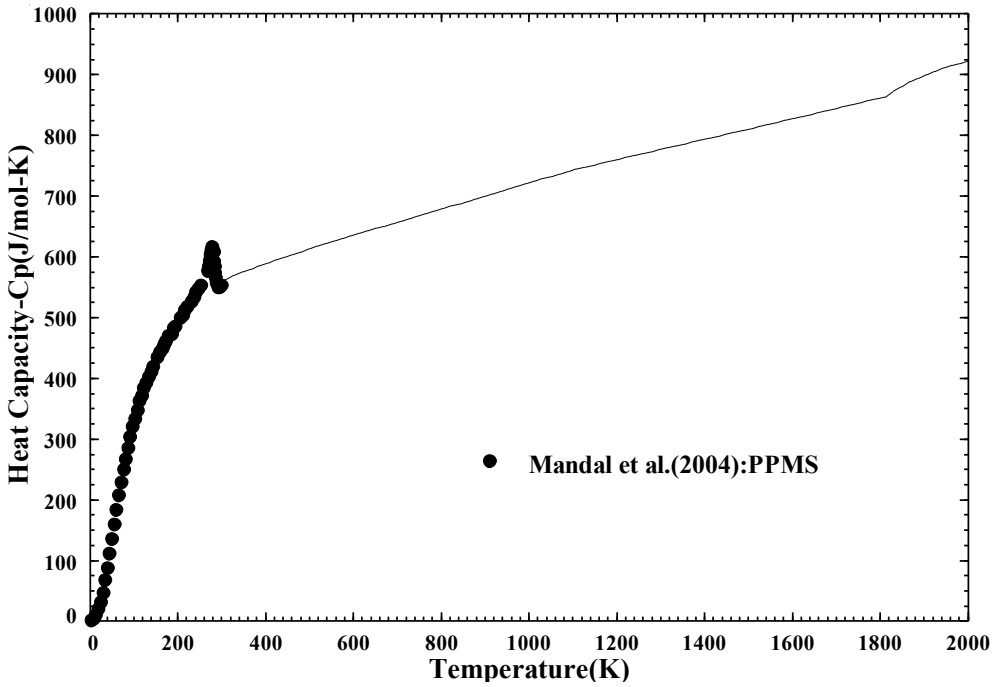

Fig. 3.3.2. Low temperature heat capacity value for Pr_2Fe_{17}.

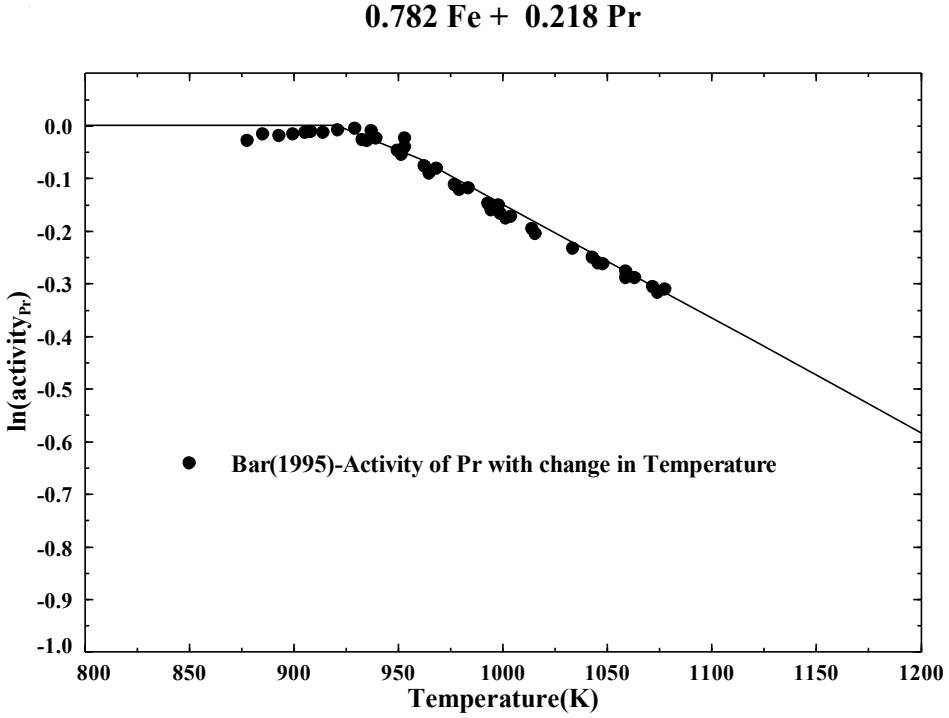

Fig. 3.3.3. Temperature dependence of activity measured on an alloy of 21.8 at. % Pr.

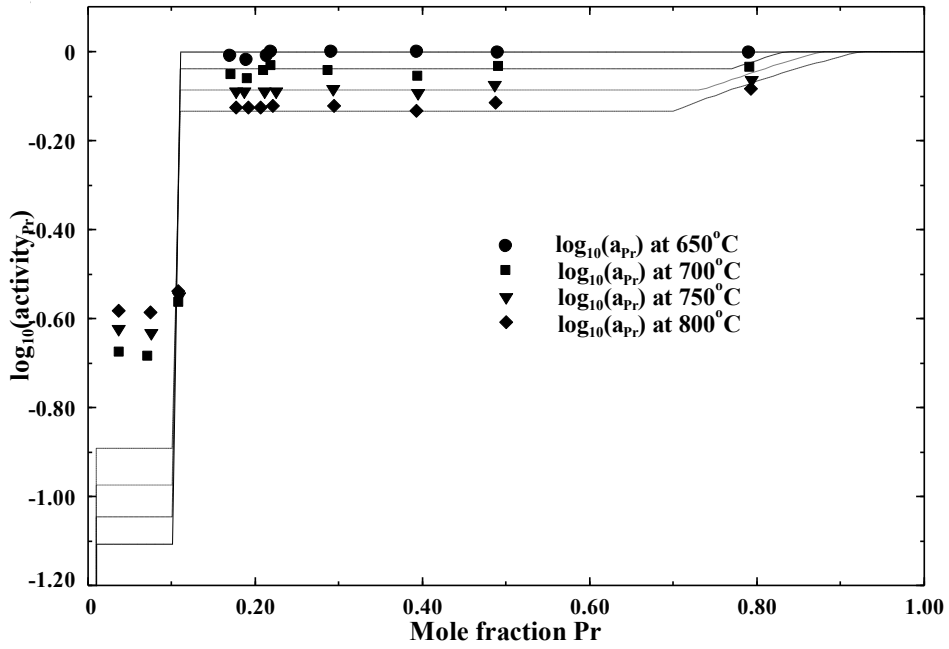

Fig. 3.3.4. Activity of praseodymium Pr-Fe alloys.

3.4. The Fe-Nd(Iron Neodymium) system

The Fe-Nd system was assessed by Zhang *et al.* [1], Okamoto [2] and Marazza *et al.* [3]. The first assessment by Zhang [1] reported only one intermetallic compound Nd_2Fe_{17}, based on the experimental study of Schneider [4]. Landgraf [5] discovered another stable phase of the Fe-Nd system, the intermetallic compound Nd_5Fe_{17}. The assessment of [2] and [3] included the new intermetallic compound.

3.4.2. Phase diagram data

Phase relations in the Fe-Nd system were experimentally determined by Terekhova *et al.* [6] using thermal analysis and XRD, Che *et al.* [7] with XRD and DTA, Schneider *et al.* [8] by metallography XRD and DTA, Faudot *et al.* [9], Landgraf *et al.* [5] and Hennemann *et al.* [13] using DTA. The experimental phase diagram data are given in Fig. 3.4.1.

Solubility of Nd in bcc Fe were measured by He *et al.* [10] and Wang *et al.* [11] using the positron annihilation technique, Zhang *et al.* [12] with the aid of XRD lattice parameter measurements and EPMA, Hennemann *et al.* [13] using XRD lattice parameter measurements and Li and Xing [14] using EPMA. The experimental data are plotted in Fig. 3.4.2. The solid solutions of Nd in bcc and fcc Fe are modeled using the Compound Energy Formalism, where the first sublattice contains the substitutional species (Fe and Nd), and the second sublattice contains interstitials (vacancies). As no data were available regarding the solubility of Nd in fcc Fe, the same model parameters as for the bcc solid solution were used.

3.4.2. Thermodynamic data

The only experimental data on the heat capacity were reported by Aune and Seetharaman [15] for the compound Nd_2Fe_{17} by means of the DSC. However, insufficient information was given to convert their data into SI units. The heat capacity function for Nd_5Fe_{17} and Nd_2Fe_{17} were, therefore, determined based on the heat capacity functions of the constituents Fe and Nd.

The standard Gibbs energy of formation of Nd_2Fe_{17} was determined between 973 and 1073 K by Hennemann *et al.* [13] and between 966 and 1022 K by Xi and Ji [16] from EMF measurements (galvanic cells using CaF_2 as a solid electrolyte). More recently, Gozzi *et al.* [17] evaluated the standard Gibbs energy of formation of Nd_2Fe_{17} using the same type of galvanic cell. The optimized heat capacity of the Nd_2Fe_{17} compound (obtained using the heat capacity functions of the elemental constituents Fe and Nd) was decreased by 27 J mol^{-1} K^{-1} in order to fit the experimental data on the Gibbs energy of formation and to have the compound stable at room temperature. Henneman *et al.* [13] also determined the standard Gibbs energy of formation of Nd_5Fe_{17} between 973 and 1073 K by EMF measurements in the (Nd_2Fe_{17} + Nd_5Fe_{17}) two-phase field and using the standard Gibbs energy of formation of Nd_2Fe_{17}. The experimental data and optimized functions for the Gibbs energy functions of the compounds Nd_2Fe_{17} and Nd_5Fe_{17} are shown in Fig. 3.4.3 and Fig. 3.4.4, respectively. The calculated chemical potential of Nd is compared with the experimental data of Hennemann *et al.* [13] in Fig. 3.4.5.

Experimental data on liquid were not found in literature. The thermodynamic optimization of the Fe-Nd system was performed using the Gibbs energy of formation of the intermetallic compounds Nd_2Fe_{17} and Nd_2Fe_{17} and the critically assessed phase diagram data. The optimized values for the model parameters are listed in Table 3.4.1. The phase diagrams and other thermodynamic properties calculated with the optimized set of model parameters are shown in Figs. 3.4.1 to 3.4.5 and compared with experimental data. The calculated curves are in good agreement with the measured values.

3.4.3. Magnetic Data

The magnetic properties of the intermetallic compound Nd_2Fe_{17} were taken from the thermodynamic optimization by Hennemann *et al.* [13].

3.4.4. References

1. Zhang, W., G. Liu and K. Han, J. Phase Equilib., **13**, 645-648 (1992).
2. Okamoto, H., J. Phase Equilib., **18**, 106 (1997).
3. Marazza, R., P. Riani and G. Cacciamani, Inorg. Chim. Acta, **361**, 3800-3806 (2008).
4. Schneider, G., E. T. Henig, G. Petzow and H. H. Stadelmaier, Z. Metallkde, **78**, 694-696 (1987).
5. Landgraf, F. J. G., G. S. Schneider, V. Villas-Boas and F. P. Missel, J. Less-Common Met., **163**, 209-218 (1990).
6. Terekhova, V. F., E. V. Maslova and Ye. M. Savitskiy, Russian Metall., 50-52 (1965).
7. Che, G., J. Liang and X. Wang, Scientia Sinica series A, **29**, 1172-1185 (1986).
8. Schneider, G., E. T. Henig, G. Petzow and H. H. Stadelmaier, Z. Metallkde, **78**, 694-696 (1987).
9. Faudot, F., M. Harmelin and J. Bigot, Scripta Metall., **23**, 795-798 (1989).
10. He, Y., X. R. Chang, Z. Z. Tian, C. M. Hsiao, M. H. Wang, H. B. Lu, Y. Y. Wang and N. Q. Liu, Scripta Metall., **19**, 79-82 (1985).
11. Wang, Y. Y., N. Q. Liu, Z. Z. Tian and X. R. Chang, Acta Metall. Sinica, **23**, B149-B151 (1987).
12. Zhang, F., L. Gu, L. Qu, W. Liu and Y. Yan, Acta Metall. Sinica, **23**, A503-A506 (1987).
13. Hennemann, K., H. L. Lukas and H. J. Schaller, Z. Metallkde, **84**, 668-674 (1993).
14. Li, L., and Z. Xing, Acta Metall. Sinica, **29**, A136-A141 (1993).
15. Aune R. E., and S. Seetharaman, High Temp. Mater. Proc., **17**, 299-311 (1998).
16. Xi, Z., and C. Ji, Nonferrous Met., **41**, 68-71 (1989).
17. Gozzi, D., M. Iervolino and A. Latini, J. Chem. Eng. Data, **52**, 2350-2358 (2007).

Table 3.4.1. Optimized thermodynamic data of the Fe-Nd system.

Liquid phase (Quasichemical model parameters)			
Coordination numbers: $Z^{Fe}_{FeFe} = Z^{Nd}_{NdNd} = Z^{Nd}_{NdFe} = Z^{Fe}_{FeNd} = 6$ $\Delta g_{FeNd} = 418.4 + 5439.2 X_{FeFe}$ J mol^{-1}			
Solid phases			
***ΔH_f°₂₉₈* (kJ mol^{-1})**			
Compound	**Optimized elements as reference**	**Experimental elements as reference**	**Reference**
Nd_2Fe_{17}	10.0	-	
Nd_5Fe_{17}	11.5	-	
***S°₂₉₈* (J mol^{-1} K^{-1})**			
Compound	***S°₂₉₈* Optimized**	***S°₂₉₈* Experimental**	**Reference**
Nd_2Fe_{17}	669.5	-	
Nd_5Fe_{17}	893.5	-	
***C_p* (J mol^{-1} K^{-1})**			
Compound	**Optimized**		**Reference**
Nd_2Fe_{17} 298-2000 K	480 + 0.14729118 T + 3.8318154 10^{-5} T^2 - 2769754 T^{-2}		2 Cp(Nd) + 17 Cp(Fe)
Nd_5Fe_{17} 298-2000 K	561.2574 + 0.14395443 T + 8.6779554 10^{-5} T^2 - 2979076 T^{-2}		5 Cp(Nd) + 17 Cp(Fe)
Magnetic properties			
Compound	**Magnetic moment**	**Curie Temperature (K)**	**Reference**
Nd_2Fe_{17}	43.7	327	[13]
Solid Solution (parameters of the Compound Energy Formalism with two-sublattice			

approach $(\mathrm{Fe,Nd})_1^{\mathrm{I}}(\mathrm{Va})_1^{\mathrm{II}}$ **)**	
FCC	${}^0L_{\mathrm{Fe,Nd}} = 41840$
BCC	${}^0L_{\mathrm{Fe,Nd}} = 41840$

Figures

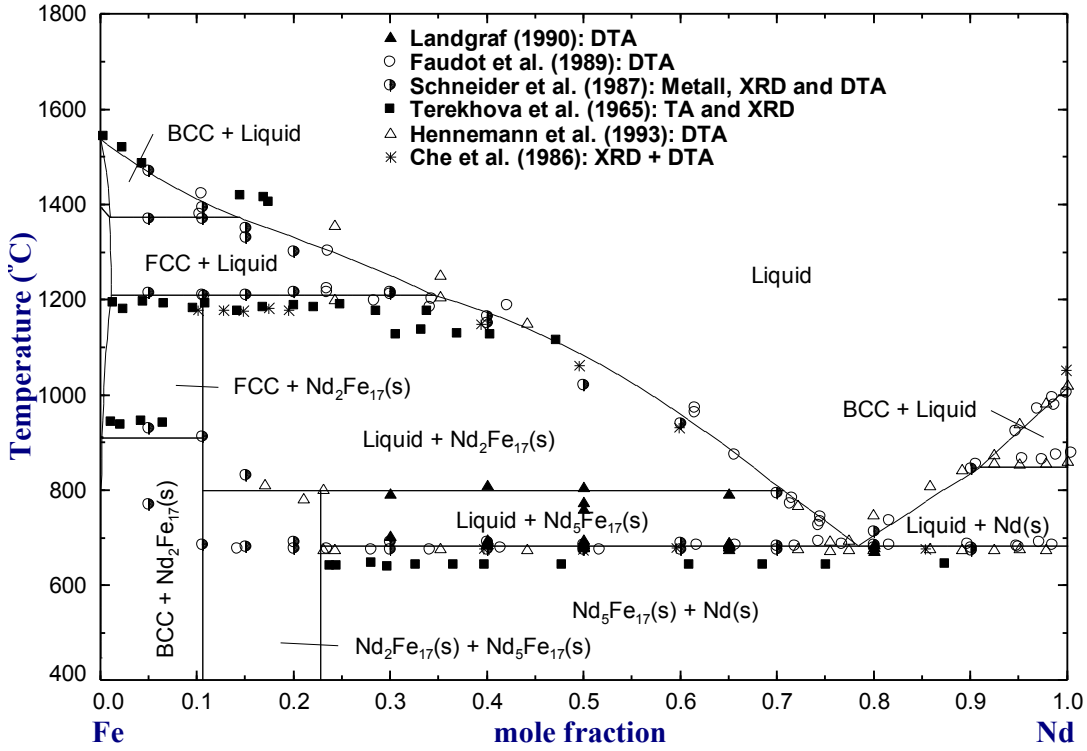

Fig. 3.4.1. The optimized Fe-Nd system.

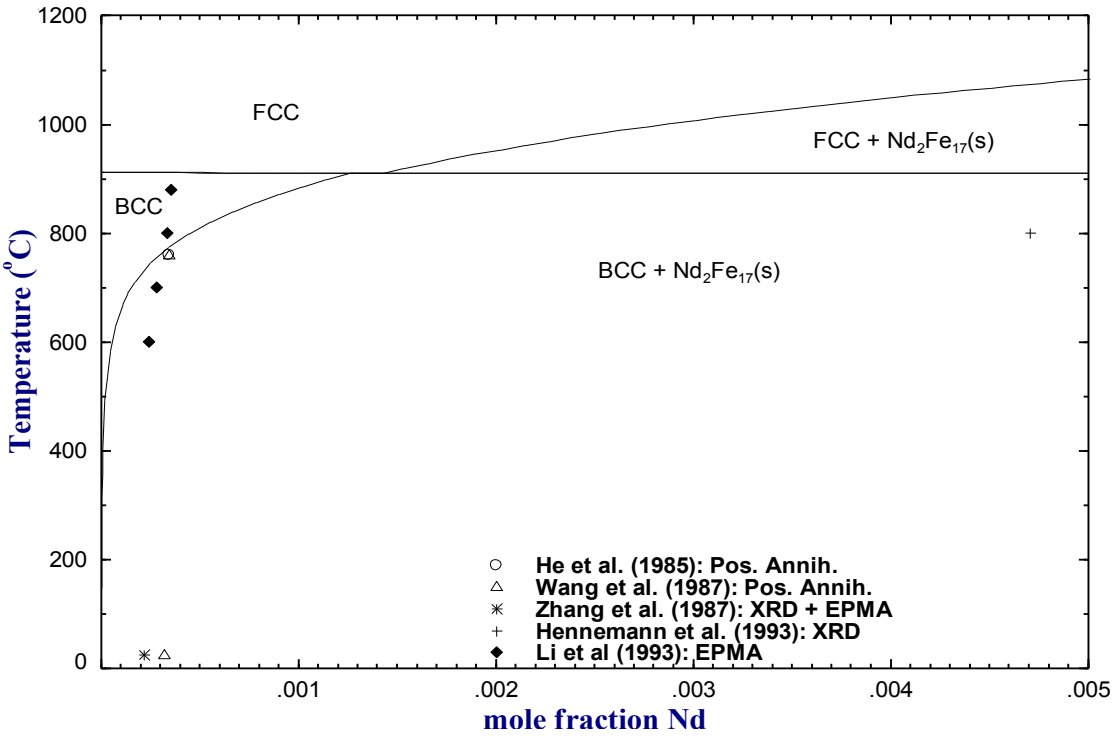

Fig. 3.4.2. Optimized Fe-rich corner of the Fe-Nd phase diagram.

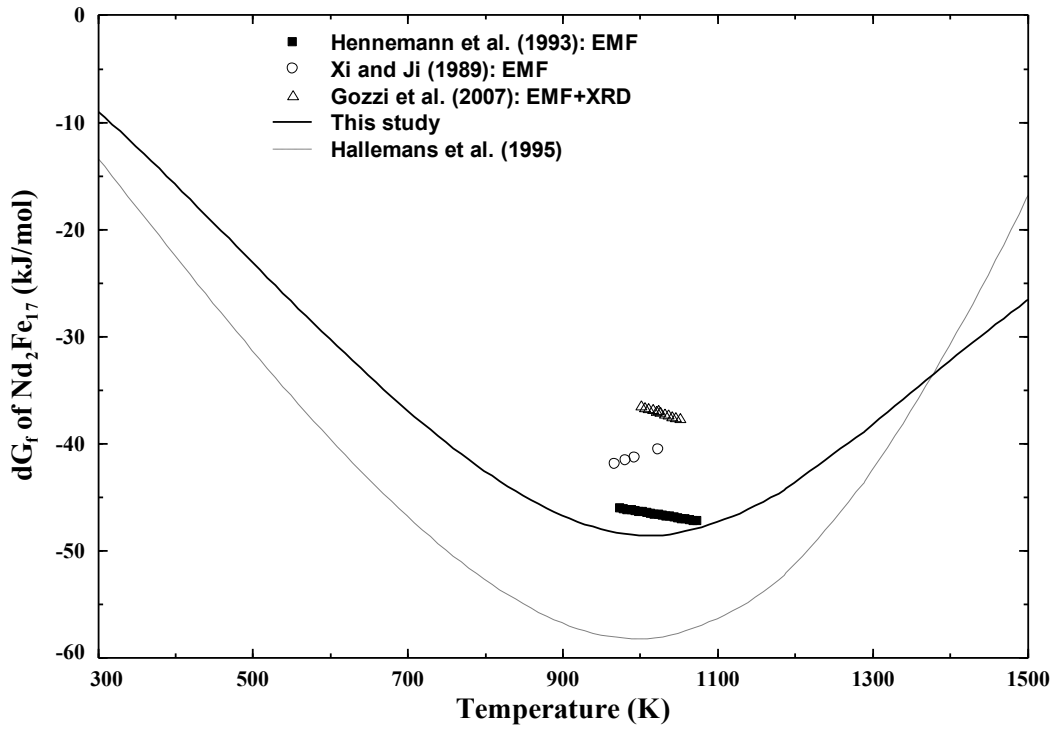

Fig. 3.4.3. Evolution of the Gibbs Energy of formation of Nd_2Fe_{17} with temperature.

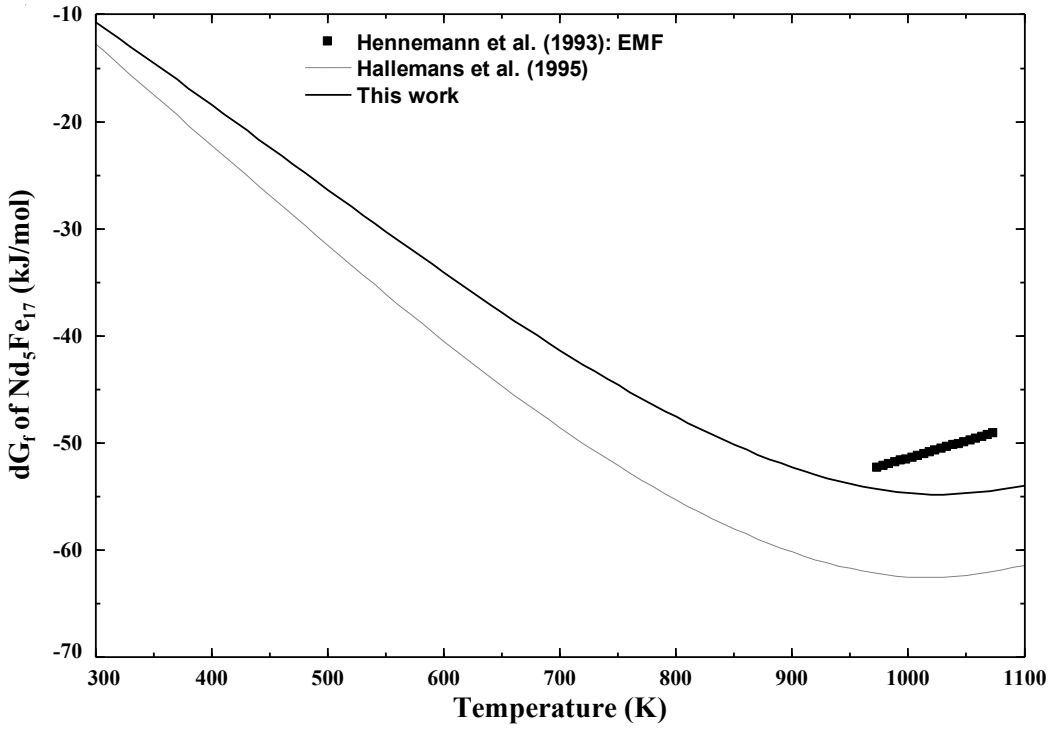

Fig. 3.4.4. Evolution of the Gibbs Energy of formation of Nd_5Fe_{17} with temperature.

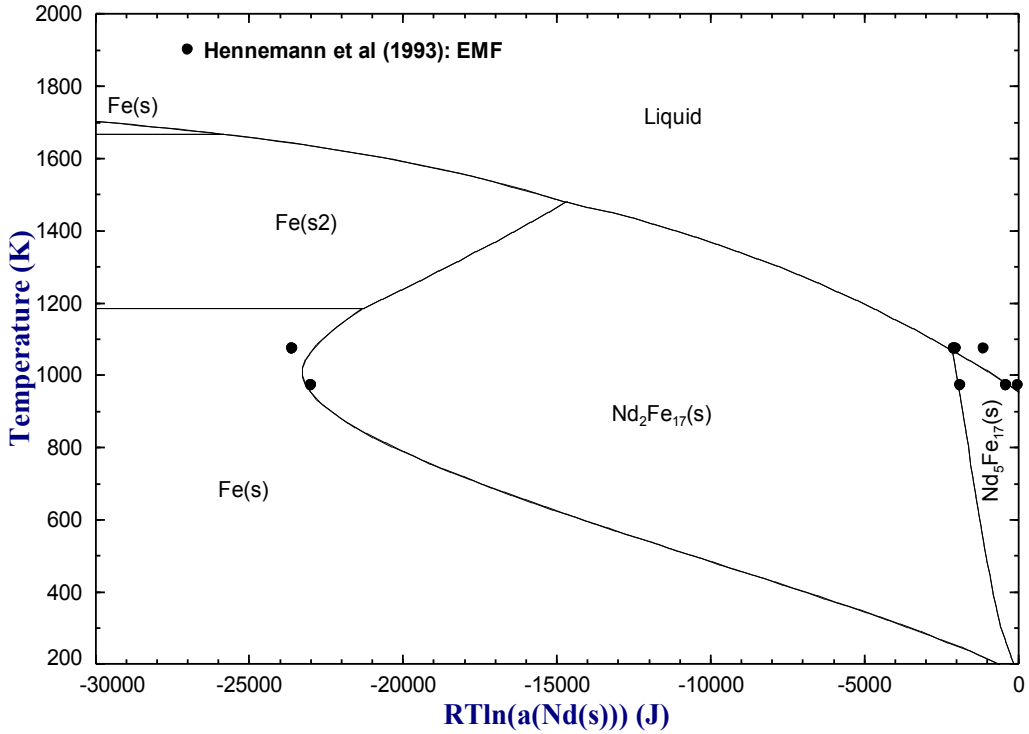

Fig. 3.4.5. Calculated evolution of the chemical potential of Nd with temperature, compared with measured values.

3.5.The Fe-Sm (Iron-Samarium) system

3.5.1. Phase diagram data

The Samarium Iron phase diagram was experimentally investigated by Buschow[1]. He used X-ray diffraction technique, metallography and thermal analysis (with a DTA) to determine the crystal structure of the phases and compounds, the type of invariant reaction, respective temperatures and several points on the liquidus line. There are three stoichiometric intermetallic compounds in the binary system formed by peritectic reactions: Sm_2Fe_{17} [2] (Th_2Zn_{17}-type), $SmFe_3$ [3] ($PuNi_3$-type) and $SmFe_2$ [4, 5]. All the compounds show ferromagnetic behavior. Zinkevich et. al [6] in their assessment did a detailed study about the magnetic characteristic(Magnetic moment and the Curie temperature) of the compounds in the system which are otherwise all ferromagnetic. The $SmFe_7$ and $Sm_{23}Fe_6$ single crystals are prepared by a modified self flux method by Samata et al.[7, 8]. The thermodynamic stability of these phases is not verified by any thermal analysis hence not considered. While studying the ternary Sm-Fe-Ti system by using diffusion triple technique and electron microprobe analysis Liu et al.[9] found only $SmFe_2$, $SmFe_3$ and Sm_2Fe_{17} phases after annealing the Fe Sm sample for 500hrs at 600^{o}C. They also found an appreciable homogeneity range for each of the intermetallic phases which was different as stated by Buschow[1]. The maximum solubility of Sm in α-Fe is very small (0.3at.% or less) and the solubility of Fe in α-Sm was undetectable[6]. Due to lack of experimental details about the Sm solubility in α-Fe it is not considered in the present assessment. Fig. 3.5.1. shows the phase diagram obtained from the current assessment.

3.5.2. Thermodynamic data

For the compounds no enthalpy of formation data is reported by any of the previous experimentation. Zinkevich[6] measured the low temperature heat capacity for the Sm_2Fe_{17} phase by using PPMS quantum Design instrument from 5 to 298K. They also presented a value of S_{298} experimental by integrating the heat capacity curve from 0 to 298.15 K which is 36.6J/mol-K. In our current optimization we found that the error in integration and the standard deviation (5% as reported by Zinkevich) is around 15%, the S298 value used in this current modeling is 31.6J/mol-K.

Berezutskii[10] measured the mixing enthalpies in homogeneous melts of Samarium with Iron system by using high temperature calorimetric methods for the entire composition range. The mixing enthalpy is negative with a minimum for Fe- Sm system at 1556^{o}C to be -4.20±0.93kJ/mol. He reported the partial enthalpies of the samarium and iron in the melt. Fig. 3.5.3. shows the partial enthalpy and integral enthalpy obtained from the current assessment against the experimental data.

3.5.3. Magnetic Data

The magnetic moment for the compounds $SmFe_2$ and $SmFe_3$ are obtained from Buschow's compilation of magnetic data[11]. The magnetic data of $SmFe_3$ as measured by [12] is quite similar to that mentioned by Buschow. While that of $SmFe_2$ the value of Bohr magneton reported by Buschow is close to that of [13] who measured the magnetic properties at room temperature. The magnetic properties for Sm_2Fe_{17} were obtained from [6] assessment and is 1.83(μ_B per mole of atoms) and 394K as the bohr magneton and curie temperature respectively.

Table 3.5.1. Optimized thermodynamic data of the Sm-Fe system.

Liquid phase (Quasichemical model parameters)			
Coordination numbers: $Z^{Fe}_{FeFe} = Z^{\mathrm{Sm}}_{\mathrm{SmSm}} = Z^{\mathrm{Sm}}_{\mathrm{Sm}Fe} = Z^{\mathrm{Sm}}_{\mathrm{FeSm}} = 6$ $\Delta g_{FeSm} = -1337.6 + 6270X_{FeFe}$			
Solid phases			
$\Delta H_f°_{298}$ **(kJ mol^{-1})**			
Compound	**Optimized elements as reference**	**Experimental elements as reference**	**Reference**
$SmFe_2$	-23.6	-	-
$SmFe_3$	-24.8		
Sm_2Fe_{17}	-32.54	-	-
$S°_{298}$ **(J mol^{-1} K^{-1})**			
Compound	$S°_{298}$ **Optimized**	$S°_{298}$ **Experimental**	**Reference**
$SmFe_2$	116	-	-
SmFe3	147	-	-
Sm_2Fe_{17}	620	695.4	[6, 14]

C_p (J mol^{-1} K^{-1})		
Compound	**Optimized**	**Reference**
$SmFe_2$		C_p = $C_p(Sm_{(hcp)})$ + $2C_p(Fe_{(bcc)})$
298-700 K	48.6771+ 0.11809808T -145100T^{-2} +-5.9913576E-5T^2	
700-1190 K	149.6936-0.07731432T-8032976T^{-2} +4.5937422E-5T^2	
1190-1345K	-334.3912202-0.527562756T +79894768T^{-2} - 0.000164365788T^2	
1345-1811K	97.2366+0.01759008T -309436T^{-2}+7.07124E-7T^2	
1811-2100K	142.208-4.132854E33T^{-10}	
$SmFe_3$		
298-700K	72.1914+0.12689312T -299818T^{-2}-5.9560014E-5T^2	C_p = $C_p(Sm_{(hcp)})$ + $3C_p(Fe_{(bcc)})$
700-1190K	173.2079-0.06851928T -8187694T^{-2}+4.6290984E-5T^2	
1190-1345K	-310.8769202+0.536357796T +79740050T^{-2}- 0.000164012226T^2	
1345-1811K	120.7509+0.02638512T -464154T^{-2}+1.060686E-6T^2	
1811-2100K	188.208-6.199281E33T^{-10}	
Sm_2Fe_{17}		
298-700K		
700-1190K	472.0401+0.35053168 T -2301534 T^{-2}-0.000115230846 T^2	C_p = $2C_p(Sm_{(hcp)})$ + $17C_p(Fe_{(bcc)})$ +69
1190-1345K	674.0731-0.04029312 T -18077286 T^{-2} +9.647115E-5 T^2	
1345-1811K	-294.0965404+1.169461032T + 157778202T^{-2} -0.00032413527T^2	
1811-2000K	569.1591+0.14951568T -2630206T^{-2} +6.010554E-6T^2	

Compound	**Magnetic moment**	**Curie Temperature(K)**	**References**
$SmFe_2$	2.68	688	[11]
$SmFe_3$	4.6	650	[12]
Sm_2Fe_{17}	34.2	394	[6]

3.4.4. References

1. Buschow, K.H.J., *The samarium-iron system.* Journal of the Less Common Metals, 1971. **25**(2): p. 131-134.
2. G. Johnson, D.H.W., G.S. Smith and A.E. Ray, *Refinement of a Th_2Zn_{17} Structure.* Acta Crystallogr. Sect. B, 1968. **24**: p. 274-276.
3. Nassau, K., L.V. Cherry, and W.E. Wallace, *Intermetallic compounds between lanthanons and transition metals of the first long period. I. Preparation, existence and structural studies.* Phys. Chem. Solids, 1960. **16**,p. 123-30.
4. Geller, S., J.H.Wernick, Trans. AIME., 1960. **218**.
5. Mansey, R.C., G.V. Raynor, and I.R. Harris, *Rare-earth intermediate phases. V. The cubic Laves phases formed by rare-earth metals with iron and nickel.* J. Less-Common Metals, 1968. **14**,p. 329-36.
6. Zinkevich, M., et al., *Thermodynamics of Fe-Sm, Fe-H, and H-Sm systems and its application to the hydrogen-disproportionation-desorption-recombination (HDDR) process for the system Fe17Sm2-H2.* J. Alloys Compd., 2002. **339**,p. 118-139.
7. Samata, H., et al., *New intermetallic compound found in Sm-Fe system.* Jpn. J. Appl. Phys., Part 2, 1997. **36**,p. L476-L478.
8. Samata, H., et al., *Magnetic properties of Sm6Fe23 crystal.* J. Alloys Compd., 2001. **322**,p. 37-41.
9. Liu, Z. and Z. Jin, *Determination of phase equilibria in the Sm-Fe-Ti system at 600°C.* Zeitschrift fuer Metallkunde/Materials Research and Advanced Techniques, 1997. **88**(2): p. 174-177.
10. Berezutskii, V. and M. Ivanov, *Mixing enthalpies in samarium–transition metal melts.* Powder Metallurgy and Metal Ceramics, 2009. **48**(7): p. 454-461.
11. Buschow, K.H.J., *Intermetallic compounds of rare earth and 3d transition metals.* Rep. Prog. Phys., 1977. **40**,p. 1179-256.
12. Samata, H., et al., *Magnetic properties of SmFe3 single crystal.* Jpn. J. Appl. Phys., Part 1, 1997. **36**,p. 3492-3496.
13. Ishizaka, C., T. Yoneyama, and A. Fukuno, *Magnetic properties and phase transfer of $SmFe_2$ and $SmFe_3$ intermetallic compounds by nitrogenation.* IEEE Trans. Magn., 1993. **29**,p. 2833-5.

14. Kreyssig, A., et al., *Crystallographic phase transition within the magnetically ordered state of Ce_2Fe_{17}.* Phys. Rev. B: Condens. Matter Mater. Phys., 2007. **76**,p. 054421/1-054421/8.

Figures

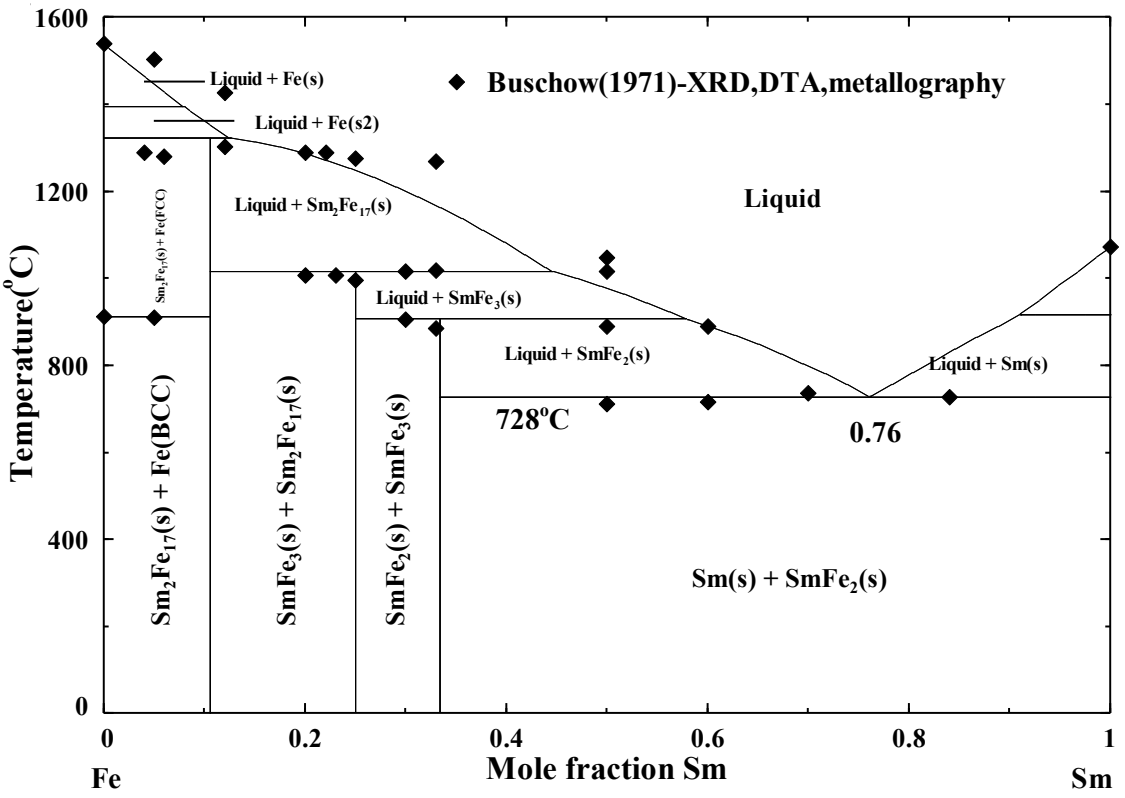

Fig 3.5.1 The optimized Fe-Sm system

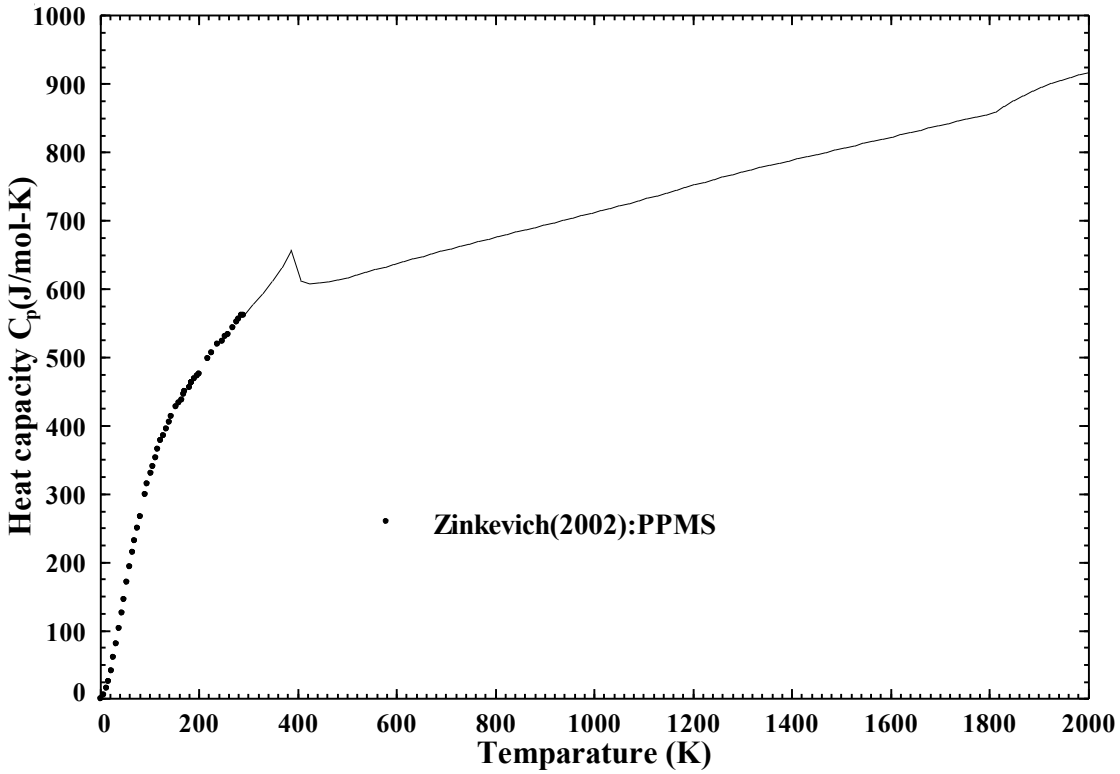

Fig. 3.5.2. Low temperature heat capacity of Sm_2Fe_{17}

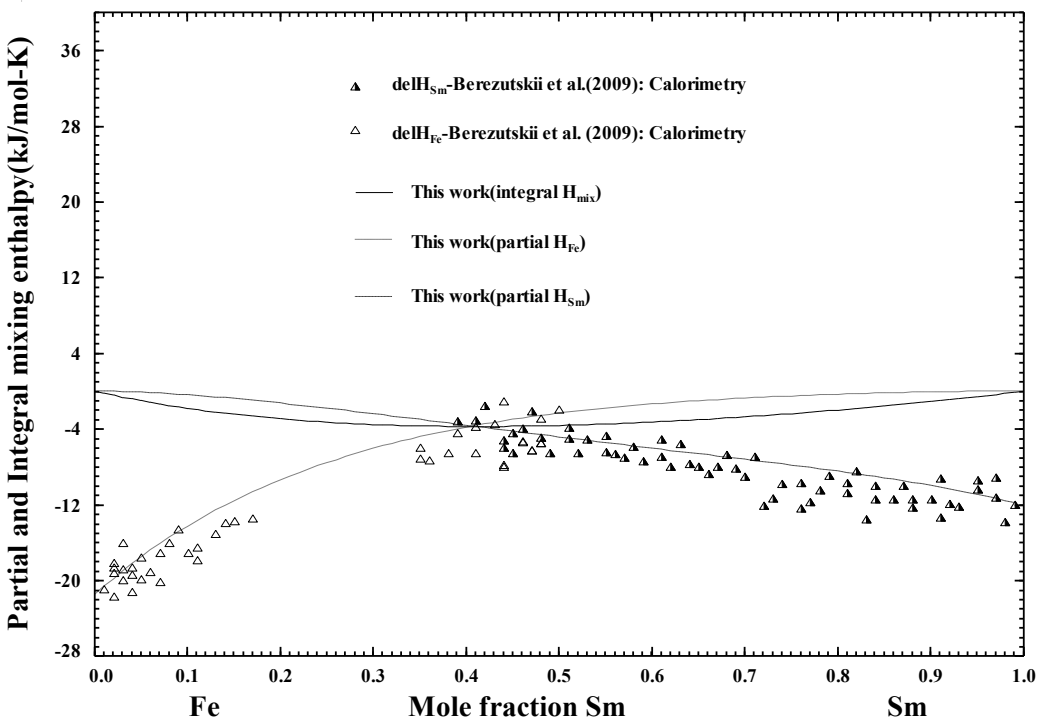

Fig. 3.5.3. Enthalpy of mixing of Fe-Sm alloy at 1829K

3.6. The Fe-Gd (Iron-Gadolinium) system

The binary Fe-Gd system was assessed by Liu et al. [1], Okamoto [2] and Zinkevich et al.[3]. They all reported Fe_2Gd, Fe_3Gd, $Fe_{17}Gd_2$ and $Fe_{23}Gd_6$.

3.6.1. Phase diagram data

The Iron Gadolinium was first investigated by Novy et al[4]. In their work they reported seven intermetallic phases with the following Gd-Fe ratios: 2:3, 1:2, 1:3, 2:7, 1:4, 1:5, and 2:17. The authors stated five invariant reactions. With the help of thermal analysis and melting point determination the eutectic reaction was established to be about 13 wt pct Fe at around 860^{o}C between Gd rich side and Gd_2Fe_3. Peritectic reactions were reported at 2:3, 1:2, 1:3 and 2:7 compounds. The liquidus determination was not complete for the whole range of composition, and only with Iron content in excess of 50 wt. % was predicted. Copeland et al.[5] also investigated the binary system and suggested three intermetallic phases $GdFe_9$, $GdFe_3$ and $GdFe_2$ all of them melting incongruently by peritectic reactions. In the investigation done by Spedding [6] similar phases were reported. Savitski and co-workers [7-9] also studied the Iron Gadolinium system and presented a complete phase diagram.

Savitski [7] reported solubility of gadolinium in iron and that of iron in gadolinium less than or equal to 0.1 at. % Gd(at 800 ^{o}C) and 0.6 at.% Fe at 700 ^{o}C, respectively. At the peritectoid temperature 932±5 ^{o}C the solubility of Gd dissolved in α-Fe and γ-Fe were estimated to be 0.7 and 0.5 at. % respectively. Eventhough the solubility of Gd and Fe at 800 ^{o}C and 700^{o}C was reproduced in the current assessment the peritectoid solubility of Gd seems to be overestimated with respect to current optimization.

Savitski et al. [7] reported two compounds Gd_2Fe_{17} and $GdFe_2$ with peritectic melting along with a eutectic at 12 wt pct.Fe at 830^{o}C between Gd rich side and Gd_2Fe_3. Later in another work [8] they reported four intermetallic phases Gd_2Fe_{17}, $GdFe_4$, $GdFe_3$ and $GdFe_2$ all formed by peritectic reactions. There is a eutectic reaction Liquid → α-Fe + $GdFe_2$, a peritectoid reaction γ-Fe + Gd_2Fe_{17} → α-Fe alongwith a couple of metatectic reactions δ-Fe → Liquid + γ-Fe and β-Fe→Liquid + α-Gd were suggested. Novy[4] presented the phase Fe_4Gd to melt congruently melting while Savitskii proposed a

incongruent melting. In line with the other Iron Rare Earth binary investigations, this phase was suggested by Kubaschewski[10] to have an formula of Gd_6Fe_{23} with an incongruent melting. In all the recent assessments [1-3], four intermetallic compounds, Gd_2Fe_{17}, Gd_6Fe_{23}, $GdFe_3$ and $GdFe_2$ and even in this assessment the same phases were considered. The present work is in agreement with the results of Savitskii et al. but inconsistent with Novy and Copeland's work [5]. Atiq et al. [11] suggested the polymorphic transformation of the Gd_2Fe_{17} phase in rhombohedral(Th_2Zn_{17} type) and hexagonal(Th_2Ni_{17} type) structures. The structural transformation takes place at around 1488±2 K but this is not included in this work. A recent assessment has also been done by Atiq et al. [12]. He also suggested a phase diagram along with some phase diagram points determined by thermal arrests. The phase diagram also points at the Gd_2Fe_{17} polymorphic transformation. As pointed out by Zinkevich[3] Liu's assessment shows deviation from the experimental values of enthalpy of formation without sufficient explanation. Both Zinkevich's and Liu's assessment fails to suggest a phase diagram till the room temperature, so the stability of the intermetallic phases cannot be estimated, where we found that Gd_2Fe_{17} is unstable at room temperature. Along with this the set of Gibb's energy equations presented by Liu was not reproducible to create the phase diagram.

3.6.2. Thermodynamic Data

Colinet et al.[13] [14] measured the enthalpy of formation at room temperature of the three intermetallic phases $GdFe_2$, $GdFe_3$ and Gd_2Fe_{17} by calorimetric method involving dissolution of the compound in molten aluminum. Deodhar et al. [15] also reported the activation energy of Iron Gadolinium compounds with temperature, but their experimental results seems to be inconsistent. The low temperature heat capacity of $GdFe_2$ was taken by the experiment of Germano and Butera [16, 17] , from this the entropy of the intermetallic phase is evaluated.

The intermetallic compounds formed by Fe-Gd were termed as daltonides which means having a non-measurable homogeneity range [7]. The solubility of gadolinium in iron and and that of iron in gadolinium was reported by Copeland, Burov and Savitskii. The

solubility of gadolinium in iron is less than or equal to 0.1 at.% Fe(1073 K)and 0.6 at.% Fe(973 K) respectively as reported by Savitskii[6].

The heat of mixing in the liquid was measured by Nikolaenko and Nosova[18]at 1850K. The enthalpies of formation of Gd_2Fe_{17}, $GdFe_3$ and $GdFe_2$ are taken from the work of Colinet et al.[19].

3.6.3. Magnetic Data

The magnetic properties such as the Bohr magnetons per mole and Curie temperature of the intermetallic phases are taken from the Wallace and Segal[20] which was also referred in the previous assessment by [1].

Table 3.6.1. Optimized thermodynamic data of the Gd-Fe system.

Liquid phase (Quasichemical model parameters)			
Coordination numbers: $Z_{FeFe}^{Fe} = Z_{\mathrm{GdGd}}^{\mathrm{Gd}} = Z_{GdFe}^{\mathrm{Gd}} = Z_{\mathrm{FeGd}}^{\mathrm{Fe}} = 6$ $\Delta g_{FeGd} = -8987 + 5.434T - 3762X_{GdGd}^2 + 3.762TX_{GdGd}^2 + 7106X_{FeFe}^2 - 4.18TX_{FeFe}^2$			
Solid phases			
$\Delta H_f°_{298}$ **(kJ mol^{-1})**			
Compound	**Optimized elements as reference**	**Experimental elements as reference**	**Reference**
$GdFe_2$	-26.7	-34.8±8.7	[14]
$GdFe_3$	-30.4	-37.2±13.6	[14]
Gd_6Fe_{23}	-170.0	-	-
Gd_2Fe_{17}	-47.5	-43.7±3.8	[14]
$S°_{298}$ **(J mol^{-1} K^{-1})**			
Compound	$S°_{298}$ **Optimized**	$S°_{298}$ **Experimental**	**Reference**
$GdFe_2$	109.6	115.596674	[17]
GdFe3	142.4	-	-
Gd_6Fe_{23}	1042.5		-
Gd_2Fe_{17}	641	-	-
C_p **(J mol^{-1} K^{-1})**			
Compound	Optimized		Reference
$GdFe_2$			C_p =
298-1000 K	83.0579031+0.02329489042T -292104.53304T^{-2}+2.595168456E-6T^2		$C_p(Gd_{(hcp)})$ +
1000-1508 K	83.9963197+0.02129458022T-309436T^{-2} +4.674393642E-6T^2		

1508-1811K	161.136687-0.0125387692T +-59023216.6T^{-2} +4.542119688E-6T^2	2C_p(Fe$_{(bcc)}$) +11.31
$GdFe_3$		
298-1000 K	107.5722031+0.03208993042T -446822.53304T^{-2}+2.948730456E-6T^2	C_p = C_p(Gd$_{(hcp)}$) + 3C_p(Fe$_{(bcc)}$) +12.3
1000-1508 K	107.5106197+0.03008962022T -464154T^{-2}+5.027955642E-6T^2	
1508-1811K	161.136687-0.0125387692T -59023216.6T^{-2}+4.542119688E-6T^2	
1811-3600K	206.108087-0.0301288492T -58713780.6T^{-2}+3.834995688E-6T^2-4.132854E33T^{-10}	
Gd_6Fe_{23}		
298-1000 K	763.0047186+0.23651478252T-3454525.19824T^{-2}+1.9460192736E-5T^2	C_p = 6C_p(Gd$_{(hcp)}$) + 23C_p(Fe$_{(bcc)}$)+73.84
1000-1508 K	762.6352182+0.22451292132T -3558514T^{-2}+3.1935543852E-5T^2	
1508-1811K	1225.477422-0.0215128248T -355841197.6T^{-2}+3.1141900128E-5T^2	
1811-3600K	1742.648522-0.1807730952T -352282683.6T^{-2}+2.3009974128E-5T^2-4.7527821E34T^{-10}	
Gd_2Fe_{17}		
298-700K		C_p = 2C_p(Sm$_{(hcp)}$) + 17C_p(Fe$_{(bcc)}$) +24.6158
298-1000 K	473.8017062+0.16092530084T-2595543.06608T^{-2}+9.786642912E-6T^2	
1000-1508 K	473.6785394+0.15692468044T -2630206T^{-2}+1.3945093284E-5T^2	
1508-1811K	627.959274+0.0892579816T -120057767.2T^{-2}+1.3680545376E-5T^2	
1811-3600K	1010.216174-0.0602576984T -117427561.2T^{-2}+7.669991376E-6T^2-3.5129259E34T^{-10}	
Solid Solution (parameters of the Compound Energy Formalism with two-sublattice approach) $(Fe, Gd)_1^I(Va)_1^{II}$		
FCC	$^0L_{Fe,Gd}$ = 44726	
BCC	$^0L_{Fe,Gd}$ = 12.54+20.9T	
HCP	$^0L_{Fe,Gd}$ = 31350+16,72T	

Compound	Magnetic moment	Curie Temperature(K)	References
$GdFe_2$	3.35	782	[20]
$GdFe_3$	1.6	728	[20]
Gd_6Fe_{23}	14.8	468	[20]
Gd_2Fe_{17}	21.2	472	[20]

3.6.4. References

1. Liu, Z.-K., W. Zhang, and B. Sundman, *Thermodynamic assessment of the Co-Fe-Gd systems.* J. Alloys Compd., 1995. **226**,p. 33-45.
2. Okamoto, H., *Fe-Gd (Iron-Gadolinium).* Journal of Phase Equilibria, 1996. **17**(6): p. 552.
3. Zinkevich, M., N. Mattern, and H.J. Seifert, *Reassessment of the Fe-Gd (Iron-Gadolinium) system.* J. Phase Equilib., 2000. **21**,p. 385-394.
4. Novy, V.F., R.C. Vickery, and E.V. Kleber, *The gadolinium-iron system.* Trans. Am. Inst. Min., Metall. Pet. Eng., 1961. **221**,p. 580-5.
5. Copeland, M.I., C.E. Armantrout, and H. Kato, *Iron-Gadolinium Phase Diagram*, in *Report of Investigations*1962, Bureau of Mines, U.S.
6. Spedding, F., A.D., B. Beaudry, I. Haefling, F. Hunter, M. Michel, H. Rider, F. Smidt, R. Valletta and W. Wunderlin, 1963, U.S. Atom. Energy Commun. p. p. C15.
7. Savitskii , E.M., V.F. Terekhova, I.V. Burov, and O.D. Chistyakov, *Equilibrium Diagram for Alloys of the Gadolinium-Iron System.* Russ. J. Inorganic Chem., 1961. **6**(7): p. 883–885.
8. Savistkii, E.M., V.F. Terekhova, R.S. Torchinova, I.A. Markova, O.P. Naumkin, V.E. Kolesnichenko, and V.F. Stroganova. *Etudes des Proprietes physiques et chemiques D'alliages de terres rares*. in *Proc. Conf. Les Elements des Terres Rares*. 1969. Paris-Grenole.
9. Burov, I.V., V.F. Terekhova, and E.M. Savitskii, *Phase diagrams for states containing gadolinium.* Vopr. Teorii i Primeneniya Redkozem. Metal., Akad. Nauk SSSR, 1964,p. 116-23.
10. Kubaschewski, O., *IRON-Binary Phase Diagrams*1982, Berlin: Springer.
11. Atiq, S., R.D. Rawlings, and D.R.F. West, *Crystal structure of compounds iron-gadolinium ($Fe_{17}Gd_2$) and iron-terbium ($Fe_{17}Tb_2$).* Mater. Sci. Technol., 1990. **6**,p. 778-80.
12. Atiq, S., R.D. Rawlings, and D.R.F. West, *The Fe-Gd Phase Diagram.* Pak. J. Sci. Ind. Res., 2005. **48**(4): p. 231-235.
13. Colinet, C. and A. Pasturel, *Electronic structure and enthalpies of formation of gadolinium-nickel-cobalt-iron ($Gd(Ni, Co, Fe)_2$) compounds.* J. Less-Common Met., 1986. **119**,p. 167-74.

14. Colinet, C., A. Pasturel, and K.H.J. Buschow, *Study of the enthalpies of formation in the gadolinium-(iron, cobalt, palladium, platinum) systems.* Metall. Trans. A, 1987. **18A**,p. 903-7.

15. Deodhar, S.S. and P.J. Ficalora, *Reaction kinetics for the formation of rare earth-transition metal Laves compounds.* Metall. Trans., A, 1975. **6A**,p. 1909-14.

16. Germano, D.J., R.A. Butera, and K.A. Gschneidner, Jr., *Heat capacity and thermodynamic functions of the RFe2 compounds (R = gadolinium, terbium, dysprosium, holmium, erbium, thulium, lutetium) over the temperature region 8 to 300 K.* J. Solid State Chem., 1981. **37**,p. 383-9.

17. Germano, D.J. and R.A. Butera, *Heat capacity of, and crystal-field effects in, the RFe2 intermetallic compounds (R = Gd, Tb, Dy, Ho, Er, Tm, and Lu).* Phys. Rev. B: Condens. Matter, 1981. **24**,p. 3912-27.

18. Nikolaenko, I.V. and V.V. Nosova, *Enthalpy of mixing of gadolinium with manganese and iron.* Soviet progress in chemistry, 1989. **55**(12): p. 30-33.

19. Colinet, C. and A. Pasturel, *A data base for enthalpies of formation of transition rare-earth metal alloys.* CALPHAD: Comput. Coupling Phase Diagrams Thermochem., 1987. **11**,p. 323-34.

20. Segal, E., W.E. Wallace., *Rare Earth Intermetallics*. .1973 New York: Academic Press.

Figures

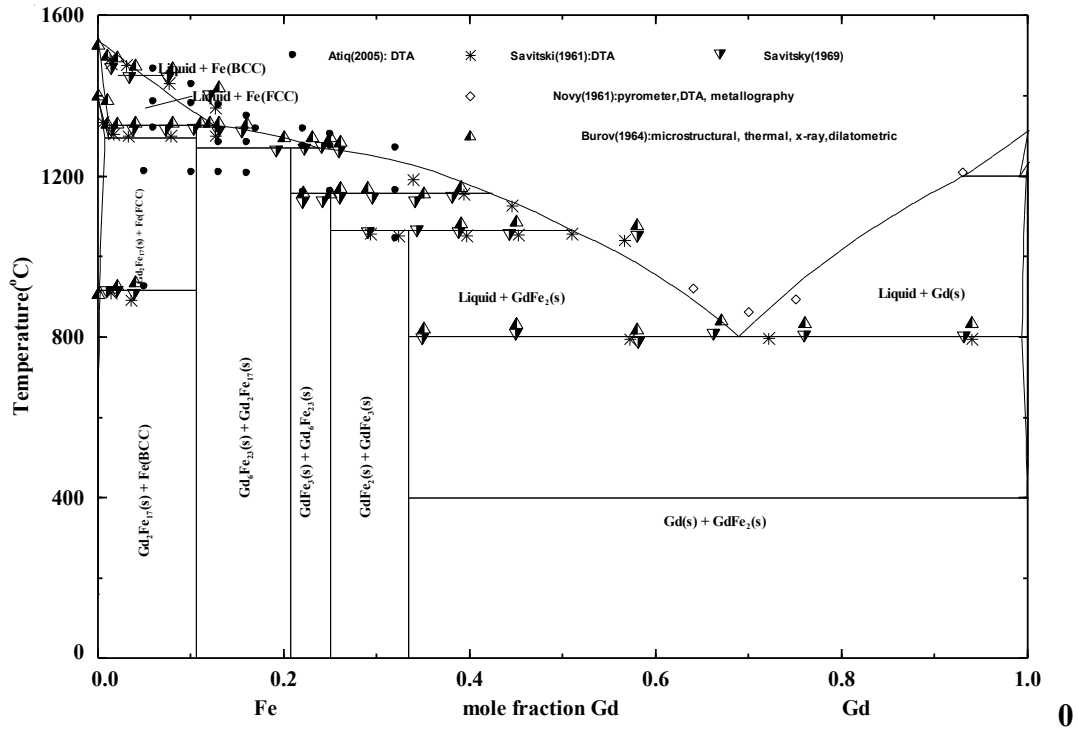

Fig. 3.6.1 The optimized Fe-Gd system.

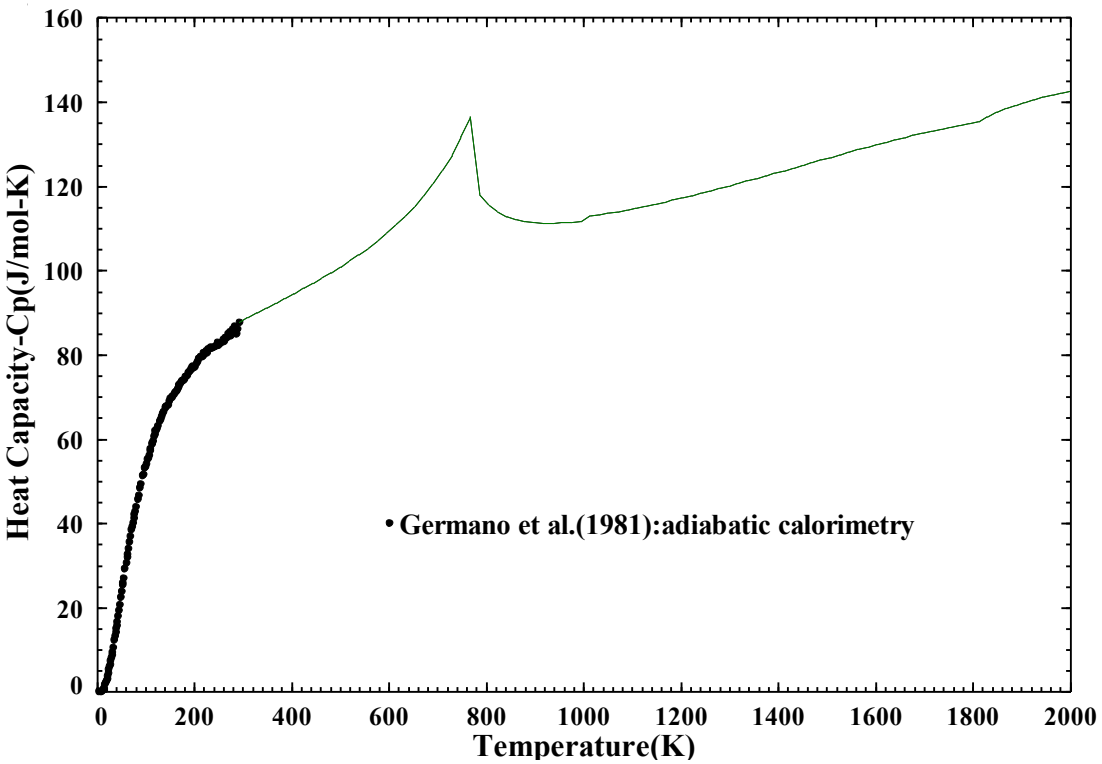

Fig. 3.6.2. Low temperature heat capacity of $GdFe_2$.

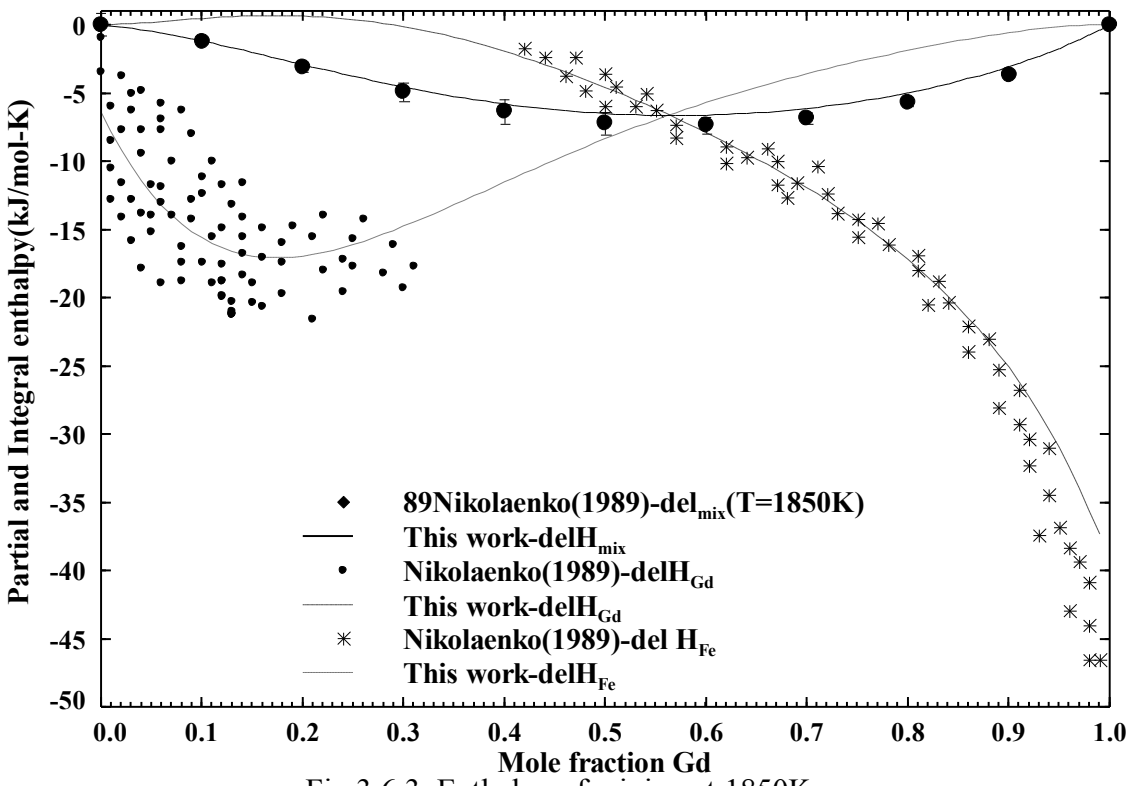

Fig.3.6.3. Enthalpy of mixing at 1850K.

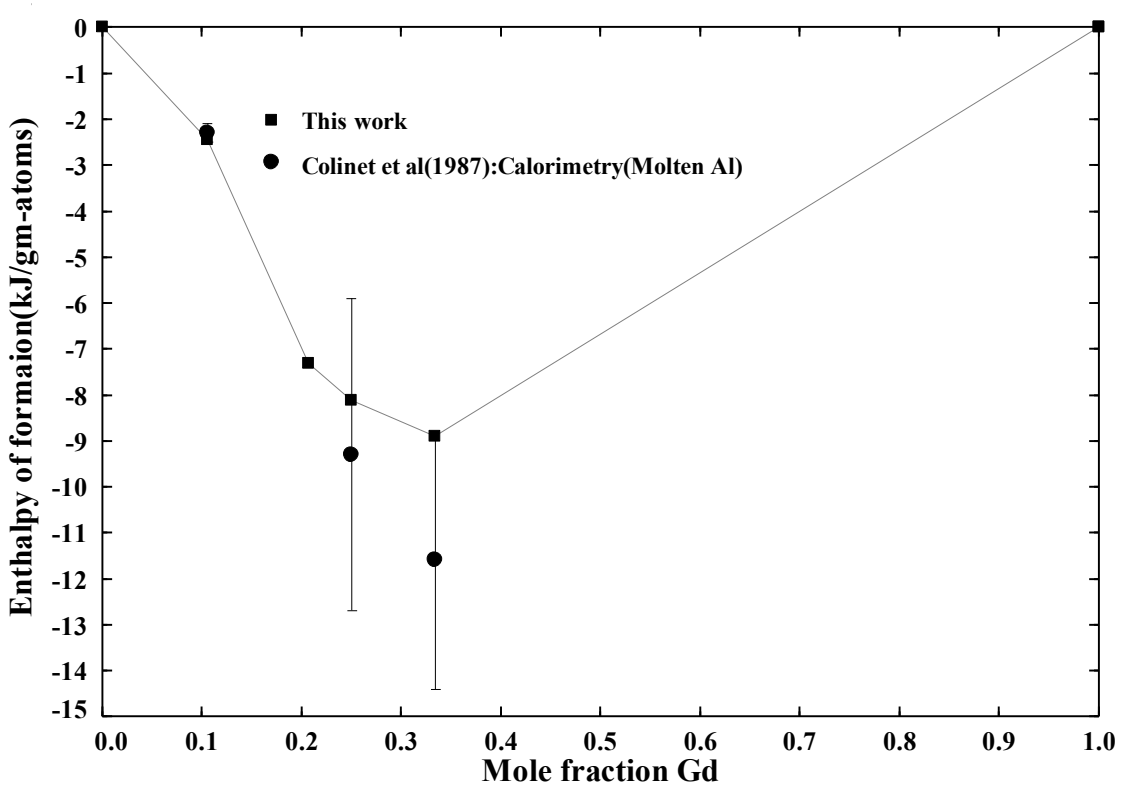

Fig. 3.6.4 Formation Enthalpies of Fe-Gd compounds.

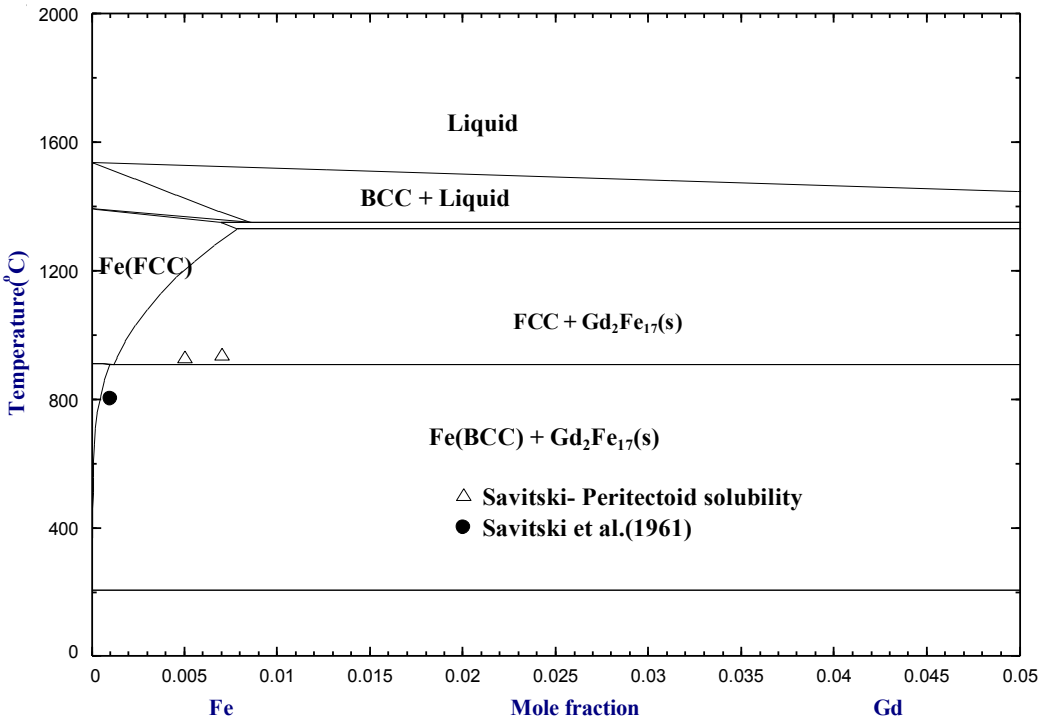

Fig. 3.6.5. Iron-rich side of the Fe-Gd phase diagram.

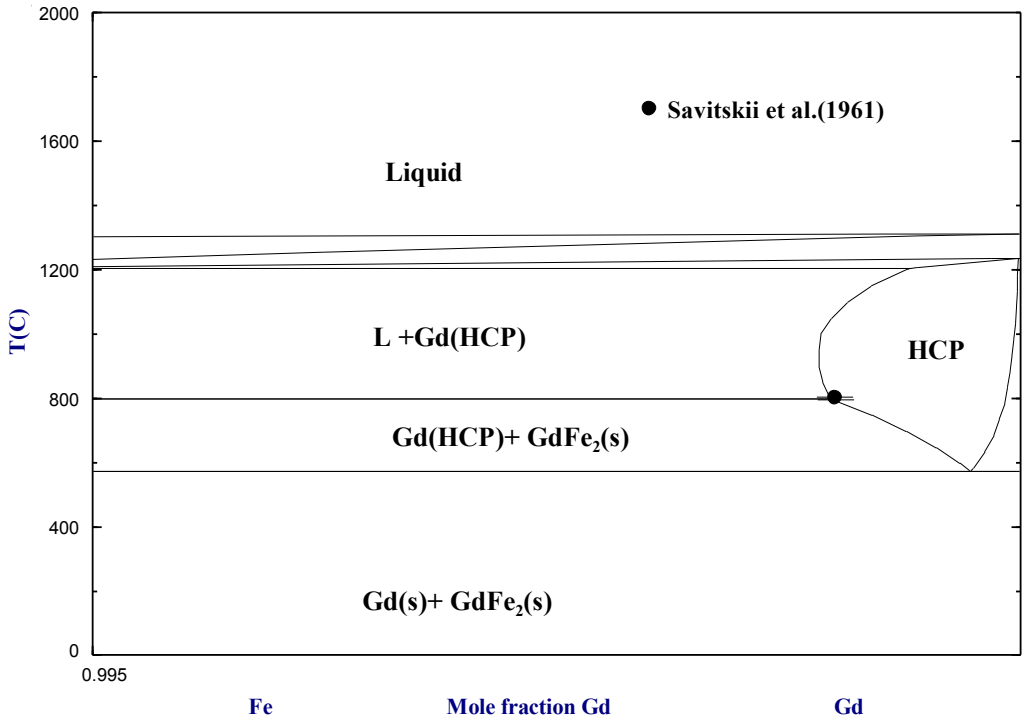

Fig. 3.6.6. Gadolinium-rich side of the Fe-Gd phase diagram.

3.7. The Fe-Tb (Iron Terbium) system

The Iron terbium system was assessed by Susanne et al.[1] and Okamoto[2] . They reported four intermetallic phases $TbFe_2$, $TbFe_3$, Tb_6Fe_{23} and Tb_2Fe_{17}. Even though the laves phase $TbFe_2$ has important magneto-strictive properties this system is not being reviewed much.

3.7.1. Phase Diagram data

The Iron terbium phase diagram was reported by Dariel et al. [3] and Orlova et al.[4]. Both of them reported the four intermetallic compounds which is characteristic of Iron-heavy Rare-Earth alloys. Dariel et al. [3] conducted X-ray analysis, metallography and thermal analysis. Orlova[4] determined the melting point of the compounds with an pyrometer with an error of ±50 K and then the elemental composition of the samples were determined by chemical analysis and neutron activation which also had a reported error of 3%. The phase diagram reported as stated by Okamoto [2] possesses thermodynamically improbable features. Thus the data from their experiments were not used to verify the present assessment. Dariel et al. [3] presented the phase diagram based on metallographic, DTA, X-ray diffraction and electron probe microanalysis techniques. The solubility of Tb in δFe is not reported, but Okamoto [2] hints of some solubility. Dariel et al. [3] reported that the solubility of Tb in α-Fe as 0.07±0.03at. % which was in agreement to his EPMA experiments which suggested solubility of 0.1±0.05 at. %. The current assessment does not include Tb solubility in α-Fe. The Tb_2Fe_{17} has two polymorphic forms: α-Tb_2Fe_{17} (Th_2Zn_{17}-type rhombohedral) and β-Tb_2Fe_{17} (Th_2Ni_{17}-type hexagonal) with some ambiguous behavior as reported by Okamoto [2]. Tb_2Fe_{17} exhibits a peritectic melting at 1312 ^oC[3], Orlova et al. reported a congruent melting at about 1500 ^oC which seems improbable considering the trend of the same compound in other Iron-Rare Earth binary systems. Tb_6Fe_{23} forms peritectically from Tb_2Fe_{17} and Liquid at 1276 ^oC [3]. The room temperature stability of Tb_2Fe_{17} and Tb_6Fe_{23} has been questioned by Okamoto [2] as also stated by Buschow[5], who did X-ray analysis of quenched and annealed samples to get elementary Fe and $TbFe_3$ after decomposition. $TbFe_3$ also have a peritectic melting at 1212^{o}C [3]. $TbFe_2$ and α-Tb reacts eutectically at 847^{o}C as reported by Dariel[3] which is 1050^{o}C by Orlova[4] this could not be reproduced by this work

considering the pyrometer technique to erroneously overestimate the melting temperature. $TbFe_2$ has a peritectic melting point of 1186^oC [3]. It us cubic at high temperatures, however it is distorted to a rhombohedral structure below the curie temperature due to the magnetostriction[6].

3.7.2. Thermodynamic data

Gozzi et al. [7] reported the enthalpy of formation for the Tb_2Fe_{17} phase by using galvanic cells, CaF_2 single crystal serving as the electrolyte. The reported value was found to be very low. Later Meschel et al.[8] in their work related to shape memory alloy calculated the formation enthalpy of the same phase by direct synthesis calorimetry. There reported value has more than cent percent error range. In their tabulation the value referenced as Gozzi et al.'s data [7] is -3.3kJ/g-atom which in the original paper is -1.3kJ/g-atom. Eventually the enthalpy values are approximated very similar to that of Iron-Dysprosium system. The enthalpy of formation of Tb_2Fe_{17} phase lies well within the data reported by Meschel et al. [8]. For the $TbFe_2$ phase Meschel et al. [8] reported enthalpy of formation with almost 50% error, which is found lower than the optimized value in this assessment. The value in the assessment is chosen considering the trend of the other heavy rare earth-Iron alloys with similar stoichiometry. There is no liquid data available for the Iron Terbium binary system. The liquid Gibbs energy data is used similar to Iron-Dysprosium system.

3.7.3. Magnetic data

The four phases $TbFe_2$, $TbFe_3$, Tb_6Fe_{23} and Tb_2Fe_{17} are magnetic in nature. The value of magnetic moment and the Curie temperature are obtained from Buschow [9].

Table 3.7.1. Optimized thermodynamic data of the Tb-Fe system.

Liquid phase (Quasichemical model parameters)			
Coordination numbers: $Z^{Fe}_{FeFe} = Z^{\mathrm{Tb}}_{\mathrm{TbTb}} = Z^{\mathrm{Tb}}_{TbFe} = Z^{\mathrm{Fe}}_{\mathrm{FeTb}} = 6$ $\Delta g_{FeTb} = -2717 - 0.64372T - 2926X_{TbTb} - 5016X_{FeFe}$			
Solid phases			
$\Delta H_f°_{298}$ **(kJ mol^{-1})**			
Compound	**Optimized elements as reference**	**Experimental elements as reference**	**Reference**
$TbFe_2$	-33.30	-16.5±7.2	[8]
$TbFe_3$	-30.79	-	-
Tb_6Fe_{23}	-163.00	-	-
Tb_2Fe_{17}	-41.00	-39.9±58.9	[8]
		-24.7	[7]
$S°_{298}$ **(J mol^{-1} K^{-1})**			
Compound	$S°_{298}$ **Optimized**	$S°_{298}$ **Experimental**	**Reference**
$TbFe_2$	117.5	122.67	[10]
TbFe3	162.8	-	-
Tb_6Fe_{23}	1193	-	-
Tb_2Fe_{17}	701.34	-	-
C_p **(J mol^{-1} K^{-1})**			
Compound	**Optimized**		**Reference**
$TbFe_2$			$C_p = C_p(Tb_{(hcp)}) + 2C_p(Fe_{(bcc)}) + 9.0954$
298-600 K	$133.624668-0.14886292T-1434296T^{-2}+0.000154744122T^2$		
600-1200 K	$81.98996799+0.02310409-654146.000000002T^{-2}+5.54215200000002E-6T^2$		
1200-1562 K	$82.08246799+0.02094275T-309436T^{-2}+7.11291599999999E-6T^2$		
1654-1811K	$256.3397629-0.0656402380000001T-130397016T^{-2}+1.2975306E-5T^2$		
1811-3000K	$301.311163-0.0832303179999998T-130087580T^{-2}+1.2268182E-5T^2-4.132854E33T^{-10}$		
$TbFe_3$			$C_p = C_p(Tb_{(hcp)}) + 3C_p(Fe_{(bcc)})$
298-600 K	$148.0435-0.14006788T-1589014T^{-2}+0.000155097684T^2$		
600-1200 K	$96.4088+0.03189913T-808864T^{-2}+5.895714E-6T^2$		
1200-1562K	$96.5013+0.02973779T-464154T^{-2}+7.466478E-6T^2$		
1562-1811K	$270.7585949-0.056845198T-130551734T^{-2}+1.3328868E-5T^2$		
1811-3000K	$338.2156949-0.083230318T-130087580T^{-2}+1.2268182E-5E-6T^2-6.199281E33T^{-10}$		

Tb_6Fe_{23}		
298-600 K	1005.8325 -0.79643208T-10307674T^{-2}+0.000932353914 T^2	C_p = $6C_p(Tb_{(hcp)})$ + $23C_p(Fe_{(bcc)})$
600-1200 K	696.0243+0.23536998T -5626774T^{-2}+3.7142094E-5T^2	
1200-1562 K	696.5793+0.22240194T -3558514T^{-2}+4.6566678E-5T^2	
1562-1811K	1742.1230694-0.297095988T -784083994T^{-2}+8.1741018E-5T^2	
1811-3000K	2259.2941694-0.499381908T -780525480T^{-2}+7.3609092E-5T^2-4.7527821E34T^{-10}	
Tb_2Fe_{17}		
298-600 K	554.7443-0.18339032 T-4879926 T^{-2}+0.00031408455 T^2	C_p = $2C_p(Tb_{(hcp)})$ + $17C_p(Fe_{(bcc)})$
600-1200K	451.4749+0.1605437T -3319626T^{-2}+1.568061E-5T^2	
1200-1562K	451.6599+0.15622102T -2630206T^{-2}+1.8822138E-5T^2	
1562-1811K	800.1744898-0.016944956T-262805366T^{-2}+3.0546918E-5T^2	
1811-3000K	1182.4313898-0.166460636T -260175160T^{-2}+2.4536364E-5T^2-3.5129259E34T^{-10}	

Compound	Magnetic moment	Curie Temperature(K)	References
$TbFe_2$	4.47	704	[9]
$TbFe_3$	3.13	652	[9]
Tb_6Fe_{23}	14.8	574	[9]
Tb_2Fe_{17}	17.9	408	[9]

3.7.4. Reference

1. Landin, S. and J. Ågren, *Thermodynamic assessment of Fe---Tb and Fe---Dy phase diagrams and prediction of Fe---Tb---Dy phase diagram.* Journal of Alloys and Compounds, 1994. **207-208**: p. 449-453.
2. Okamoto, H., *Fe-Dy (Iron-Dysprosium).* Journal of Phase Equilibria, 1996. **17**(1): p. 80.
3. Dariel, M.P., J.T. Holthuis, and M.R. Pickus, *The terbium-iron phase diagram.* Journal of the Less Common Metals, 1976. **45**(1): p. 91-101.
4. Orlova, I.G., A.A.Eliseev., G.E. Chuprikov and F. Rukk, *The Fe-Tb system.* Russian Journal of Inorganic Chemistry, 1977. **22**(9): p. 1387-1389.
5. Buschow, K.H.J., *Crystal structures of the rare-earth compounds of the form R_2Ni_{17}, R_2Co_{17}, and R_2Fe_{17}.* J. Less-Common Met., 1966. **11**,p. 204-8.
6. Dwight, A.E. and C.W. Kimball, *$TbFe_2$, a rhombohedral Laves phase.* Acta Crystallographica Section B, 1974. **30**(11): p. 2791-2793.
7. Gozzi, D., M. Iervolino, and A. Latini, *Thermodynamics of Fe-rich intermetallics along the rare earth series.* Journal of Chemical and Engineering Data, 2007. **52**(6): p. 2350-2358.
8. Meschel, S.V., J. Pavlu, and P. Nash, *The thermochemical behavior of some binary shape memory alloys by high temperature direct synthesis calorimetry.* Journal of Alloys and Compounds, 2011. **509**(17): p. 5256-5262.
9. Buschow, K.H.J., *Intermetallic compounds of rare earth and 3d transition metals.* Rep. Prog. Phys., 1977. **40**,p. 1179-256.
10. Germano, D.J. and R.A. Butera, *Heat capacity of, and crystal-field effects in, the RFe2 intermetallic compounds (R = Gd, Tb, Dy, Ho, Er, Tm, and Lu).* Phys. Rev. B: Condens. Matter, 1981. **24**,p. 3912-27.

Figures

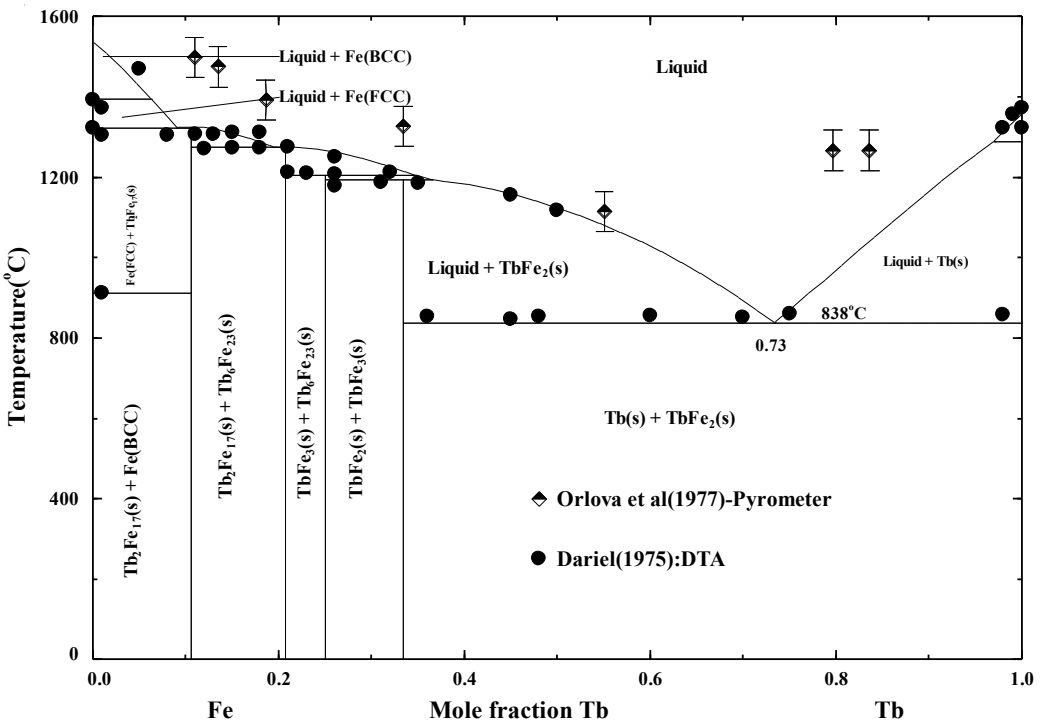

Fig 3.7.1. The optimized Fe-Tb system

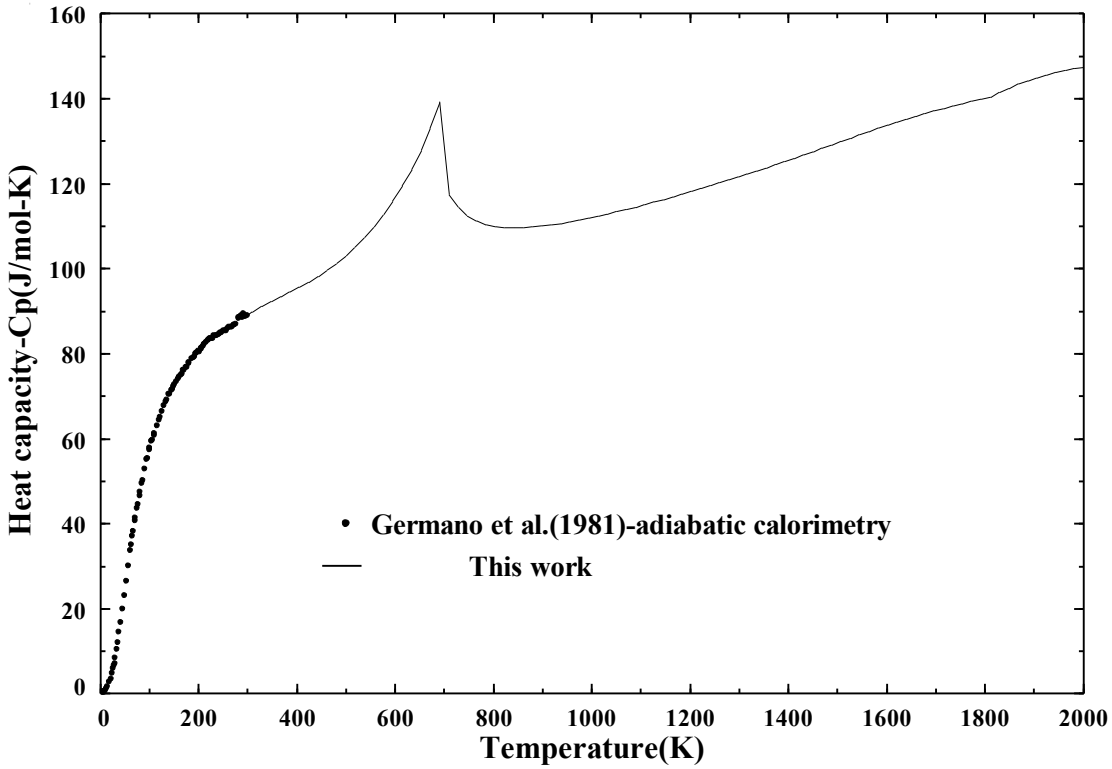

Fig.3.7.2. Low temperature heat capacity of $TbFe_2$

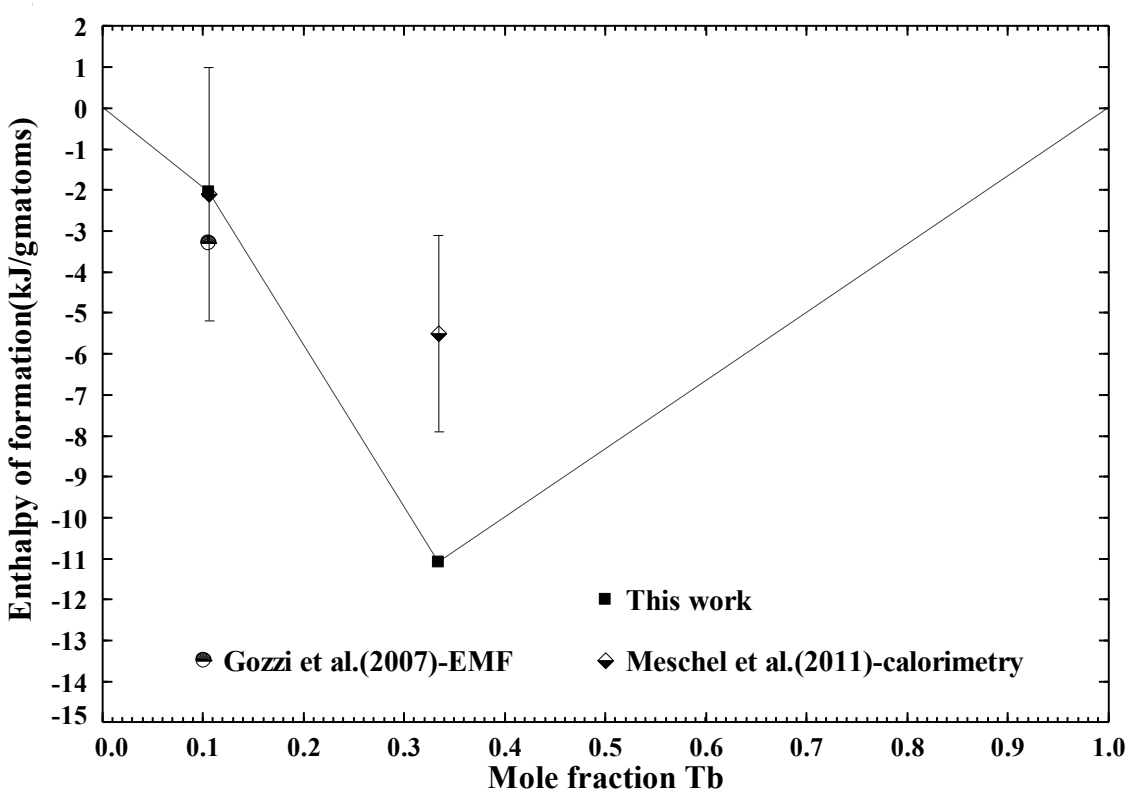

Fig. 3.7.3 Formation Enthalpies of Fe-Tb compounds

3.8. The Fe-Dy (Iron Dysprosium) system

Thermodynamic assessment of Fe-Dy system was conducted by Landin et al. [1] and Okamoto [2]. In both of this review the four compounds were suggested $DyFe_2$, $DyFe_3$, Dy_6Fe_{23} and Dy_2Fe_{17}.

3.8.1. Phase diagram data

The Fe-Dy system was investigated by Van der Goot et al.[3] over the whole composition range by means of X-ray diffraction, thermoanalysis and metallography. According to VanderGoot et al. [3] $DyFe_2$ is the phase with highest Dysprosium concentration has a cubic $MgCu_2$ structure, the compound with 75% Fe is $DyFe_3$ with a rhombohedral $PuNi_3$ type of structure, the Dy_6Fe_{23} phase has cubic Th_6Mn_{23}-type of structure and the iron rich intermetallic phase is Dy_2Fe_{17} has a hexagonal Th_2Ni_{17} type of crystal structure. Based on the experimental micrographs Vandergoot [3] suggested congruent melting for $DyFe_3$ and Dy_2Fe_{17} and $DyFe_2$ and Dy_6Fe_{23} melt peritectically. Susanne et al. [1] in their assessment suggested that the formation of Dy_6Fe_{23} is by a peritectoid reaction rather than a peritectic reaction. Susanne also reported that in order to have a eutectic or peritectic reaction the liquidus curve would be very un-symmetric and such liquid behavior is thermodynamically improbable.

3.8.2. Thermodynamic data

The enthalpy of formation of the $DyFe_2$, $DyFe_3$ and Dy_2Fe_{17} was measured by Norgren et al. [4] by indirect solution calorimetry in liquid aluminum at 1100 K. The $\Delta H_f^\circ{}_{298}$ (kJ mol^{-1}) for $Dy_{1/3}Fe_{2/3}$, $Dy_{1/4}Fe_{3/4}$ and $Dy_{2/19}Fe_{17/19}$ to be -11.1, -7.7 and -1.9 respectively. In Fig. 3.8.2. the enthalpy of formation by current assessment along with Norgren's result[4], and Colinet's band calculation and Miedema's method, are presented. Recently Gozzi et al. [5] and Meschel et al. [6] have also reported enthalpy of formation of Dy_2Fe_{17} and $DyFe_2$ by EMF and direct synthesis calorimetry which do not follow the trend exhibited by the other heavy rare earth-Iron compounds, thus are not reproduced in this assessment. The enthalpy of formation data available in literature are presented with the present assessment values in Fig. 3.8.3. The entropy[S°_{298} (J mol^{-1} K^{-1})] of $DyFe_2$ was derived by integrating the low temperature heat capacity data. The present assessment

agrees well with the experimental data available for the compounds. No experimental data have been reported in the literature to determine the Gibbs energy for the liquid.

3.8.3. Magnetic data

The magnetic properties such as the Bohr magnetons per mole and Curie temperature of the intermetallic phases are taken from the Buschow [7], which are tabulated below.

Table 3.8.1. Optimized thermodynamic data of the Dy-Fe system.

Liquid phase (Quasichemical model parameters)			
Coordination numbers: $Z_{FeFe}^{Fe} = Z_{\mathrm{DyDy}}^{\mathrm{Dy}} = Z_{DyFe}^{\mathrm{Dy}} = Z_{\mathrm{FeDy}}^{\mathrm{Fe}} = 6$ $\Delta g_{FeDy} = -2926 - 0.627T - 5016X_{FeFe} - 2926X_{DyDy} - 1254X_{FeFe}^{3}$			
Solid phases			
$\Delta H_f°_{298}$ **(kJ mol^{-1})**			
Compound	**Optimized elements as reference**	**Experimental elements as reference**	**Reference**
$DyFe_2$	-33.30	-33.3±4.2	[4]
		-4.8±8.7	[6]
$DyFe_3$	-30.78	-30.8±5.2	[4]
Dy_6Fe_{23}	-163.5755	-	-
Dy_2Fe_{17}	-38.9028	-36.1±26.6	[4]
		-100.7±32.3	[6]
		-87.4	[5]
$S°_{298}$ **(J mol^{-1} K^{-1})**			
Compound	$S°_{298}$ **Optimized**	$S°_{298}$ **Experimental**	**Reference**
$DyFe_2$	118.6	124.792289	[8]
DyFe3	166.584	-	-
Dy_6Fe_{23}	1212.05		-
Dy_2Fe_{17}	715.44	-	-
C_p **(J mol^{-1} K^{-1})**			
Compound	**Optimized**		**Reference**
$DyFe_2$			C_p = $C_p(Dy_{(hcp)})$ + $2C_p(Fe_{(bcc)})$ +10.8
298-1000 K	84.2203167+0.019113447314T -317457.8113T^{-2}+4.22860875E-6T^2		
1000-1654 K	101.6569359-0.01579188024T-309436.034723975T^{-2} +2.168929416E-5T^2		
1654-1811K	329.952552-0.0980702562T -219541912T^{-2}+1.727727288E-5T^2		

1811-3000K	374.923952-0.1156603362T -219232476T^{-2}+1.657014888E-5T^2-4.132854E33T^{-10}	
$DyFe_3$		
298-1000 K	96.9346167+0.027908487314T -472175.8113T^{-2}+4.58217075E-6T^2	$C_p = C_p(Dy_{(hcp)}) + 3C_p(Fe_{(bcc)})$
1000-1654 K	114.3712359-0.00699684024T -464154.034723975T^{-2}+2.204285616E-5T^2	
1654-1811K	342.666852-0.0892752162T -219696630T^{-2}+1.763083488E-5T^2	
1811-3000K	206.108087-0.0301288492T -58713780.6T^{-2}+3.834995688E-6T^2-4.132854E33T^{-10}	
Dy_6Fe_{23}		
298-1000 K	699.1792002+0.211426123884T-3606644.8678T^{-2}+2.92608345E-5T^2	$C_p = 6C_p(Dy_{(hcp)}) + 23C_p(Fe_{(bcc)})$
1000-1654 K	803.7989154+0.00199415856000001T -3558514.20834385T^{-2}+0.00013402494696T^2	
1654-1811K	2173.572612-0.4916760972T -1318953370T^{-2}+0.00010755281928T^2	
1811-3000K	2690.743712-0.6939620172T -1315394856T^{-2}+9.942089328E-5T^2-4.7527821E34T^{-10}	
Dy_2Fe_{17} 298-700K		
298-1000 K	452.5265334+0.152562414628T-2646249.6226T^{-2}+1.30535235E-5T^2	$C_p = 2C_p(Dy_{(hcp)}) + 17C_p(Fe_{(bcc)})$
1000-1654 K	487.3997718+0.08275175952T -2630206.06944795T^{-2}+4.797489432E-5T^2	
1654-1811K	943.991004-0.0818049924T -441095158T^{-2}+3.915085176E-5T^2	
1811-3000K	1326.247904-0.2313206724T -438464952T^{-2}+3.314029776E-5T^2-3.5129259E34T^{-10}	

Compound	Magnetic moment	Curie Temperature(K)	References
$DyFe_2$	5.75	635	[7]
$DyFe_3$	3.97	606	[7]
Dy_6Fe_{23}	14.9	534	[7]
Dy_2Fe_{17}	16.1	371	[7]

3.8.4. Reference

1. Landin, S. and J. Ågren, *Thermodynamic assessment of Fe-Tb and Fe-Dy phase diagrams and prediction of Fe-Tb-Dy phase diagram.* Journal of Alloys and Compounds, 1994. **207-208**: p. 449-453.
2. Okamoto, H., *Fe-Dy (Iron-Dysprosium).* Journal of Phase Equilibria, 1996. **17**(1): p. 80.
3. van der Goot, A.S. and K.H.J. Buschow, *The dysprosium-iron system: Structural and magnetic properties of dysprosium-iron compounds.* Journal of the Less Common Metals, 1970. **21**(2): p. 151-157.
4. Norgren, S., et al., *Experimental investigation on the enthalpies of formation of the $DyFe_2$, $DyFe_3$, Dy_2Fe_{17}, $ErFe_2$, and $ErFe_3$ intermetallic compounds.* Metallurgical and Materials Transactions A, 1998. **29**(5): p. 1367-1374.
5. Gozzi, D., M. Iervolino, and A. Latini, *Thermodynamics of Fe-rich intermetallics along the rare earth series.* Journal of Chemical and Engineering Data, 2007. **52**(6): p. 2350-2358.
6. Meschel, S.V., J. Pavlu, and P. Nash, *The thermochemical behavior of some binary shape memory alloys by high temperature direct synthesis calorimetry.* Journal of Alloys and Compounds, 2011. **509**(17): p. 5256-5262.
7. Buschow, K.H.J., *Intermetallic compounds of rare earth and 3d transition metals.* Rep. Prog. Phys., 1977. **40**,p. 1179-256.
8. Germano, D.J. and R.A. Butera, *Heat capacity of, and crystal-field effects in, the RFe_2 intermetallic compounds (R = Gd, Tb, Dy, Ho, Er, Tm, and Lu).* Phys. Rev. B: Condens. Matter, 1981. **24**,p. 3912-27.

Figures

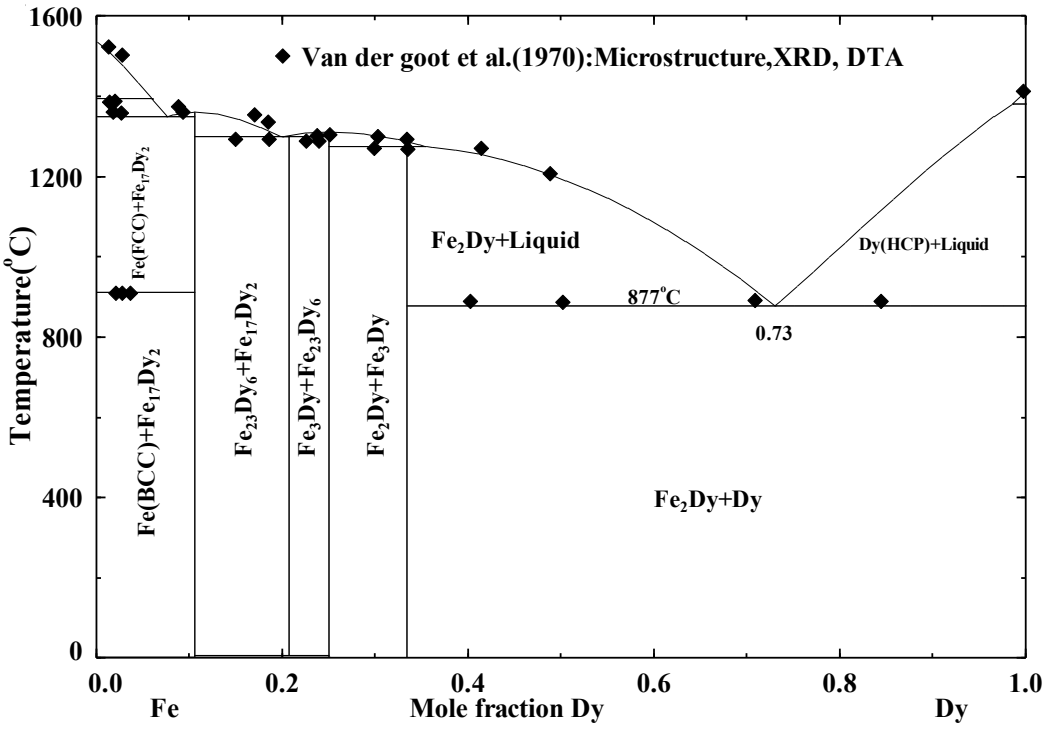

Fig. 3.8.1. The optimized Fe-Dy phase diagram.

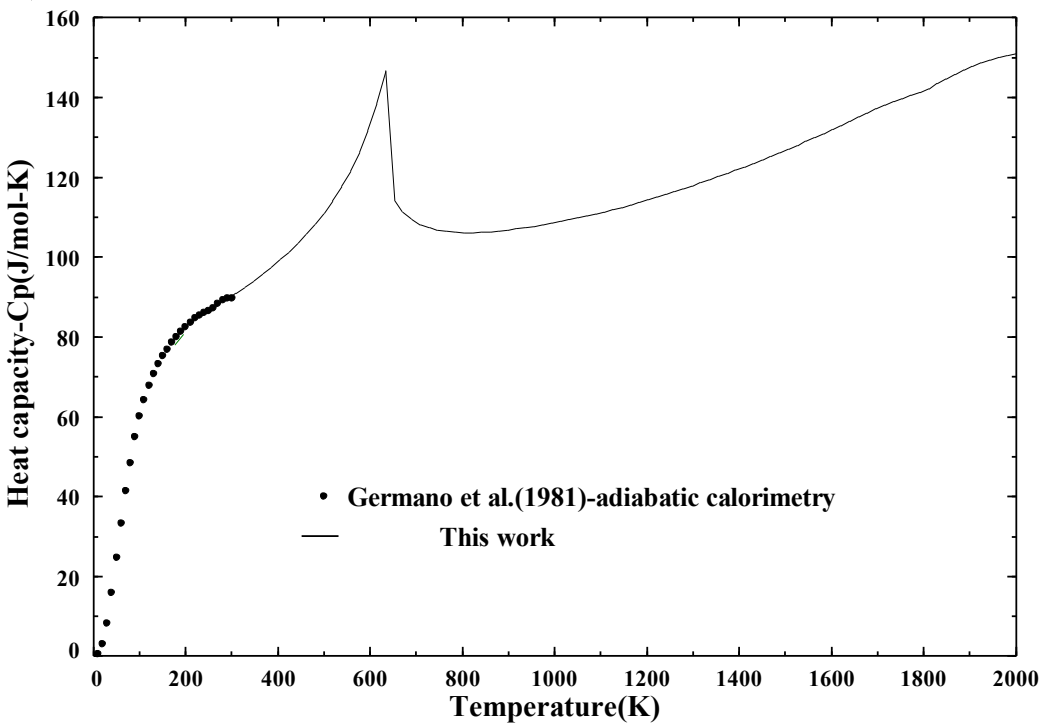

Fig. 3.8.2. Low temperature heat capacity of $DyFe_2$.

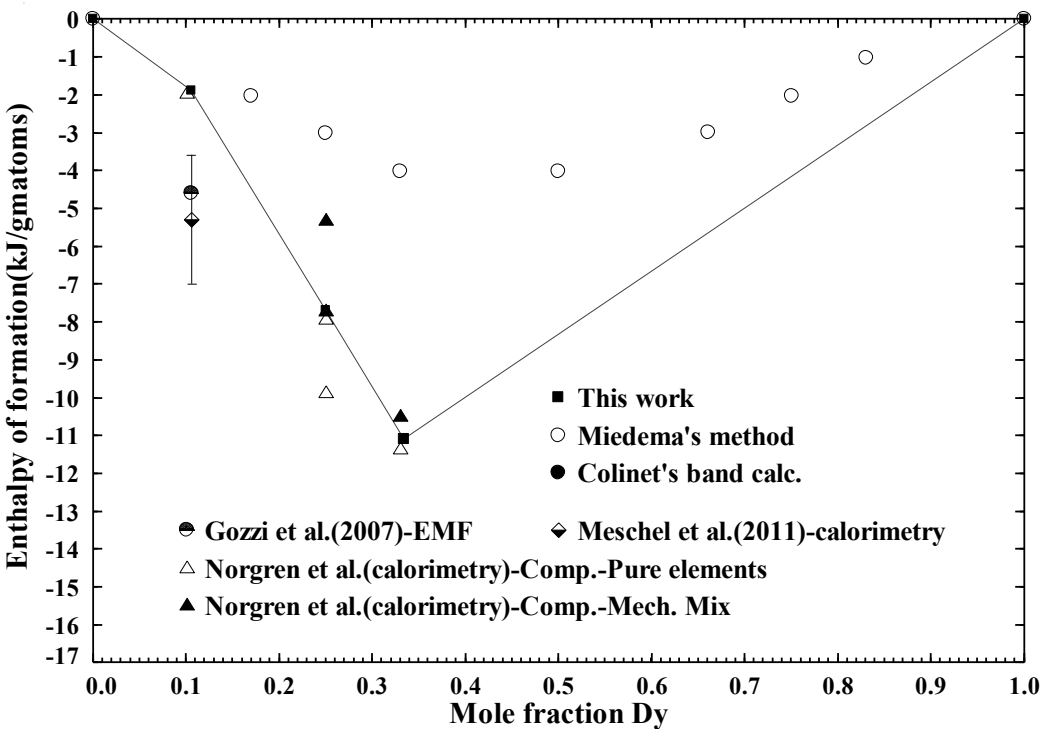

Fig. 3.8.3 Formation Enthalpies of Fe-Dy compounds.

3.9. The Fe-Ho (Iron Holmium) system

The Fe-Ho phase diagram was investigated by Roe et al.[1], and also reported by Kubaschewski[2]. Okamoto [3] also presented the binary phase diagram.

3.9.1. Phase Diagram data

This system was investigated till the eutectic reaction at about 16.5 wt. % Ho by Roe et al.[1] who established the phase diagram by doing X-ray diffraction, metallographic and differential thermal analysis techniques. The reported four intermetallic compounds $HoFe_2$, $HoFe_3$, Ho_6Fe_{23} and Ho_2Fe_{17}. They reported eutectic reactions at 16.5 wt.% Fe at 875^oC between $HoFe_2$ and Ho, 61 wt. pct Fe at 1284^oC Ho_2Fe_{17} and Ho_6Fe_{23} and at 79 wt.% between Fe and Ho_2Fe_{17} with a error of ±3^oC barring the Ho-$HoFe_2$ eutectic reaction. They reported that Ho_6Fe_{23} and Ho_2Fe_{17} melt congruently at 1332^oC and 1343^oC respectively. $HoFe_2$ and $HoFe_3$ have peritectic melting at 1288^oC and 1293^oC, respectively. With X-ray diffraction technique they determined the crystal structure of the intermetallic phases The Ho_6Fe_{23} and the $HoFe_2$ have a cubic crystal structure, Ho_2Fe_{17} and $HoFe_3$ has a hexagonal and rhombohedral crystal structure respectively.

3.9.2. Thermodynamic Data

The low temperature heat capacity measurement for the $HoFe_2$ was done by Germano et al. [4] which was integrated to obtain the S_{298} value. No enthalpy of formation or entropy data for any other intermetallic phases. The enthalpy of formation is estimated considering the experimental data obtained for other Heavy rare earth alloys. The liquid data was kept similar to that of Fe-Dy system which has enthalpy of formation data.

3.9.3. Magnetic data

The magnetic properties such as the Bohr magnetons per mole and Curie temperature of the intermetallic phases are taken from the Buschow [7], which are tabulated below.

Table 3.9.1 Optimized thermodynamic data of the Ho-Fe system.

Liquid phase (Quasichemical model parameters)
Coordination numbers: $Z^{Fe}_{FeFe} = Z^{Ho}_{HoHo} = Z^{Ho}_{HoFe} = Z^{Fe}_{FeHo} = 6$

$\Delta g_{FeHo} = -4180 - 0.418T - 2926X_{HoHo} - 5852X_{FeFe}$			
Solid phases			
$\Delta H_f°_{298}$ (kJ mol^{-1})			
Compound	**Optimized elements as reference**	**Experimental elements as reference**	**Reference**
$HoFe_2$	-33.0028	-	-
$HoFe_3$	-31.448	-	-
Ho_6Fe_{23}	-178.0515	-	-
Ho_2Fe_{17}	-46.55	-	-
$S°_{298}$ (J mol^{-1} K^{-1})			
Compound	**$S°_{298}$ Optimized**	**$S°_{298}$ Experimental**	**Reference**
$HoFe_2$	121.2	127.403431	[5]
HoFe3	166.90	-	-
Ho_6Fe_{23}	1217.07	-	-
Ho_2Fe_{17}	718.31	-	-
C_p (J mol^{-1} K^{-1})			
Compound	**Optimized**		**Reference**
$HoFe_2$			$C_p = C_p(Ho_{(hcp)}) + 2C_p(Fe_{(bcc)}) +10.367$
298-600 K	$80.88+ 0.03413638T -309436T^{-2} -1.3545678E-5T^2$		
600-900 K	$97.09 -0.01881122T -309436T^{-2} + 2.9685522E-5T^2$		
900-1200K	$9.34+ 0.10251688T+ 14062364T^{-2} -1.8691674E-5T^2$		
1200-1703K	$49.11+ 0.03924458T+ 12058264T^{-2}+7.381236E-6T^2$		
1703-1811K	$616.35-0.260633728T-440215382T^{-2}+4.1655036E-5T^2$		
1811-3000K	$661.32-0.278223808T-439905946T^{-2}+4.0947912E-5T^2 - 4.132854E33T^{-10}$		
$HoFe_3$			$C_p = C_p(Ho_{(hcp)}) + 3C_p(Fe_{(bcc)})$
298-600 K	$94.0308+ 0.04293142T -464154T^{-2} -1.3192116E-5T^2$		
600-900 K	$110.2361-0.01001618T+13907646T^{-2} + 3.0039084E-5T^2$		
900-1200K	$22.4834+ 0.11131192T+ 14062364T^{-2}-1.8338112E-5T^2$		
1200-1703K	$62.25682+ 0.04803962T+ 11903546T^{-2}+7.734798E-6T^2$		
1703-1811K	$629.4935818-0.251838688T-440370100T^{-2}+4.2008598E-5T^2$		
1811-3000K	$696.9506818-0.278223808T-439905946T^{-2}+4.0947912E-5T^2 - 6.199281E33T^{-10}$		
Ho_6Fe_{23}			$C_p = 6C_p(Ho_{(hcp)}) + 23C_p(Fe_{(bcc)})$
298-600 K	$681.7563+ 0.30156372T -3558514T^{-2}+0.000182002314T^2$		
600-900 K	$778.9881-0.01612188T -3558514T^{-2}+0.000182002314T^2$		
900-1200 K	$252.4719+ 0.71184672T +70647686T^{-2}-0.000108260862T^2$		
1200-1703K	$491.11242+ 0.33221292T -5257102T^{-2}+ 4.8176598E-5T^2$		
1703-1811 K	$3894.5329908-1.467056928T -2642994190T^{-2}+ 0.000253819398T^2$		

1811-3000K	4411.7040908+-1.669342848T-2639435676T^{-2}+ 0.000245687472T^2 -4.7527821E34T^{-10}	
Ho_2Fe_{17}		
298-600 K	446.7189+ 0.18260828T -2630206T^{-2}+ -2.249505E-5T^2	C_p = $2C_p(Ho_{(hcp)})$ + $17C_p(Fe_{(bcc)})$
600-900K	479.1295+ 0.07671308T -2630206T^{-2}+ 6.396735E-5T^2	
900-1200K	303.6241+ 0.31936928T+ 26113394T^{-2} -3.2787042E-5T^2	
1200-1703K	383.17094+ 0.19282468T +22105194T^{-2}+1.9358778E-5T^2	
1703-1811K	1517.6444636-0.406931936T-882442098T^{-2}+8.7906378E-5T^2	
1811-3000K	1899.9013636-0.556447616T-879811892T^{-2}+8.1895824E-5T^2 -3.5129259E34T^{-10}	

Compound	Magnetic moment	Curie Temperature(K)	References
$HoFe_2$	5.54	608	[6]
$HoFe_3$	4.53	571	[6]
Ho_6Fe_{23}	14.6	530	[6]
Ho_2Fe_{17}	14.8	325	[6]

3.9.4. References

1. Roe, G. and T. O'Keefe, *The Fe–Ho binary system.* Metallurgical and Materials Transactions B, 1970. **1**(9): p. 2565-2568.
2. Kubaschewski, O., *IRON-Binary Phase Diagrams,* 1982, Berlin: Springer.
3. Okamoto, H., *Phase Diagrams of Binary Iron Alloys*. J. Phase Equilib., ed. H. Okamoto, 1993, Materials Park, Ohio: Materials Information Society.
4. Germano, D.J., R.A. Butera, and K.A. Gschneidner, Jr., *Heat capacity and thermodynamic functions of the RFe_2 compounds (R = gadolinium terbium, dysprosium, holmium, erbium, thulium, lutetium) over the temperature region 8 to 300 K.* J. Solid State Chem., 1981. **37**,p. 383-9.
5. Germano, D.J. and R.A. Butera, *Heat capacity of, and crystal-field effects in, the RFe2 intermetallic compounds (R = Gd, Tb, Dy, Ho, Er, Tm, and Lu).* Phys. Rev. B: Condens. Matter, 1981. **24**,p. 3912-27.
6. Buschow, K.H.J., *Intermetallic compounds of rare earth and 3d transition metals.* Rep. Prog. Phys., 1977. **40**,p. 1179-256.

Figures

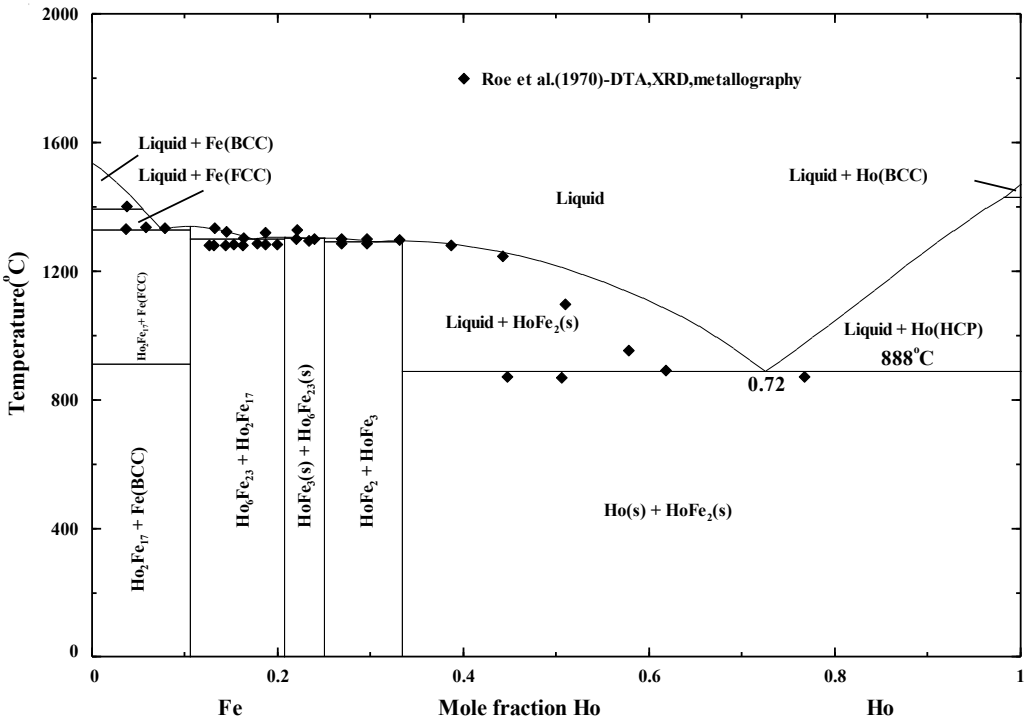

Fig. 3.9.1. The optimized Fe-Ho phase diagram

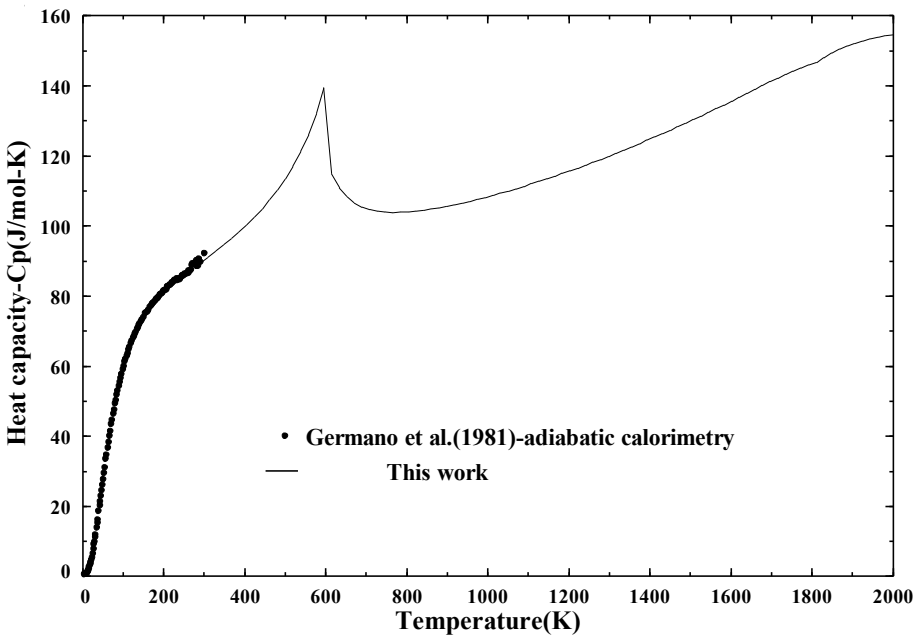

Fig. 3.9.2. Low temperature heat capacity value for Fe_2Ho

3.10.The Fe-Er (Iron-Erbium) system

The phase diagram for this binary system was reported by Buschow [1], Meyer [2] and Koleshnikov [3].

3.10.1.Phase diagram data

Buschow [1] used differential thermal analysis(DTA), X-ray diffraction and microstructure evolution. The Iron Erbium binary system is comprised of four intermetallic compounds. These four stoichiometric compounds $ErFe_2$, $ErFe_3$, Er_6Fe_{23} and Er_2Fe_{17} have $MgCu_2$-type(cubic), Be_3Nb type(hexagonal), Th_6Mn_{23}-type(cubic) and Th_2Ni_{17}-type(hexagonal) compounds. Except $ErFe_2$ which had a congruent melting at 1360 ^oC, $ErFe_3$, Er_6Fe_{23} and $Er_{17}Fe_2$ have peritectic melting at 1345 ^oC, 1330 ^oC and 1355 ^oC respectively. Hence they reported two eutectic and three peritectic reactions in the proposed phase diagram. No significant solubility of the constituent elements was found with x-ray analysis. Although Meyer[2] have reported the same stoichiometric compounds involving similar phase diagram analysis methods of DTA, X-ray analysis and metallographic methods, the melting points of the compounds are significantly lower. As stated by Buschow [1] this is due to the reduction of the crucible material by the molten erbium. This was rectified in their experiments by taking sample amount a order more than that used by Meyer[2]. Kolesnikov [3] also found the melting points similar to that of Buschow's making it more acceptable.

3.10.2. Thermodynamic Data

Norgren et al. [4] conducted indirect solution calorimetry in liquid aluminium at 1100 K in order to determine the enthalpies of formation of compounds Fe_2Er and Fe_3Er. The mean values of $\Delta_f H_{298.15K}$ are -12.5 and -7.9 in kJ/mol of atoms respectively. Gozzi et al. also reported the enthalpy of formation for Er_2Fe_{17}. These values within the error ranges are all well reproduced by the current optimization.

Germano and Butera [5] reported the low temperature heat capacity data obtained by using adiabatic calorimeter system in the temperature range of 15K to 300K with an absolute error of 1%. Due to the increment in error below 15K upto 4.2K the heat

capacity measurements were verified by a pulse calorimeter with similar error of 1%. S_{298} was calculated for the $ErFe_2$ phase with the low temperature heat capacity data.

3.10.3. Magnetic data

All the compounds in Fe-Er binary system are magnetic. The Bohr magneton and Curie point data used to define the magnetic properties of these compounds are obtained from the compilation of magnetic data by Buschow [6].

Table 3.10.1 Optimized thermodynamic data of the Er-Fe system.

Liquid phase (Quasichemical model parameters)			
Coordination numbers: $Z^{Fe}_{FeFe} = Z^{\mathrm{Er}}_{\mathrm{ErEr}} = Z^{\mathrm{Er}}_{ErFe} = Z^{\mathrm{Fe}}_{\mathrm{FeEr}} = 6$ $\Delta g_{FeEr} = -5852 - 8151X_{FeFe} - 1672X^3_{FeFe} - 6688X_{ErEr}$			
Solid phases			
$\Delta H_f°_{298}$ **(kJ mol^{-1})**			
Compound	**Optimized elements as reference**	**Experimental elements as reference**	**Reference**
$ErFe_2$	-33.00	-37.5±4.2	[4]
$ErFe_3$	-33.033	-31.6±5.6	[4]
Er_6Fe_{23}	-178.052	-	-
Er_2Fe_{17}	-41.55	-38	[7]
$S°_{298}$ **(J mol^{-1} K^{-1})**			
Compound	$S°_{298}$ **Optimized**	$S°_{298}$ **Experimental**	**Reference**
$ErFe_2$	128.6	133.79	[5]
ErFe3	165.3	-	-
Er_6Fe_{23}	1209.8		-
Er_2Fe_{17}	723	-	-
C_p **(J mol^{-1} K^{-1})**			
Compound	**Optimized**		**Reference**
$ErFe_2$			$C_p = C_p(Er_{(hcp)}) + 2C_p(Fe_{(bcc)}) +9.0954$
298-1802 K	80.8272744+0.015598496T-328598T^{-2}+6.422466E-6T^2		
1802-1811K	350.5777305-0.114311026T-248255834T^{-2} +1.8955554E-5T^2		
1811-3200K	395.5491305-0.131901106T-247946398T^{-2} +1.824843E-5T^2		

$ErFe_3$ 298-1802 K 1802-1811K 1811-3200K	 148.0435-0.14006788T -1589014T^{-2}+0.000155097684T^2 104.3415744+0.024393536T -483316T^{-2}+6.776028E-6T^2 96.5013+0.02973779T -464154T^{-2}+7.466478E-6T^2	C_p = $C_p(Er_{(hcp)})$ + 3$C_p(Fe_{(bcc)})$
Er_6Fe_{23} 298-1802K 1802-1811 K 1811-3200K	 743.6209464+ 0.190336416T -3673486T^{-2}+ 4.2423978E-5T^2 2362.123683 -0.589120716T -1491236902T^{-2}+ 0.000117622506T^2 2879.294783 -0.791406636T -1487678388T^{-2}+ 0.00010949058T^2- -4.7527821E34T^{-10}	C_p = 6$C_p(Er_{(hcp)})$ + 23$C_p(Fe_{(bcc)})$
Er_2Fe_{17} 298-600 K 1802-1811K 1811-3000K	 467.3404488+ 0.145532512 T -2668530T^{-2}+ 1.7441238E-5T^2 1006.841361 -0.114286532T -498523002T^{-2} +4.2507414E-5T^2 1389.098261 -0.263802212T -495892796T^{-2}+ 3.649686E-5T^2- 3.5129259E34T^{-10}	C_p = 2$C_p(Er_{(hcp)})$ + 17$C_p(Fe_{(bcc)})$

Compound	Magnetic moment	Curie Temperature(K)	References
$ErFe_2$	4.47	704	[6]
$ErFe_3$	3.13	652	[6]
Er_6Fe_{23}	14.8	574	[6]
Er_2Fe_{17}	17.9	408	[6]

3.10.4. References

1. Buschow, K.H.J. and A.S. Van-der Goot, *Phase relations, crystal structures, and magnetic properties of erbium-iron compounds.* Phys. Status Solidi, 1969. **35**,p. 515-22.
2. Meyer, A., *Erbium-iron system.* J. Less-Common Metals, 1969. **18**,p. 41-8.
3. Kolesnikov, V.E., V.F. Trekhova and E.M.Savitskii, Neorg. Mater., 1971. **7**(3): p. 495.
4. Norgren, S., et al., *Experimental investigation on the enthalpies of formation of the $DyFe_2$, $DyFe_3$, Dy_2Fe_{17}, $ErFe_2$, and $ErFe_3$ intermetallic compounds.* Metallurgical and Materials Transactions A, 1998. **29**(5): p. 1367-1374.
5. Germano, D.J. and R.A. Butera, *Heat capacity of, and crystal-field effects in, the RFe_2 intermetallic compounds (R = Gd, Tb, Dy, Ho, Er, Tm, and Lu).* Phys. Rev. B: Condens. Matter, 1981. **24**,p. 3912-27.

6. Buschow, K.H.J., *Intermetallic compounds of rare earth and 3d transition metals.* Rep. Prog. Phys., 1977. **40**,p. 1179-256.

7. Gozzi, D., M. Iervolino, and A. Latini, *Thermodynamics of Fe-rich intermetallics along the rare earth series.* Journal of Chemical and Engineering Data, 2007. **52**(6): p. 2350-2358.

Figures

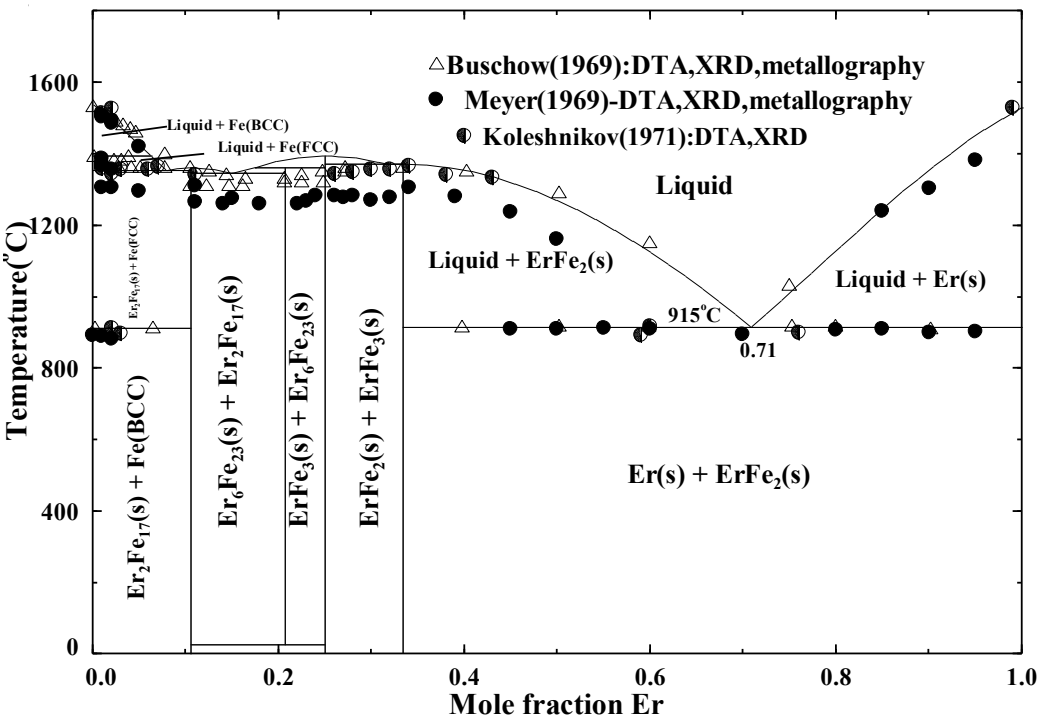

Fig 3.10.1 The optimized Fe-Er system.

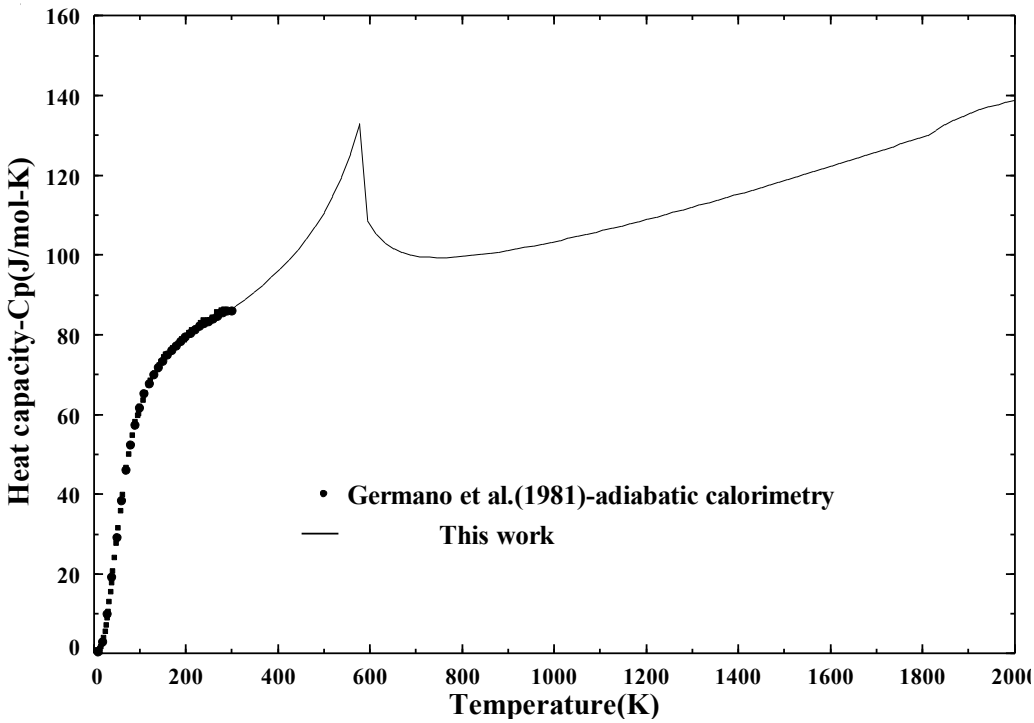

Fig. 3.10.2. Low temperature heat capacity value for $ErFe_2$.

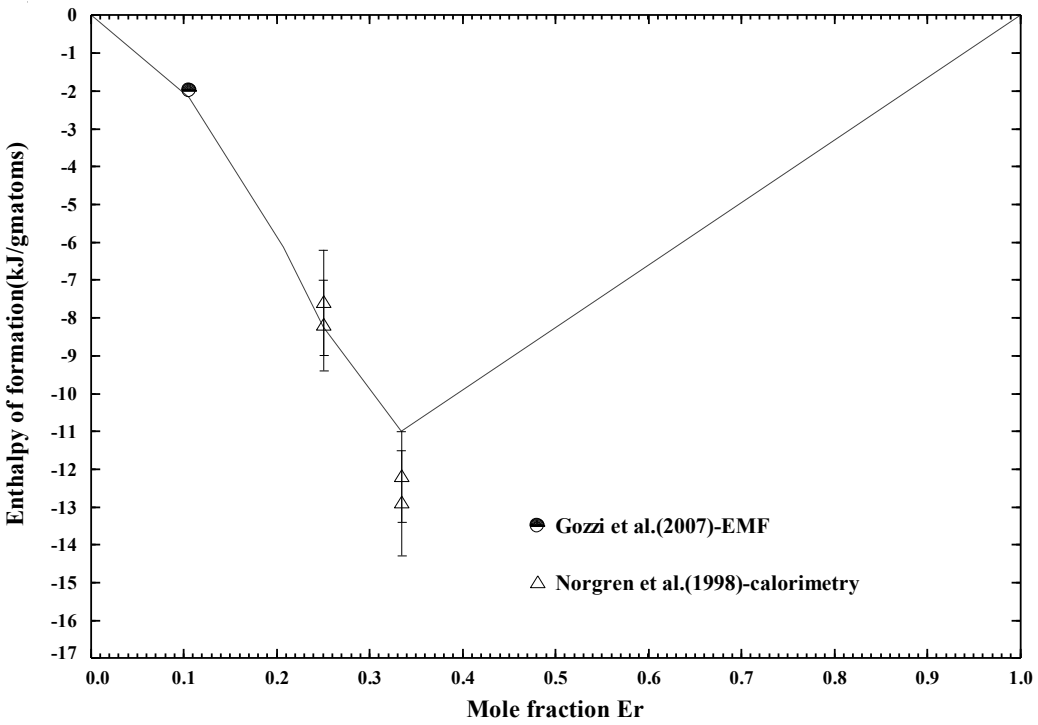

Fig. 3.10.3. Formation Enthalpies of Fe-Er compound.

3.11. The Fe-Tm(Iron Thulium) system

The phase equilibria have been determined by Kolesnichenko et al.[1]. The phase diagram information was taken by Kubaschewski [2] and Okamoto [3] and represented in their respective phase diagram compilations.

3.11.1. Phase Diagram data

The phase diagram reported by Kolesnichenko et al [1] by X-ray diffraction and thermal analysis consists of four binary compounds $TmFe_2$ and $Tm_6Fe_{23}$with cubic structure and $TmFe_3$ and Tm_2Fe_{17} with hexagonal structure. $TmFe_2$ melts congruently at 1200 °C and the remaining compounds $TmFe_3$, Tm_6Fe_{23} and Tm_2Fe_{17} form by peritectic reactions at 1180 ^oC, 1170 ^oC, and 1200 °C, respectively. The system forms two eutectic reactions at 1037 °C and 27 at. % Fe and at 1255°C and 82 at. % Fe[1]. In the current assessment the phase diagram experimental data is well reproduced.

3.11.2. Thermodynamic Data

The low temperature heat capacity measurements for the $TmFe_2$ was done by Germano et al .[4] which was integrated to obtain the S_{298} value. No other enthalpy of formation or entropy data for any other intermetallic phases was available in literature. The Liquid Gibbs energy is also assumed following trends in heavy rare-earth-Iron binary alloys.

3.11.3. Magnetic data

The magnetic properties such as the Bohr magnetons per mole and Curie temperature of the intermetallic phases are taken from the Buschow [7], which are tabulated below.

Table 3.11.1 Optimized thermodynamic data of the Tm-Fe system.

Liquid phase (Quasichemical model parameters)			
Coordination numbers: $Z^{Fe}_{FeFe} = Z^{Tm}_{TmTm} = Z^{Tm}_{TmFe} = Z^{Fe}_{FeTm} = 6$ $\Delta g_{FeTm} = -4180 - 2926X_{TmTm} - 7942X_{FeFe} - 2.1TX_{FeFe} - 0.836X^2_{FeFe}$			
Solid phases			
$\Delta H_f°_{298}$ (kJ mol^{-1})			
Compound	**Optimized elements as reference**	**Experimental elements as reference**	**Reference**
$TmFe_2$	-34.60	-	-
$TmFe_3$	-33.63	-	-
Tm_6Fe_{23}	-185.20	-	-
Tm_2Fe_{17}	-45.48	-	-
$S°_{298}$ (J mol^{-1} K^{-1})			
Compound	**$S°_{298}$ Optimized**	**$S°_{298}$ Experimental**	**Reference**
$TmFe_2$	128	127.5541	[5]
TmFe3	171	-	-
Tm_6Fe_{23}	1228	-	-
Tm_2Fe_{17}	723.9	-	-
C_p (J mol^{-1} K^{-1})			
Compound	**Optimized**		**Reference**
$TmFe_2$			$C_p = C_p(Tm_{(hcp)}) + 2C_p(Fe_{(bcc)})+5.26$
298-700 K	$86.6550974+ -0.00663185T -501400T^{-2} + 2.369406E-5T^2$		
700-1600 K	$84.4837269+ 0.016700574T -2492764T^{-2} + 3.087288E-6T^2$		
1600-1811K	$77.4702969+ 0.024359206T -309436T^{-2} +7.07124E-7T^2$		
1811-1818K	$122.4416969+ 0.006769126T -4.132854E33T^{-10}$		
1818-2300K	$-436.822763+ 0.38186078T+ 360764440T^{-2} -7.013511E-5T^2 -4.132854E33T^{-10}$		
$TmFe_3$			$C_p = C_p(Tm_{(hcp)}) + 3C_p(Fe_{(bcc)})$
298-700 K	$104.9093974+ 0.00216319T -656118T^{-2} 2.4047622E-5T^2$		
700-1600 K	$102.7380269+ 0.025495614T -2647482T^{-2} +3.44085E-6T^2$		
1600-1811K	$95.7245969+0.033154246T-464154T^{-2}+ 1.060686E-6T^2$		
1811-1818K	$163.1816969+0.006769126T-6.199281E33T^{-10}$		
1818-2300K	$-396.082763+ 0.38186078T+ 360764440T^{-2} -7.013511E-5T^2-6.199281E33T^{-10}$		
Tm_6Fe_{23}			$C_p = 6C_p(Tm_{(hcp)}) +$
298-700 K	$747.0278844+ 0.05695434T -4710298T^{-2}+0.000146053542T^2$		
700-1600 K	$733.9996614+0.196948884T -16658482T^{-2}+2.241291E-5T^2$		

1600-1811K	$691.9190814+ 0.242900676T -3558514^{-2}+8.131926E-6T^2$	$23C_p(Fe_{(bcc)})$
1811-1818K	$1209.0901814+0.040614756T -4.7527821E34T^{-10}$	
1818-2300K	$-2146.496578+ 2.29116468T + 2164586640T^{-2} - 0.00042081066T^2-4.7527821E34T^{-10}$	
Tm_2Fe_{17}		
298-700 K	$468.4760948+ 0.10107182T -3014134T^{-2}+ 5.1984426E-5T^2$	$C_p = 2C_p(Tm_{(hcp)}) + 17C_p(Fe_{(bcc)})$
700-1600K	$464.1333538+ 0.147736668T -6996862T^{-2}+ 6.396735E-5T^2$	
1600-1811K	$450.1064938+ 0.163053932T+ -2630206T^{-2} + 6.010554E-6T^2$	
1811-1818K	$832.3633938+ 0.013538252+ -3.5129259E34T^{-10}$	
1818-2300K	$-286.165526+ 0.76372156T +721528880T^{-2}+ 0.00014027022E-5T^2 -3.5129259E34T^{-10}$	

Compound	Magnetic moment	Curie Temperature(K)	References
$TmFe_2$	2.61	599	[6]
$TmFe_3$	1.6	537	[6]
Tm_6Fe_{23}	18	475	[6]
Tm_2Fe_{17}	20.4	280	[6]

3.11.4. References

1. Kolesnichenko, V.E., V.F. Terekhova, and E.M. Savitskii. *Phase diagrams of thulium-iron and lutetium-iron alloys*. 1972. "Nauka".
2. Kubaschewski, O., *IRON-Binary Phase Diagrams*1982, Berlin: Springer.
3. Okamoto, H., *Phase Diagrams of Binary Iron Alloys*. J. Phase Equilib., ed. H. Okamoto1993, Materials Park, Ohio: Materials Information Society.
4. Germano, D.J., R.A. Butera, and K.A. Gschneidner, Jr., *Heat capacity and thermodynamic functions of the RFe_2 compounds (R = gadolinium terbium, dysprosium, holmium, erbium, thulium, lutetium) over the temperature region 8 to 300 K.* J. Solid State Chem., 1981. **37**,p. 383-9.
5. Germano, D.J. and R.A. Butera, *Heat capacity of, and crystal-field effects in, the RFe_2 intermetallic compounds (R = Gd, Tb, Dy, Ho, Er, Tm, and Lu).* Phys. Rev. B: Condens. Matter, 1981. **24**,p. 3912-27.
6. Buschow, K.H.J., *Intermetallic compounds of rare earth and 3d transition metals.* Rep. Prog. Phys., 1977. **40**,p. 1179-256.

Figures

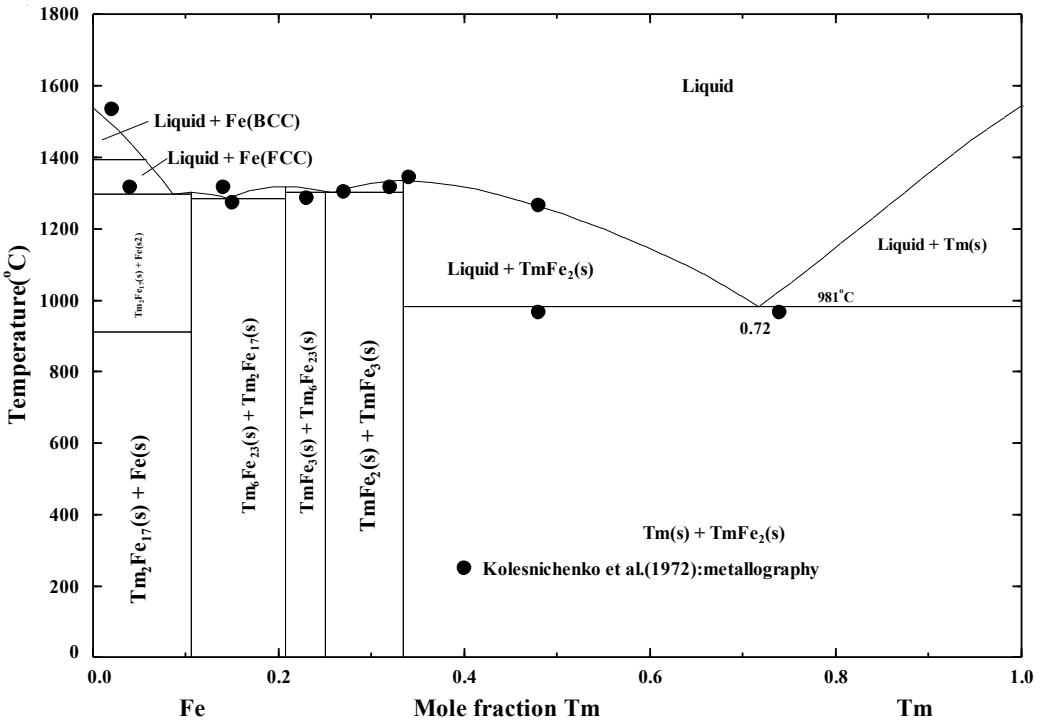

Fig 3.11.1 The optimized Fe-Tm system

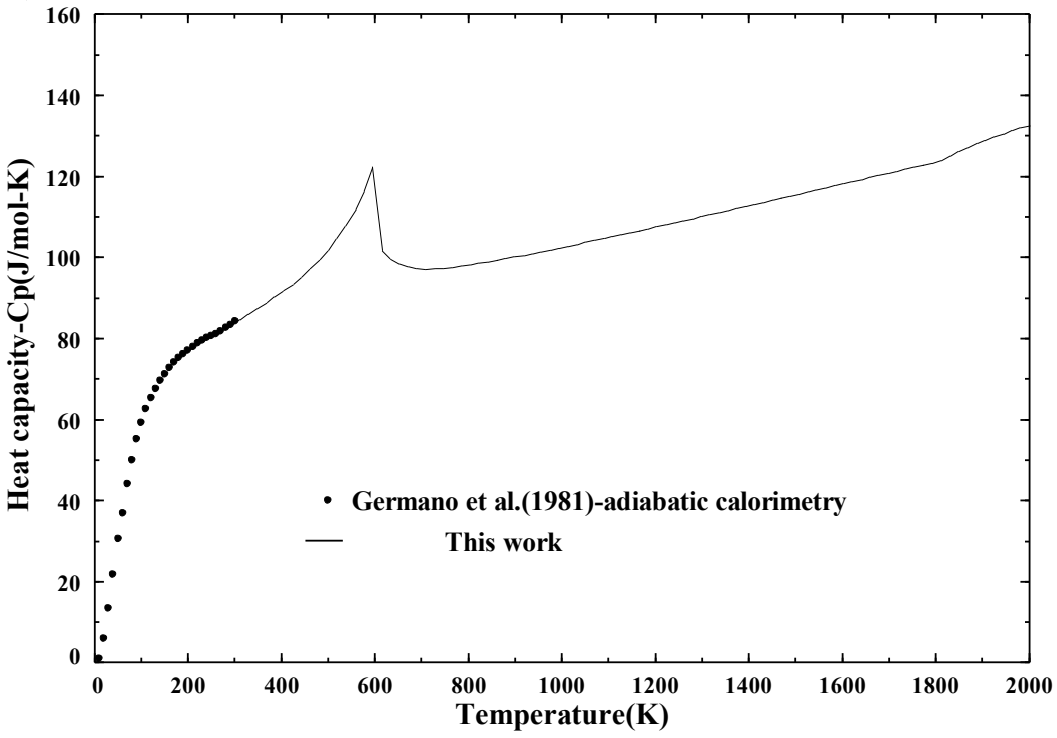

Fig.3.11.2. Low temperature heat capacity value for $TmFe_2$

3.12. The Fe-Lu (Iron lutetium) System

This Phase Diagram was first investigated by thermal analysis and X-ray diffractography by Kolesnichenko[1]. The phase diagram thus obtained was redrawn by Kubaschewski[2] and Okamoto[3].

3.12.1. Phase Diagram Data

Four intermetallic compounds form in the Lu-Fe system. $LuFe_2$ has a cubic structure; $LuFe_3$ is orthorhombic; Lu_6Fe_{23} is cubic; and Lu_2Fe_{17} is hexagonal. $LuFe_2$ melts congruently at 1345°C and the remaining compounds form by peritectic reactions at 1310, 1290, and 1320°C, respectively. The system of Lu forms two eutectic reactions at 970 °C and 27 at. % Fe and at 1275 °C and 82 at. % Fe. The alloys containing ≤ 10.6 at. % Lu has a polymorphous transition at 915°C. The γ-Fe to δ-Fe phase transition of Fe is unaffected by Lu.

3.12.2. Thermodynamic data

For the four compounds reported no enthalpy of formation data was reported by experimentation. Germano et al.[4] did low temperature heat capacity measurements for the $LuFe_2$ phase by adiabatic calorimeter. This low temperature heat capacity data was integrated to obtain the S_{298} for the intermetallic phase and adjusted with the high temperature heat capacity predicted by the algebraic Cp addition of the elemental constituents was also adjusted. Tereshina et al. [5] by using a PPMS magnetometer machine determined the low temperature heat capacity measurements for Lu_2Fe_{17} phase. For this intermetallic phase S_{298} calculation and high temperature heat capacity adjustment was also done as mentioned above.

3.12.3. Magnetic data

The magnetic data was taken from Buschow's compilation of magnetic data for Iron-Rare Earth system.

Table 3.12.1. Optimized thermodynamic data of the Lu-Fe system.

Liquid phase (Quasichemical model parameters)			
Coordination numbers: $Z^{Fe}_{FeFe} = Z^{\mathrm{Lu}}_{\mathrm{LuLu}} = Z^{\mathrm{Lu}}_{LuFe} = Z^{\mathrm{Fe}}_{\mathrm{FeLu}} = 6$ $\Delta g_{FeLu} = -4221{,}8 - 0.418T - 2926X_{LuLu} - 5852X_{FeFe}$			
Solid phases			
$\Delta H_f°_{298}$ **(kJ mol^{-1})**			
Compound	**Optimized elements as reference**	**Experimental elements as reference**	**Reference**
$LuFe_2$	-28.99	-	-
$LuFe_3$	-30.83	-	-
Lu_6Fe_{23}	-185.40	-	-
Lu_2Fe_{17}	-48.5	-	-
$S°_{298}$ **(J mol^{-1} K^{-1})**			
Compound	$S°_{298}$ **Optimized**	$S°_{298}$ **Experimental**	**Reference**
$LuFe_2$	108	107.4109	[4]
LuFe3	148.1	-	-
Lu_6Fe_{23}	1033.7	-	-
Lu_2Fe_{17}	647	647.7395	[5]
C_p **(J mol^{-1} K^{-1})**			
Compound	**Optimized**		**Reference**
$LuFe_2$			$C_p = C_p(Lu_{(hcp)}) + 2C_p(Fe_{(bcc)}) + 9.0954$
298-700 K	$79.6406 + 0.00720678T - 388882T^{-2} + 1.1451426E\text{-}5T^2$		
700-1700 K	$78.8381 + 0.01016176T - 592534T^{-2} + 9.715944E\text{-}6T^2$		
1700-1811 K	$51.66846 + 0.04139028T - 309436T^{-2} + 7.07124E\text{-}7T^2$		
1811-1936K	$96.63986 + 0.0238002T - 4.132854E33T^{-10}$		
$LuFe_3$			$C_p = C_p(Lu_{(hcp)}) + 3C_p(Fe_{(bcc)})$
298-700 K	$103.1549 + 0.01600182T - 543600T^{-2} + 1.1804988E\text{-}5T^2$		
700-1700 K	$102.3524 + 0.0189568T - 747252T^{-2} + 1.0069506E\text{-}5T^2$		
1700-1811K	$75.18276 + 0.05018532T - 464154T^{-2} + 1.060686E\text{-}6T^2$		
1811-1936K	$142.63986 + 0.0238002T - 6.199281E33T^{-10}$		
1936-6000K	$183.129817405107 - -2.066427E33T^{-10}$		
Lu_6Fe_{23}			$C_p = 6C_p(Lu_{(hcp)})$
298-700 K	$736.5009 + 0.13998612T - 4035190T^{-2} + 7.2597738E\text{-}5T^2$		
700-1700 K	$731.6859 + 0.157716T - 5257102T^{-2} + 6.2184846E\text{-}5T^2$		

1700-1811 K 1811-1936K 1936-6000K	568.66806+ 0.34508712T -3558514T^{-2}+ 8.131926E-6T^2 142.63986+0.0238002T -6.199281E33T^{-10} 183.129817405107-2.066427E33T^{-10}	+ 23C_p($Fe_{(bcc)}$)
Lu_2Fe_{17} 298-700 K 700-1700K 1700-1811K 1811-1936K 1936-3700K	 483.12+0.12874908 T-2789098 T^{-2}+2.7499158E-5T^2 481.51+ 0.13465904T -3196402T^{-2}+ 2.4028194E-5T^2 427.17+ 0.19711608T -2630206T^{-2} +6.010554E-6T^2 809.43+ 0.0476004T -3.5129259E34 T^{-10} 1283.79 -0.167202992T -499301860T^{-2}+1.9934088E-5T^2-3.5129259E34T^{-10}	C_p = 2C_p($Lu_{(hcp)}$) + 17C_p($Fe_{(bcc)}$)

Compound	Magnetic moment	Curie Temperature(K)	References
$LuFe_2$	2.93	596	[6]
$LuFe_3$	-	-	
Lu_6Fe_{23}	43.9	481	[6]
Lu_2Fe_{17}	34.2	268	[6]

3.12.4. References

1. Kolesnichenko, V.E., V.F. Terekhova, and E.M. Savitskii. *Phase diagrams of thulium-iron and lutetium-iron alloys*. 1972. "Nauka".
2. Kubaschewski, O., *IRON-Binary Phase Diagrams*1982, Berlin: Springer.
3. Okamoto, H., *Phase Diagrams of Binary Iron Alloys*. J. Phase Equilib., ed. H. Okamoto1993, Materials Park, Ohio: Materials Information Society.
4. Germano, D.J. and R.A. Butera, *Heat capacity of, and crystal-field effects in, the RFe_2 intermetallic compounds (R = Gd, Tb, Dy, Ho, Er, Tm, and Lu).* Phys. Rev. B: Condens. Matter, 1981. **24**, p. 3912-27.
5. Tereshina, E.A. and A.V. Andreev, *Magnetization and specific heat study of metamagnetism in Lu_2Fe_{17}-based intermetallic compounds.* Intermetallics, 2010. **18**(6): p. 1205-1210.
6. Buschow, K.H.J., *Intermetallic compounds of rare earth and 3d transition metals.* Rep. Prog. Phys., 1977. **40**, p. 1179-256.

Figures

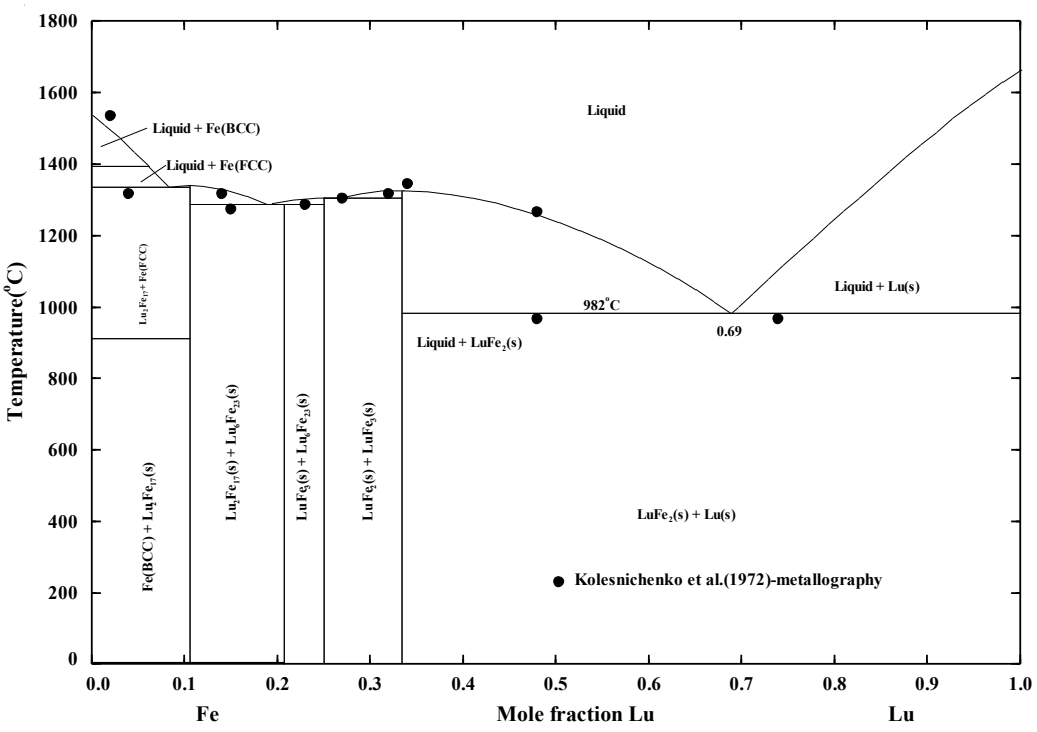

Fig 3.12.1 The optimized Fe-Lu system.

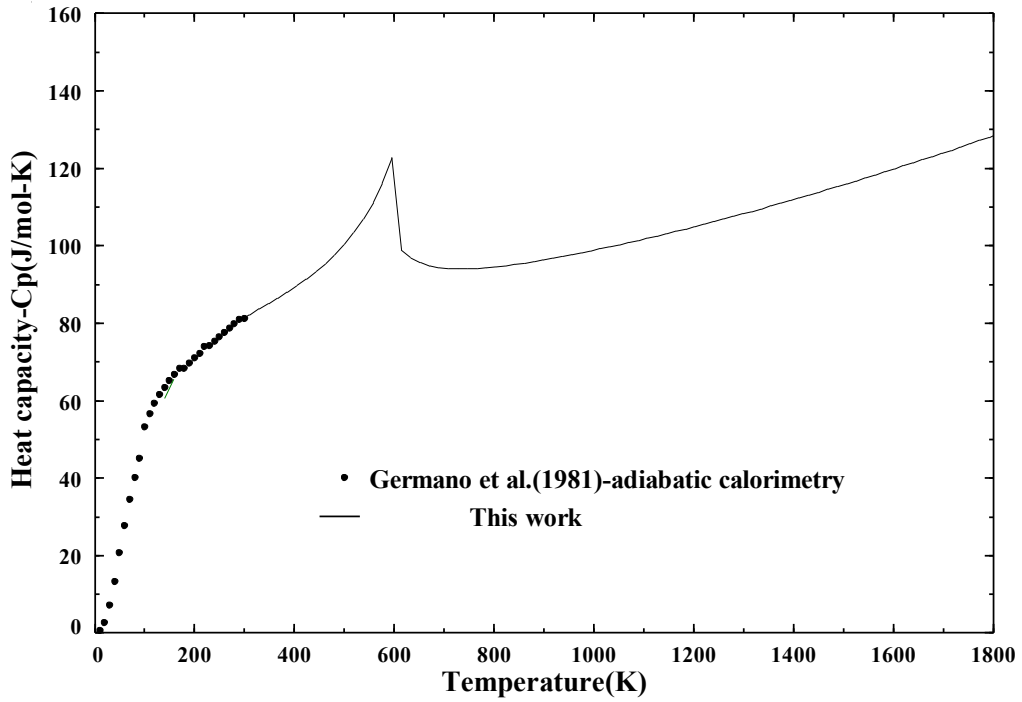

Fig.3.12.2. Low temperature heat capacity value for $LuFe_2$

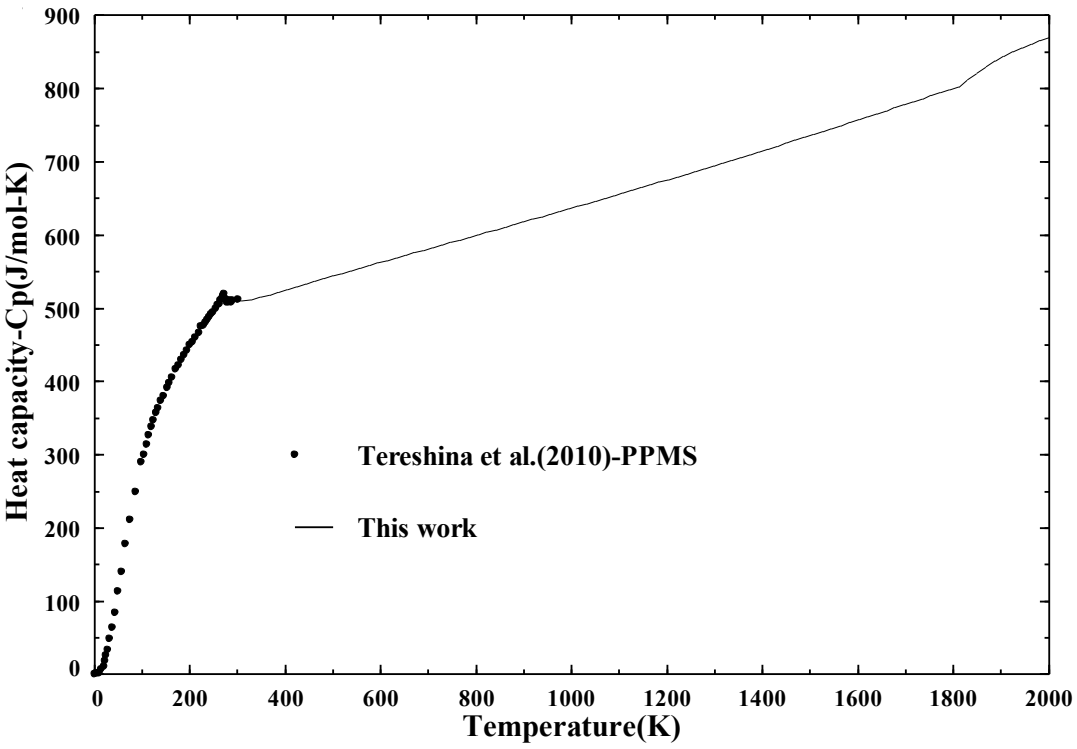

Fig. 3.12.3. Low temperature heat capacity value for Lu_2Fe_{17}

3.13. The Fe-Y (Iron-Yttrium) System

The Iron Yttrium binary system was investigated by Domagala et al.[1] , Farkas et al. [2], Assessment has been carried out by Gschneidner[3], Zhang et al. [4] and Du et al. [5].

3.13.1. Phase Diagram data

Domagala et al. [1] carried out experiments in Fe-Y binary system with the help of quenching and microstructure evaluation technique, couple with X-ray diffraction and melting point experiments. They suggested 1wt. % solubility of Fe in Y, however Yttrium undergoes a polymorphic transformation (HCP to BCC) at 1478.5^{o}C, so the solubility was considered to be in high temperature BCC structure. They reported a eutectic point at 25 wt. % ($L \rightarrow Y_{ss}+YFe_2$). The intermetallic phases suggested by him were YFe_2, YFe_3. YFe_4 and YFe_9, where YFe_2 melts peritectically and the compounds have congruent melting. In the assessment by Zhang et al. the compounds suggested were that of heavy rare-earth metals alloyed with Iron, namely YFe_2, YFe_3, Y_6Fe_{23} and Y_2Fe_{17}. The phase diagram also shows some homogeneity range of the Y_6Fe_{23} phase and the YFe_2. Due to absence of any experimental data these solubilities were not considered in the present thermodynamic assessment. Further experimentation is warranted for the liquidus also as it is present by dotted line in all the previous assessments. The melting point of the intermetallic phases as reported by Domagala et al. [6] was aimed to reproduce.

3.13.2. Thermodynamic data

The thermodynamic data available for this binary system is the Gibbs energy of formation data measured by Subramaniam et al. [6]. He used solid electrolyte electromotive force cells to determine the Gibbs free energies for the four intermetallic phases. In the current assessment we treated all the four intermetallic phases as stoichiometric compounds. The enthalpy of mixing of the liquid data was measured by Ryss et al. [7] at 1873K for the whole range of composition which agrees reasonable with our present assessment. The low temperature heat capacity of YFe_2 was reported by Dariel et al. [8], However we found while our assessment that the heat capacity tends to decrease as the temperature is increased above the Curie temperature which seems rather

strange. Low temperature heat capacity for Y_2Fe_{17} calculation data was obtained from Mandal et al. [9] with a PPMS device. This was used to evaluate the S_{298} for the intermetallic phase. When we calculated the entropy of formation for this phase at 973K the value obtained was very different from that reported by Subramaniam at al. [6] this would be due to the heat capacity which governs the temperature dependence of the entropy of formation. The current assessment the heat capacity function with respect to temperature is assumed by Kopp Newman rule (algebraic addition of constituent element heat capacity) as illustrated in the table and adjustment of the temperature independent term to match the low temperature experimental values. The specific heat anomalies of YFe_2 were measured and discussed by Dariel et al.[8]. Thus we feel similar anomalies is also expected for the other systems as the experimentally determind S_{298} for the Y_2Fe_{17} phase could also not reproduce the S_{973} of formation reported by Subramaniam et al.[6].

3.13.3. Magnetic Data

The Magnetic data for the four intermetallic phases were obtained from Buschow[10].

Table 3.13.1 Optimized thermodynamic data of the Y-Fe system.

Liquid phase (Quasichemical model parameters)			
Coordination numbers: $Z^{Fe}_{FeFe} = Z^{Y}_{YY} = Z^{Y}_{YFe} = Z^{Fe}_{FeY} = 6$ $\Delta g_{FeY} = -3762 - 5852X_{YY} - 8360X_{FeFe} - 4.18TX_{FeFe}$			
Solid phases			
$\Delta H_f^{\circ}{}_{298}$ (kJ mol^{-1})			
Compound	**Optimized elements as reference**	**Experimental elements as reference**	**Reference**
YFe_2	-26.968	-	-
YFe_3	-35.156	-	-
Y_6Fe_{23}	-213.250	-	-
Y_2Fe_{17}	-94.646	-	-
S°_{298} (J mol^{-1} K^{-1})			
Compound	**S°_{298} Optimized**	**S°_{298} Experimental**	**Reference**
YFe_2	108.812	-	-
YFe3	142.47	-	-
Y_6Fe_{23}	1056.05	-	-
Y_2Fe_{17}	595	660.7052	[9]

C_p (J mol^{-1} K^{-1})		
Compound	**Optimized**	**Reference**
YFe_2		$C_p = C_p(Y_{(hcp)}) + 2C_p(Fe_{(bcc}$
298-1000 K	$72.6942992+ 0.02110440828T -363259.018T^{-2} + 3.212494716E-6T^2$	
1000-1795 K	$70.5227827+ 0.0252324404T -309436T^{-2} +1.202331204E-6T^2$	
1795-1811K	$103.9813111+ 0.01295459242T -36463761.2T^{-2} + 1.1406318528E-6T^2$	
1811-3700K	$148.9527111 -0.00463548758T -36154325.2T^{-2} + 4.335078528E-7T^2 -4.132854E33T^{-10}$	
YFe_3		$C_p = C_p(Y_{(hcp)}) + 3C_p(Fe_{(bcc)})$
298-1000 K	$96.2085992+ 0.029899T -517977T^{-2} +3.566056716E-6T^2$	
1000-1795 K	$94.0370827+ 0.0340274804T-464154T^{-2} +1.556E-6T^2$	
1795-1811K	$127.4956+0.02174963242T-36618479.2T^{-2}+1.4941938528E-6T^2$	
1811-3700K	$194.9527111-0.00463548758T-36154325.2T^{-2} 4.335078528E-7T^2-6.199281E33T^{-10}$	
Y_6Fe_{23}		
298-1000 K	$694.8230952+ 0.22337188968T -3881452.108T^{-2}+2.3164150296E-5T^2$	$C_p = 6C_p(Y_{(hcp)}) + 23C_p(Fe_{(bcc)})$
1000-1795 K	$681.7939962+0.2481400824T -3558514T^{-2}+1.1103169224E-5T^2$	
1795-1811K	$882.5451666+ 0.17447299452T-220484465.2^{-2}+1.07329731168E-5T^2$	
1818-3700K	$1399.7162666-0.02781292548T -216925951.2T^{-2} +2.6010471168E-6T^2--4.7527821E34^{-10}$	
Y_2Fe_{17}		
298-1000 K	$509.0744984+ 0.15654433656T -2737852.036T^{-2}+ 1.1021295432E-5T^2$	$C_p = 2C_p(Y_{(hcp)}) + 17C_p(Fe_{(bcc)})-59$
1000-1795K	$504.7314654+ 0.1648004008T -2630206T^{-2}+ 7.000968408E-6\ T^2$	
1795-1811K	$882.5451666+ 0.17447299452T-220484465.2T^{-2} + 1.07329731168E-5T^2$	
1811-3700K	$1399.7162666-0.02781292548T -216925951.2T^{-2}+ 2.601E-6T^2 -4.7527821E34T^{-10}$	
Solid Solution (parameters of the Compound Energy Formalism with two-sublattice approach) $(Fe, Y)_1^I(Va)_1^{II}$		
FCC	$^0L_{Fe,Y} = -12958$	
BCC	$^0L_{Fe,Y} = 0$	
HCP	$^0L_{Fe,Y} = 16720$	

Compound	Magnetic moment	Curie Temperature(K)	References
YFe_2	2.9	542	[10]
YFe_3	5.24	569	[10]
Y_6Fe_{23}	43.1	481	[10]
Y_2Fe_{17}	32.9	324	[10]

3.13.4. References

1. Domagala, R.F., J.J. Rausch and D.W. Levinson, *The Systems Y-Fe, Y-Ni and Y-Cu.* Transactions of the ASM, 1961. **53**: p. 137-155.
2. Farkas, M.S., Bauer, A.A., 1959, USAEC Rep. p. 20.
3. Gschneidner, K.A., Jr., *Binary Alloy Systems*. Rare Earth Alloys1961, NewYork: Van Nostrand.
4. Zhang, W., G. Liu, and K. Han, *The Fe-Y (iron-yttrium) system.* J. Phase Equilib., 1992. **13**,p. 304-8.
5. Du, Z., W. Zhang, and Y. Zhuang, *Thermodynamic assessment of the Fe-Y system.* Rare Met. (Beijing), 1997. **16**,p. 52-58.
6. Subramanian, P.R. and J.F. Smith, *Thermodynamics of formation of yttrium-iron alloys.* CALPHAD: Comput. Coupling Phase Diagrams Thermochem., 1984. **8**,p. 295-305.
7. Esin, Y.O. , A.F.Ermakov, M.G. Valishev, G.M. Ryss, P.V. Geld, and E.S. Levin, *Enthalpy of Formation of Liquid Binary Alloys of Iron with Lanthanum and Cerium.* Zh. Fiz. Khim., 1981. **55**(7): p. 1665-1669.
8. Dariel, M.P., U. Atzmony, and R. Guiser, *Specific heat anomalies at the magnetic ordering temperatures of rare earth-iron Laves compounds.* J. Less-Common Metals, 1974. **34**,p. 315-19.
9. Mandal,K., A.Yan, P. Kerschl, A. Handstein, O. Gutfleisch and K.H. Muller, *The study of magnetocaloric effect in R_2Fe_{17} (R=Y, Pr) alloys.* Journal of Physics D:Applied Physics, 2004. **37**: p. 2628-2631.
10. Buschow, K.H.J., *Intermetallic compounds of rare earth and 3d transition metals.* Rep. Prog. Phys., 1977. **40**,p. 1179-256.

Figures

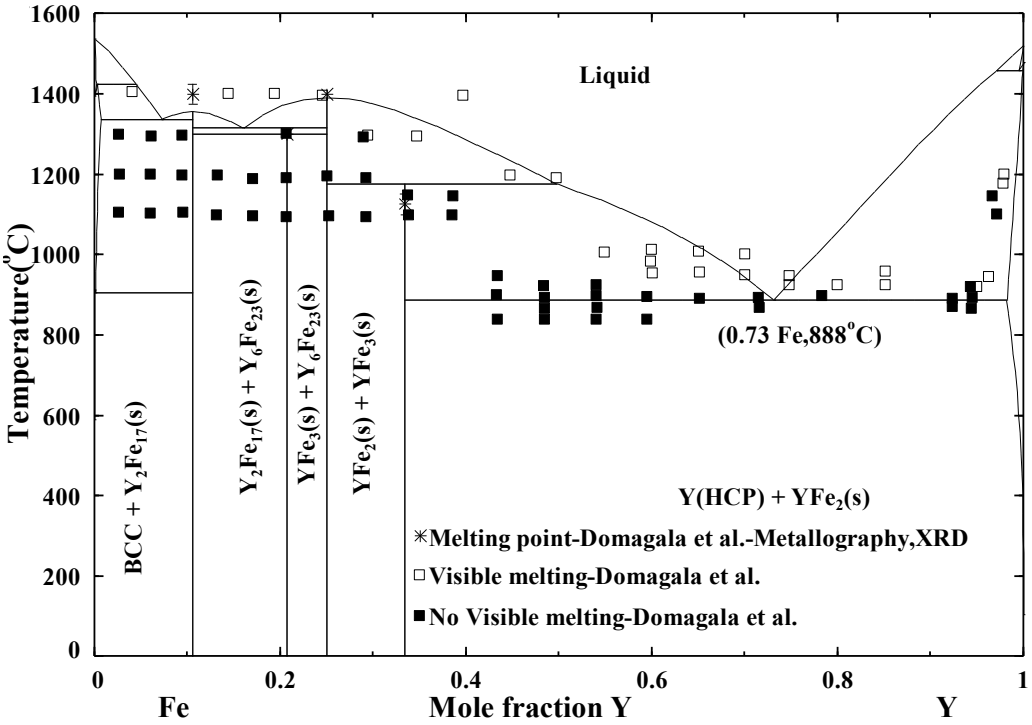

Fig 3.13.1 The optimized Fe-Y system

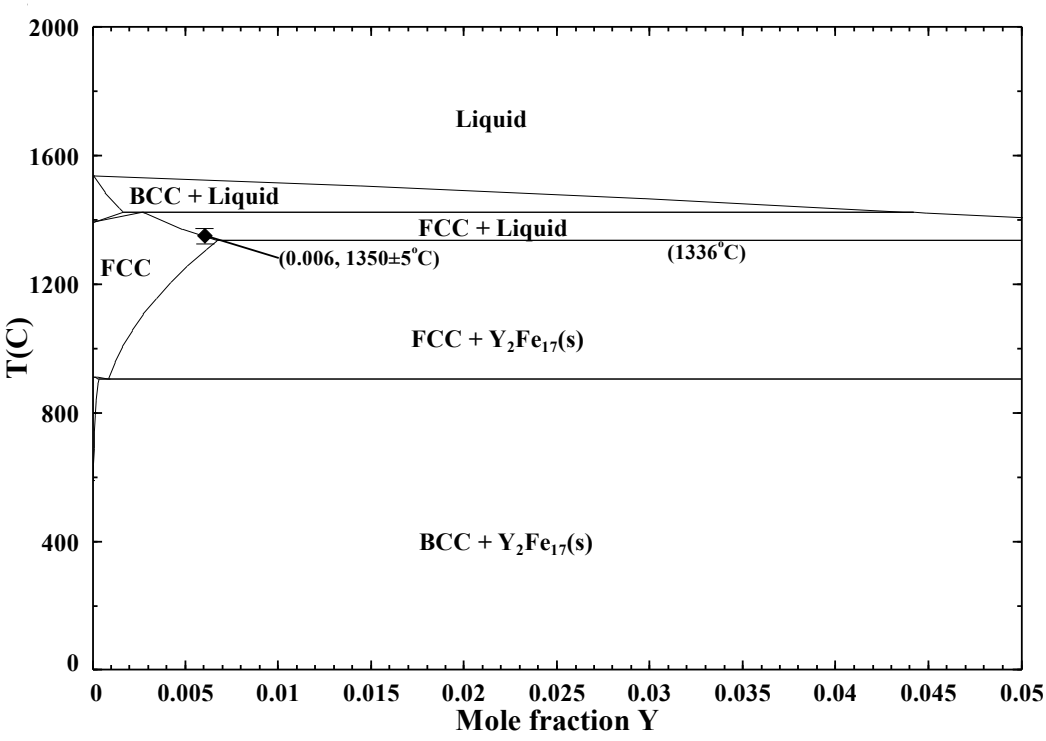

Fig 3.13.2. The solubility of Y in Fe(FCC) reported by Domagala et al.[1].

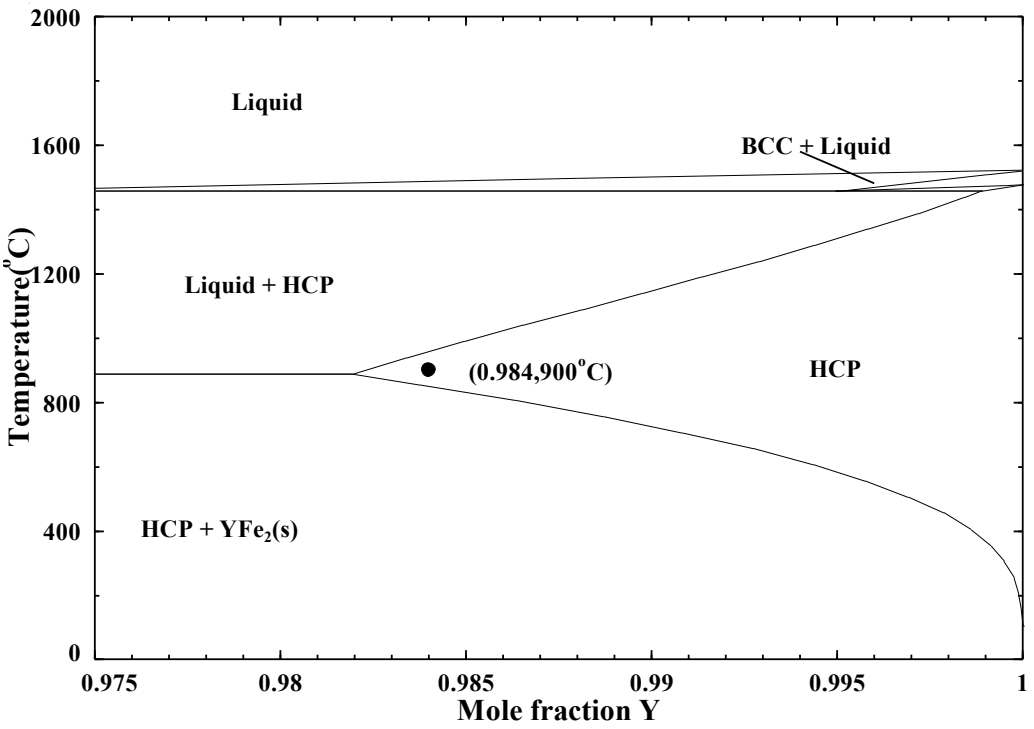

Fig 3.13.3. The solubility of Fe in Y(HCP) reported by Domagala et al.[1].

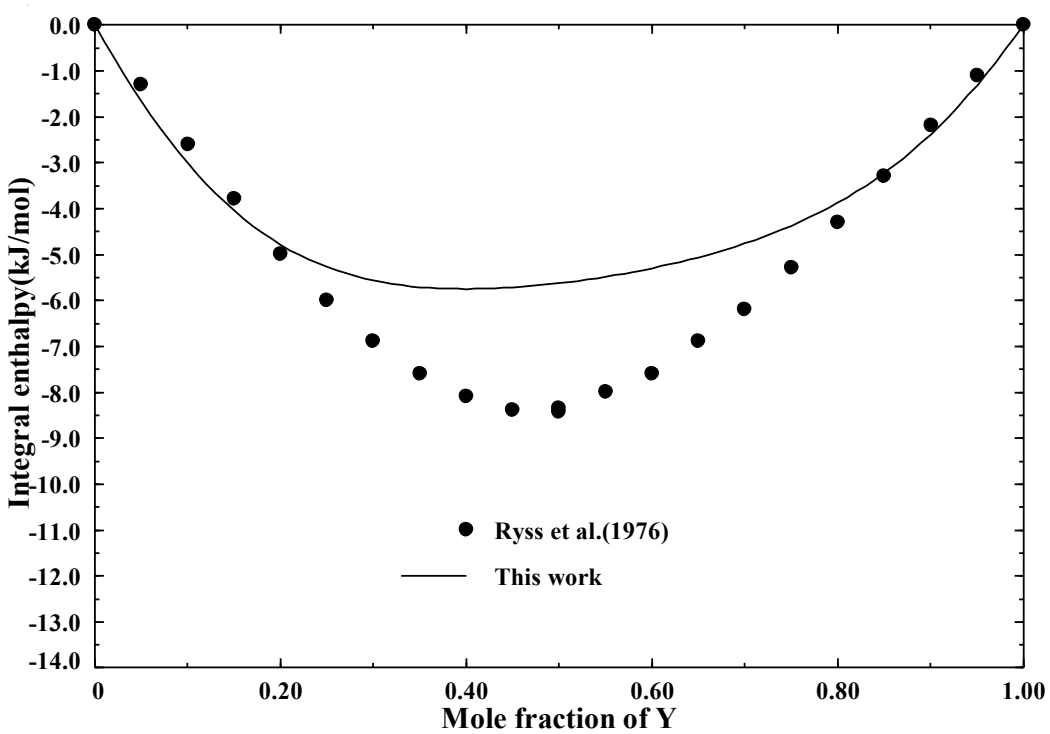

Fig.3.13.4. Enthalpy of mixing of Fe-Y at 1850K

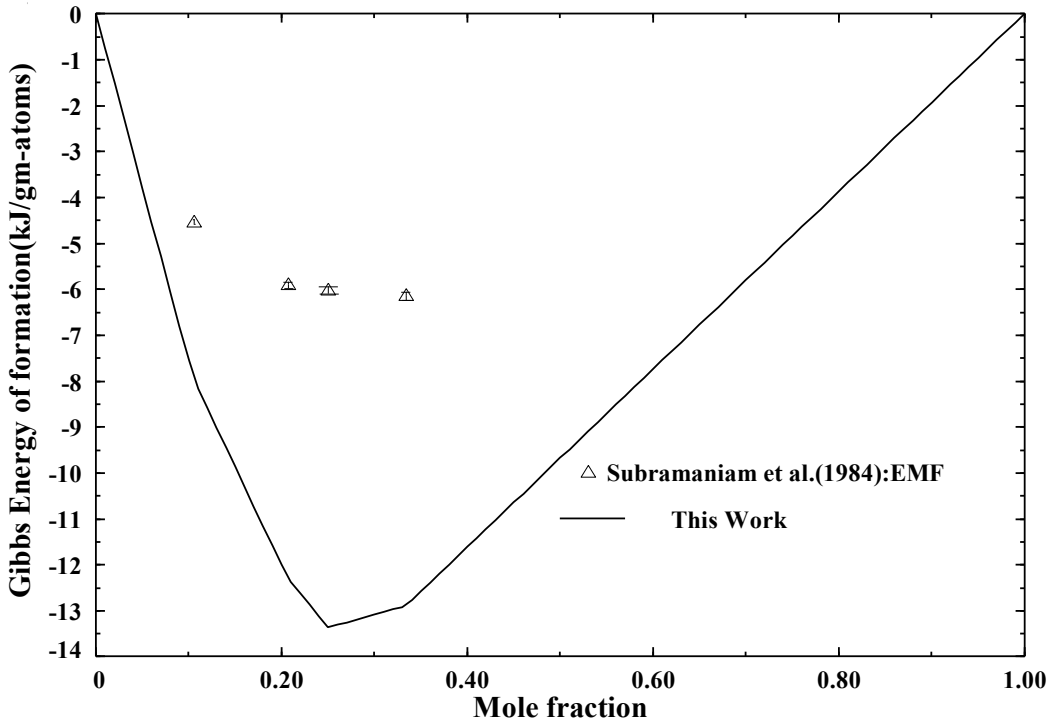

Fig.3.13.5. Gibbs energy of formation at 973K

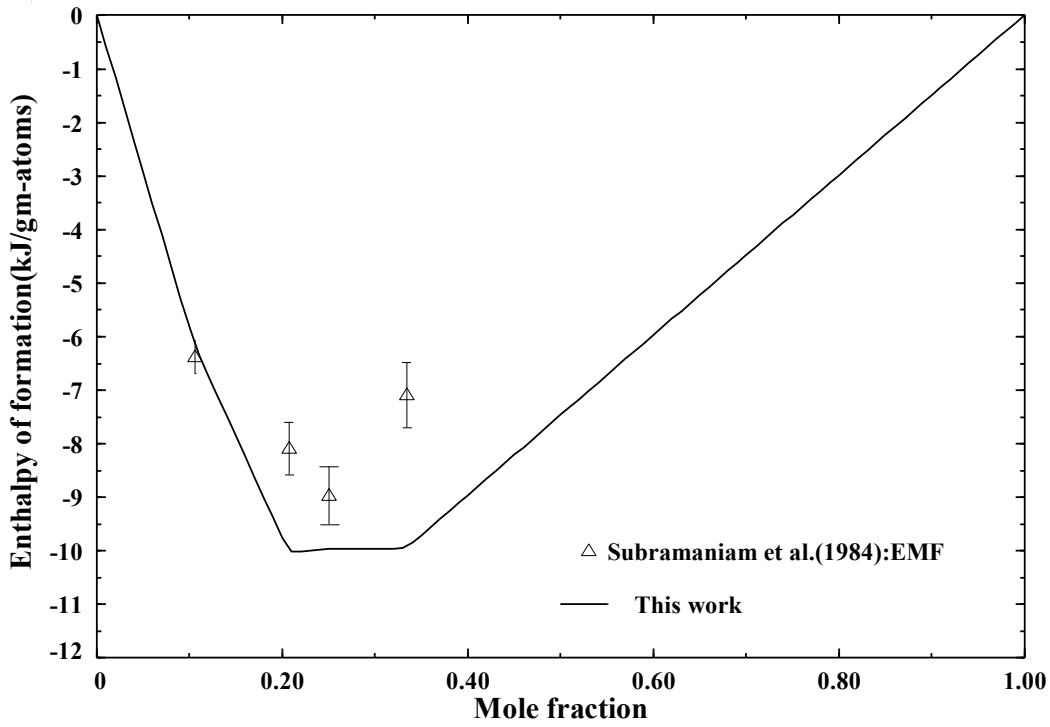

Fig.3.13.6. Enthalpy of formation at 973K

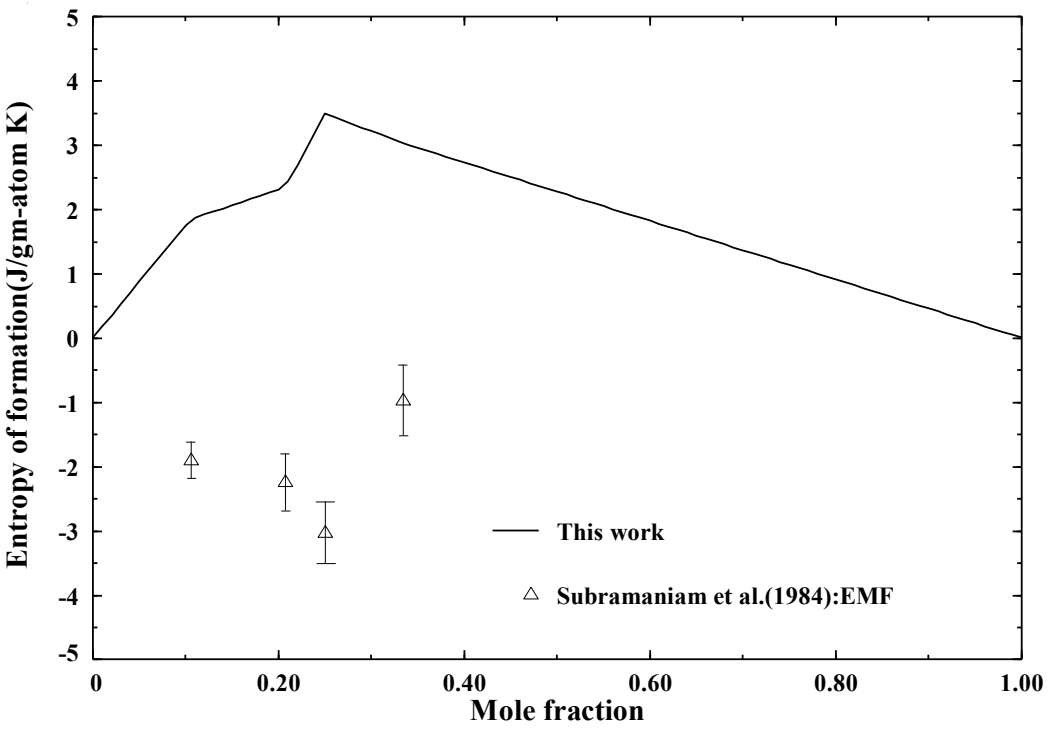

Fig.3.13.7. Entropy of formation at 973K.

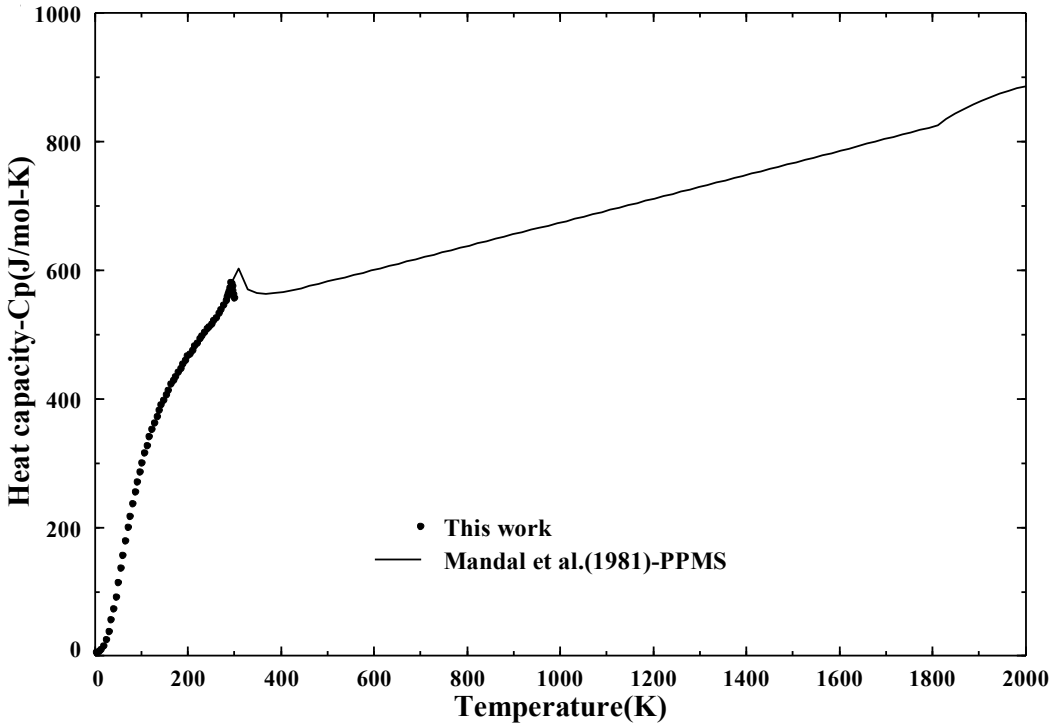

Fig.3.13.8. Low temperature heat capacity value for Y_2Fe_{17}

3.14. The Fe-Sc (Iron-Scandium) System

The Iron Scandium binary system was investigated by Naumkin et al.[1], Bodak et al. [2] and Hellawell [3] and reviewed by Okamoto[4]

3.14.1. Phase Diagram data

The Fe-Sc binary system exhibits five solution phases. Three of them due to the polymorphic transformation of Iron (α-Fe→ γ-Fe→ δ-Fe, which have BCC, FCC and BCC structures respectively) another two due to polymorphic transformation of Sc (α-Sc→ β-Sc, which has HCP and BCC structures respectively). This binary system also has four intermetallic compounds which are α-$ScFe_2$, β-$ScFe_2$, λ-$ScFe_2$ (basically $ScFe_{1.8}$) and $Sc_{29}Fe_6$. The phase diagram was first investigated by Naumkin[1]. He used X-ray diffraction and thermal analyses techniques to construct a phase diagram in compositional range from 0 to 90 at. %. Hellawell[3] reported solubility of Sc in the α-Fe to be less than 0.5at. %. Bodak et al. [2] found the polymorphic transformation of $ScFe_2$ at higher temperatures, and reported an eutectic reaction (L→ α-$ScFe_2$+ α-Sc) at 975^oC. The phase diagram had an intermetallic phase Sc_7Fe instead of Sc_3Fe (reported by Naumkin[1]) which was later reported to be $Sc_{29}Fe_6$ by Bodak et al.[5]. However in more recent studies it has been determined the true stoichiometric compound forming is $Sc_{29}Fe_6$ instead of Sc_7Fe. We found that Bodak et al.[2] did a more recent evaluation, while critically reviewing we found it more realistic. The solid solubility determined by Hellawell[3] was also reproduced. The one phase reported in Naumkin et al.'s phase diagram are all replicated except that in the Iron rich side which we feel was over estimated, and that of the Sc_3Fe which actually is $Sc_{29}Fe_6$.

3.14.2. Thermodynamic data

The enthalpy of formation for $ScFe_2$ phase was determined by Selhaoui and Kleppa [6], who performed direct synthesis calorimetry at 1473±2K with pure α-Fe and pure α-Sc. Goncharuk et al. [7] also measured the formation enthalpies of both the compounds $ScFe_2$ and $Sc_{29}Fe_6$ at 950 K by using EMF technique. However there is a divergence between the enthalpy values reported by Selhaoui et al.[6] and Goncharuk [7]. While critically reviewing the experimental procedure of Goncharuk [7] we found that the electrode used to measure EMF considers the activity of Scandium against the alloy of Sc-Si, this may be erroneous as the scandium has some probability of interacting with molten salt at the elevated temperature. In this assessment we trusted on Selhaoui et al. [6]'s data as the reference for the formation enthalpy for $ScFe_2$ as there method and experimental procedure has lesser scope of error. The formation enthalpy of Sc_5Fe_9 phase was reported by Savchenkova et. al[8] which is much overestimated as also reported by Goncharuk et. al [7]. The transformation energy of $ScFe_2$ from the low-temperature to high temperature polymorph at 1200 ^oC is 1kJ. The enthalpy of mixing of liquid phase

was measured at 1873 K by Esin et al. [9] in the compositional range from 0-18 at. % Sc at 1873 K in the Fe-Sc system. Sudavtsova et al.[10] also reported the enthalpy of scandium dissolution in molten Iron measured at 1870 K. Both Esin et al.[9]'s data and Sudavtsova et al.'s [9]data shows very low partial enthalpy of mixing for Scandium at the Iron rich side which is very hard to reproduce.

3.14.3. Magnetic data

The magnetic data for the Fe_2Sc system was obtained from Ikeda et al. [9]

Table 3.14.1 Optimized thermodynamic data of the Sc-Fe system.

Liquid phase (Quasichemical model parameters)			
Coordination numbers: $Z_{FeFe}^{Fe} = Z_{ScSc}^{Sc} = Z_{ScFe}^{Sc} = Z_{FeSc}^{Fe} = 3$ $\Delta g_{FeSc} = -9196 - 3.762T - 4598X_{ScSc} - 1.672TX_{ScSc}$			
Solid phases			
$\Delta H_f^\circ{}_{298}$ (kJ mol^{-1})			
Compound	**Optimized elements as reference**	**Experimental elements as reference**	**Reference**
$ScFe_2$(s1)	-37.899	-33.6±3.6(298.15K)	[6]
	-13.922	37.7±3.2(950K)	[7]
$ScFe_2$(s2)	-35.156	-	-
$Sc_{29}Fe_6$	-355.896		-
	-376.71	-395.5±171.5(950K)	[7]
Sc_5Fe_9	-110.677	-828.8±28	[8]
S°_{298} (J mol^{-1} K^{-1})			
Compound	**S°_{298} Optimized**	**S°_{298} Experimental**	**Reference**
$ScFe_2$	108.3705	-	-
$Sc_{29}Fe_6$	1025.54264537874	-	-
Sc_5Fe_9	566.2630144	-	-
C_p (J mol^{-1} K^{-1})			
Compound	**Optimized**		**Reference**
$ScFe_2$ 298-800 K 800-1608 K	 75.2168+ 0.01115224T -453790T^{-2} + 1.0578984E-5T^2 71.9418+ 0.01873667T -309436T^{-2} + 5.863194E-6T^2		C_p = $C_p(Sc_{(hcp)})$ + $2C_p(Fe_{(bcc)})$
$ScFe_2$(high temperature) 298-2000 K	 71.9418+ 0.01873667T -309436T^{-2} + 5.863194E-6T^2		
$Sc_{29}Fe_6$ 298-800 K	 958.5436 -0.13392712T -5114574T^{-2}+ 0.000288405312T^2		C_p = $29C_p(Sc_{(hcp)})$ +

800-1608K	$863.5686+ 0.08602135T -928308T^{-2}+ 0.000151647402T^{2}$	$6C_p(Fe_{(bcc)})$
1608-1811K	$-6860.70+ 6.8694752T +2934286914T^{-2}-0.001518603828T^{2}$	
1811-2000K	$-6725.7904732+6.816704968T +2935215222T^{-2}-$ $0.0015207252T^{2} -1.2398562E34\ T^{-10}$	
Solid Solution (parameters of the Compound Energy Formalism with two-sublattice approach) $(\mathbf{Fe, Sc})_1^{\mathbf{I}}(\mathbf{Va})_1^{\mathbf{II}}$		
FCC	${}^0L_{Fe,Sc} = 2299$	
BCC	${}^0L_{Fe,Sc} = -17138+12.54T$ ${}^1L_{Fe,Sc} = 4180$	
HCP	${}^0L_{Fe,Gd} = 8360$	

Compound	Magnetic moment	Curie Temperature(K)	References
$ScFe_2$	1.37	542	[9]

3.14.4. References

1. Naumkin, O.P., V.F. Terekhova, and E.M. Savitskii, *Phase diagram of iron-scandium alloys.* Izv. Akad. Nauk SSSR, Metal., 1969, p. 161-5.
2. Bodak, O.I., et al., *Scandium-iron system phase diagram.* Dopov. Akad. Nauk Ukr. RSR, Ser. A: Fiz.-Mat. Tekh. Nauki, 1978, p. 365-70.
3. Hellawell, A., Journal of Less Common Metals, 1962. **4**: p. 101-103.
4. Okamoto, H., *Desk Handbook-Phase Diagrams for Binary Alloys.* ASM International, 2000.
5. Kotur, B. Ya., O.I. Bodak, R.I. Andrusyak, Dokl. Akad. Nauk. Ukr. SSR, 1986, **Ser. B11**, 29-32.
6. Selhaoui, N. and O.J. Kleppa, *Standard enthalpies of formation of scandium alloys, Sc + M (M = iron, cobalt, nickel ruthenium, rhodium, palladium, iridium, platiunum) by high-temperature calorimetry.* J. Alloys Compd., 1993. **191**, p. 145-9.
7. Goncharuk, L.V. and V.R. Sidorko, *Thermodynamics of Interaction of Rare-Earth Metals with d-Metals. The Scandium — Iron System.* Powder Metallurgy and Metal Ceramics, 2001. **40**(7): p. 354-361.
8. Savchenkova, A.P., R. A. Sirotina, V.V. Burnasheva and N.S. Kudryashova, *Calorimetric study of the cubic modification of $ScFe_{1.8}$ and hydrides based on it*, Izv. Akad. Nauk SSSR, Neorgan. Materialy,1984, **20**(9), 1507-1510.

9. Esin, Yu.O., M.G.Valishev, A.F. Ermakov, S.E. Demin, P.V. Gel'd, Teprofiz. Vys. Temp., 1984. **22**(6): p. 1214-1217.

10. Sudavtsova, V.S., G.I. Batalin, V.P. Kurach, *Enthalpy of scandium dissolution in molten iron* , Izv. Akad. nauk SSSR, Neorg. Mater., 1984, **20**, p. 1925-6.

11. Ikeda, K., T.Nakamichi, T. Yamada and M. Yamamoto, J. Phys. Soc. Japan, 1974. **36**.

Figures

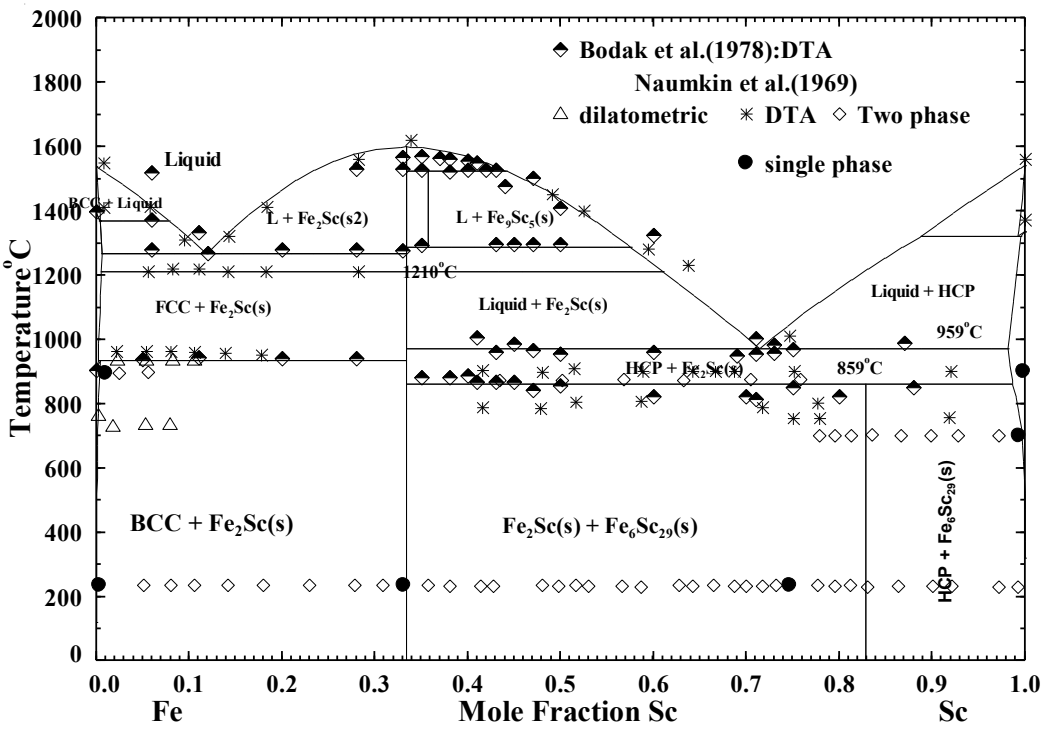

Fig 3.14.1 The optimized Fe-Sc system.

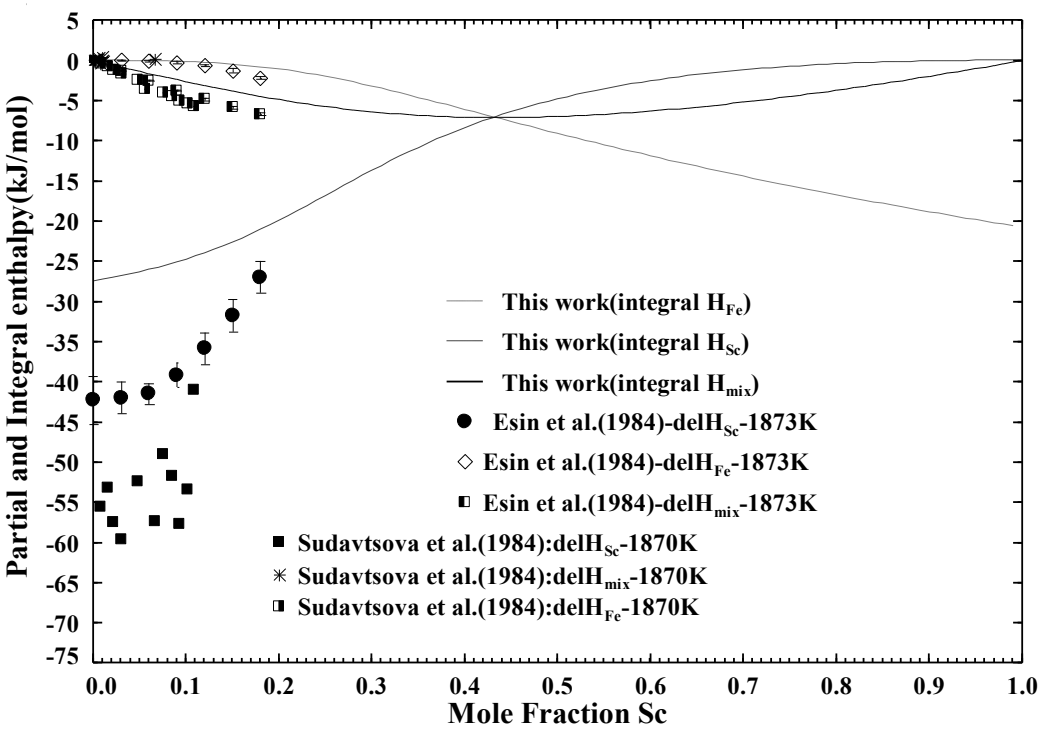

Fig 3.14.2. Enthalpy of mixing of Fe-Sc alloy at 1873K

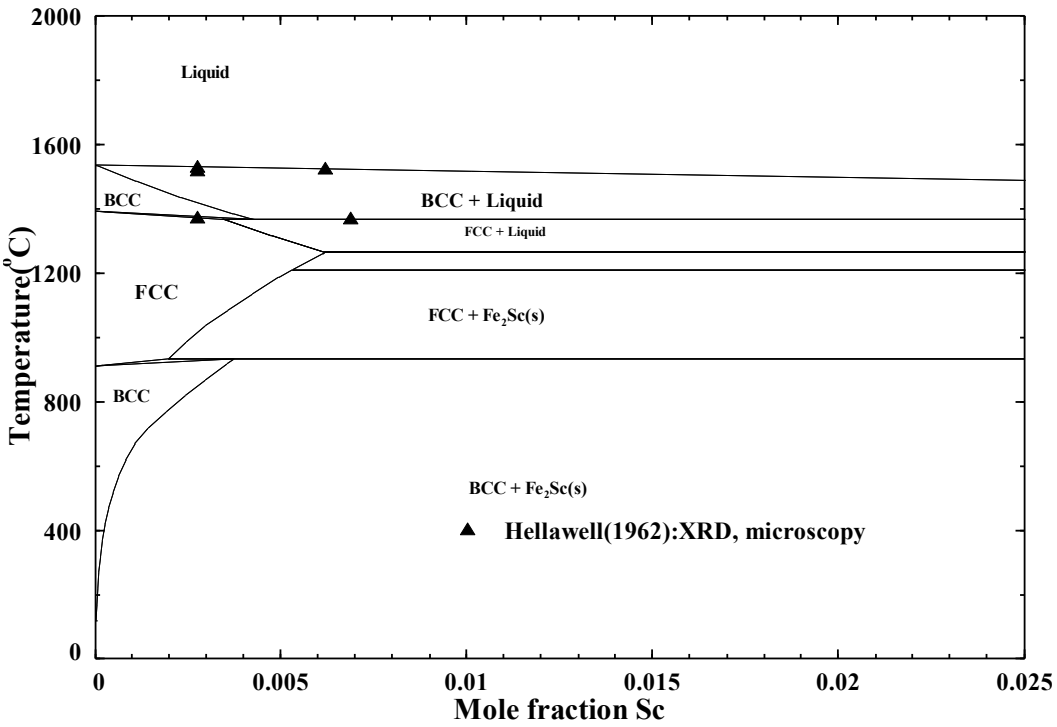

Fig. 3.14.3. Iron-rich side of the Fe-Sc phase diagram.

Chapter 4. Discussion and systematic Analysis

According to the evaluated phase diagrams in the present study, it is easily found that there is a certain trend in the phase diagram with the periodic number of Rare Earth (RE) elements. For example, the stable compounds in the Fe-RE binary groups are summarized in Table 4.1. As can be seen in the table, light RE group has less intermetallic phases than heavy RE group. In light RE group, no intermetallic phase forms in Fe-La system, then Fe_2RE, $Fe_{17}RE_2$, $Fe_{17}RE_5$ and Fe_3RE are forming with increasing periodic number of light RE elements. For the heavy RE group, intermetallic compounds Fe_2RE, Fe_3RE, $Fe_{23}RE_6$ and $Fe_{17}RE_2$ are forming for all the binary systems. This trend tells that heavy RE – Fe system has energetically more negative interaction between RE and Fe than light RE – Fe system.

Table 4.1. Summary of stable compounds in Fe-RE systems. L = Light RE (La sub-group); H= Heavy RE (Y sub-group); O = experimental thermodynamic data available; X= experimental thermodynamic data unavailable. No phase diagram data are available for Fe-Pm, Fe-Eu and Fe-Yb systems.

Type	Binary System	Phase Diagram	Enthalpy of Mixing	$REFe_2$		$REFe_3$		RE_6Fe_{23}		RE_2Fe_{17}		RE_5Fe_{17}		$RE_{29}Fe_6$		RE_5Fe_9	
				$\Delta H_f^\circ{}_{298}$	S°_{298}	$\Delta H_f^\circ{}_{298}$	S°_{298}	$\Delta H_f^\circ{}_{298}$	S°_{298}	$\Delta H_f^\circ{}_{298}$	S°_{298}	$\Delta H_f^\circ{}_{298}$	S°_{298}	$\Delta H_f^\circ{}_{298}$	S°_{298}	$\Delta H_f^\circ{}_{298}$	S°_{298}
L	Fe-La	O	O														
L	Fe-Ce	O	O	X	O					X	O						
L	Fe-Pr	O	X							X	O						
L	Fe-Nd	O	X							X	X	X	X				
L	Fe-Pm																
L	Fe-Sm	O	O	X	X	X	X			X	O						
L	Fe-Eu																
H	Fe-Gd	O	O	O	O	O	X	X	X	O	X						
H	Fe-Tb	O	X	O	O	X	X	X	X	O	X						
H	Fe-Dy	O	X	O	O	O	X	X	X	O	X						
H	Fe-Ho	O	X	X	O	X	X	X	X	X	X						
H	Fe-Er	O	X	O	O	O	X	X	X	O	X						
H	Fe-Tm	O	X	X	O	X	X	X	X	X	X						
H	Fe-Yb																
H	Fe-Lu	O	X	X	O	X	X	X	X	X	O						
H	Fe-Y	O	O	X	O	X	X	X	X	X	X						
	Fe-Sc	O	X	O	X									O	X	O	X

In order to examine this trend in more details, the thermodynamic calculations for enthalpy of formation for compounds and enthalpy of mixing for liquid phase were calculated from the present thermodynamic model parameters. In addition, the entropies of solid and liquid were also calculated and plotted in Figs. 4.1 to 4.8.

The enthalpy of formation for the binary compounds shows minimum at composition around $X_{RE} = 1/3$. The enthalpies of formation of the light-RE-Fe compounds are less negative than those of the heavy-RE-Fe compounds except samarium. The range of enthalpy of formation for the light RE – Fe binary series lies in the range of -4.5kJ/mole (FE-Ce) to -7.5kJ/mol (Fe-Sm) and for heavy RE - Fe series lies between -7.7kJ/mol (Fe-Gd) to -10.5kJ/mol (Fe-Tm). It is interesting that the enthalpies of formation for all Fe_2RE for the heavy RE elements are about -9 ± 1 kJ/mol.

The entropy of formation for both the light and heavy RE - Fe binary phase diagrams shows a trend with periodic number. The entropy decreases and becomes negative as RE elements moves across light RE - Fe binary compounds in the periodic table. Regarding heavy RE system, the entropies of formation for the compounds of Fe_3RE and $Fe_{17}RE_2$ are positive for all elements but the entropies of formation for Fe_2RE vary from ideal to negative in general with periodic number of elements.

The similar features are also reflected in liquid solution. The enthalpy of mixing for heavy RE - Fe systems is more negative than that of light RE - Fe system. The maximum or minimum of enthalpy curve for liquid solution does not have any definitive trend. The entropy of mixing of liquid phase shows almost an ideal behaviour except Gd, Sm and La which is hard to explain in the present study.

Although there are general trends in the enthalpy and entropy of solid state and liquid state as shown in Fig. 4.1 to 4.8, there are many exceptions in the system. This may be due to the less accuracy of the thermodynamic modeling induced by lack of experimental data in particular for thermodynamic properties. Thus, more experimental studies are needed in future for the Fe-RE system to obtain more accurate thermodynamics of the system.

Figures

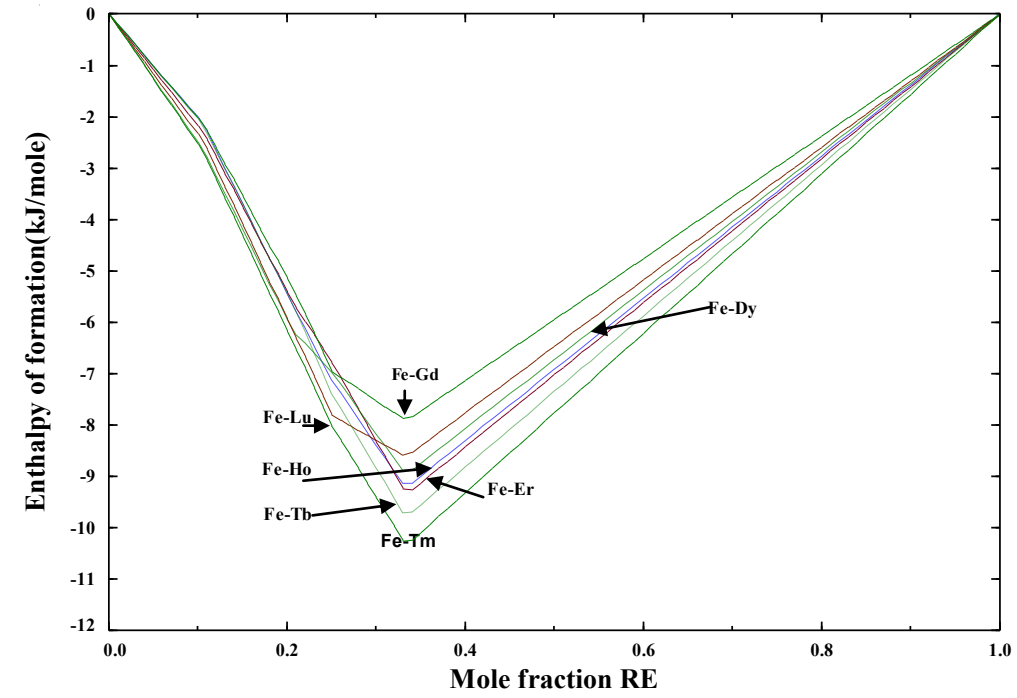

Fig. 4.1 Calculated enthalpies of formation for stable intermetallic compounds at 298 K in the heavy RE – Fe system. RE = Gd, Tb, Dy, Ho, Er, Lu and Tm.

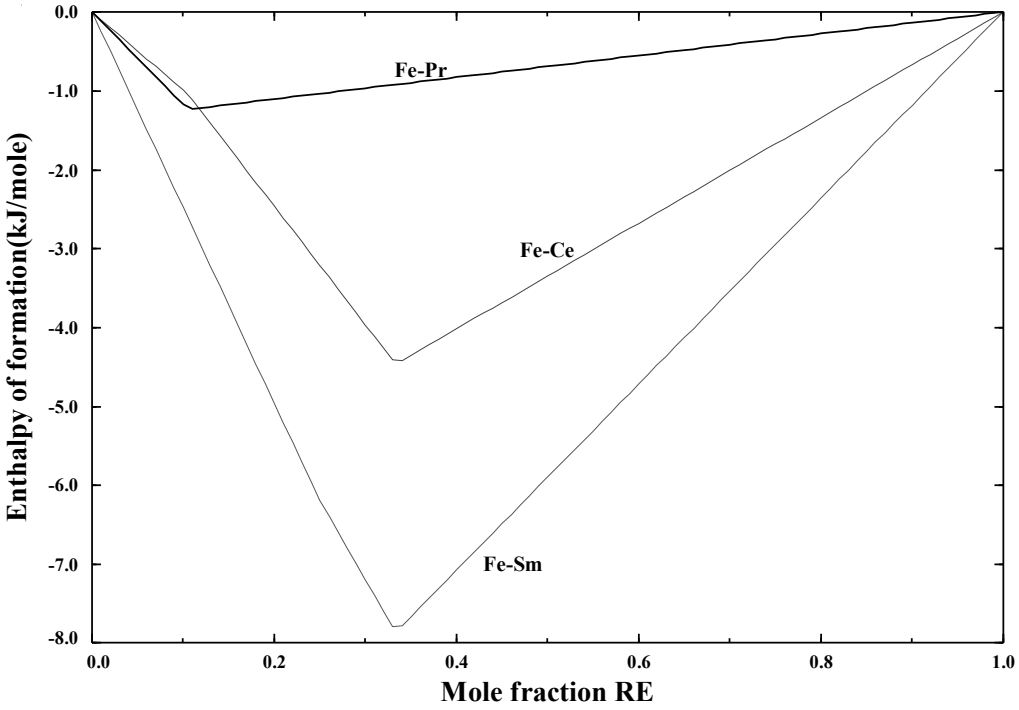

Fig. 4.2. Calculated curve of enthalpy of formation for stable intermetallic compounds at 298K in the light RE – Fe system. RE = Ce, Pr and Sm. (no compound for La)

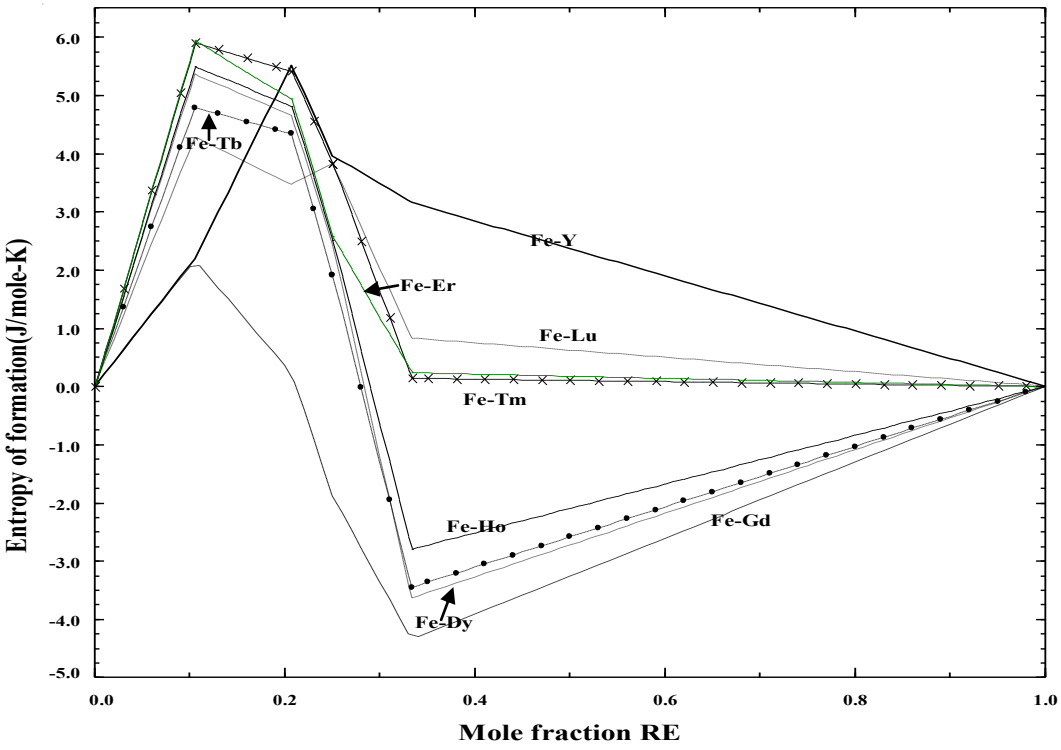

Fig. 4.3. Calculated entropies of formation for stable intermetallic compounds at 298 K in the heavy RE – Fe system. RE = Gd, Tb, Dy, Ho, Er, Lu, Tm and Y.

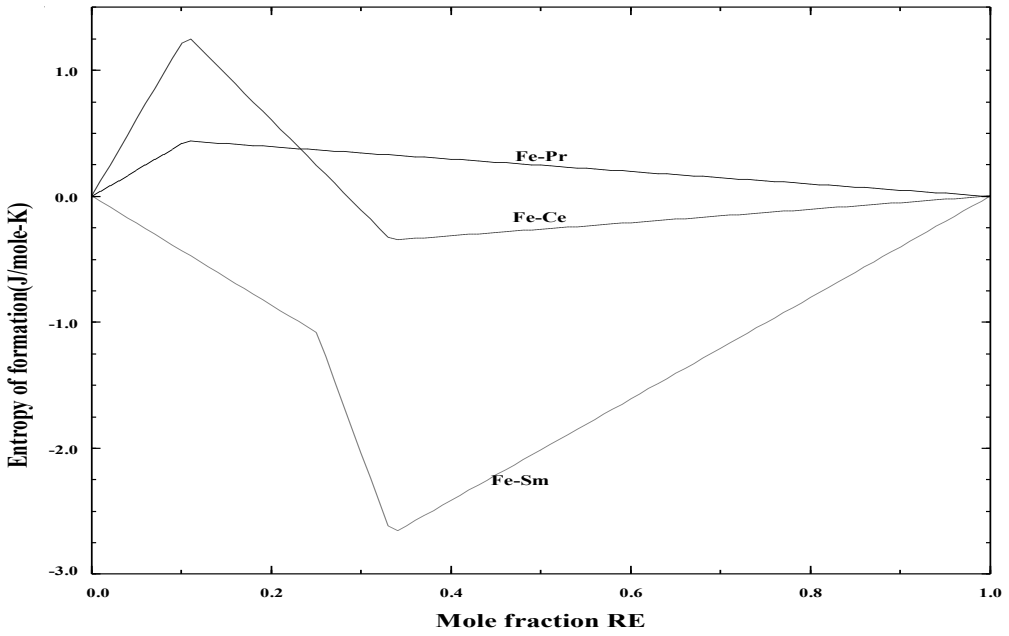

Fig. 4.4. Calculated entropies of formation for stable intermetallic compounds at 298 K in the light RE – Fe system. RE = Ce, Pr, and Sm. (no compound for La)

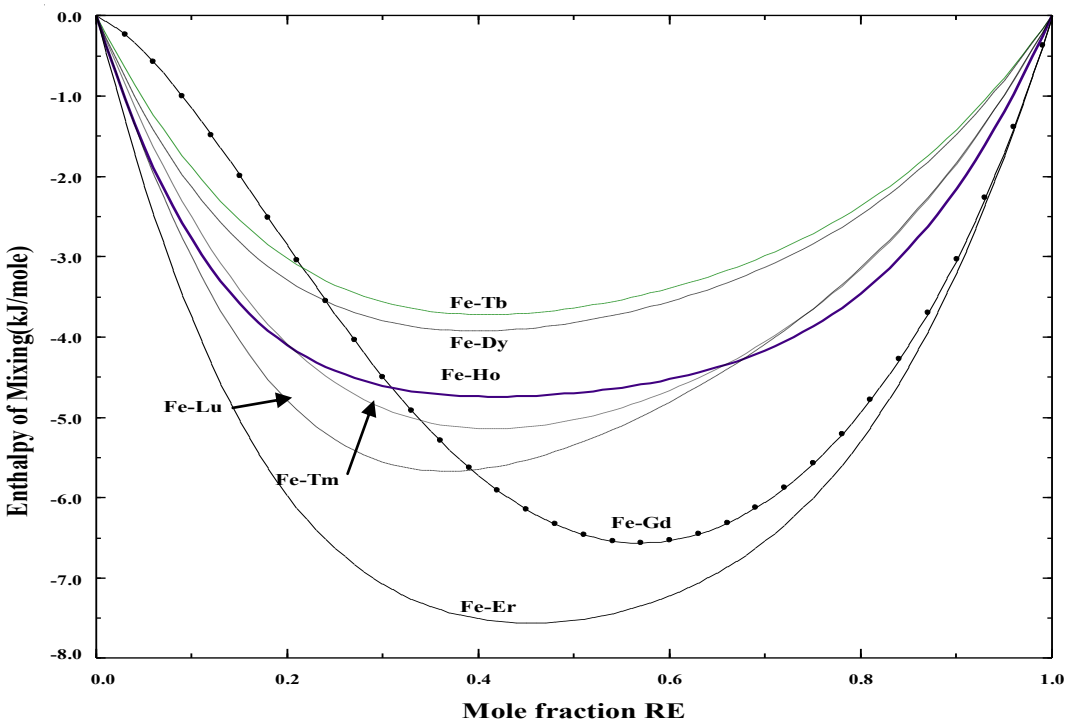

Fig. 4.5. Calculated enthalpy of mixing of liquid solution at 1973 K for the heavy RE – Fe system. RE = Gd, Tb, Dy, Ho, Er, Lu, and Tm.

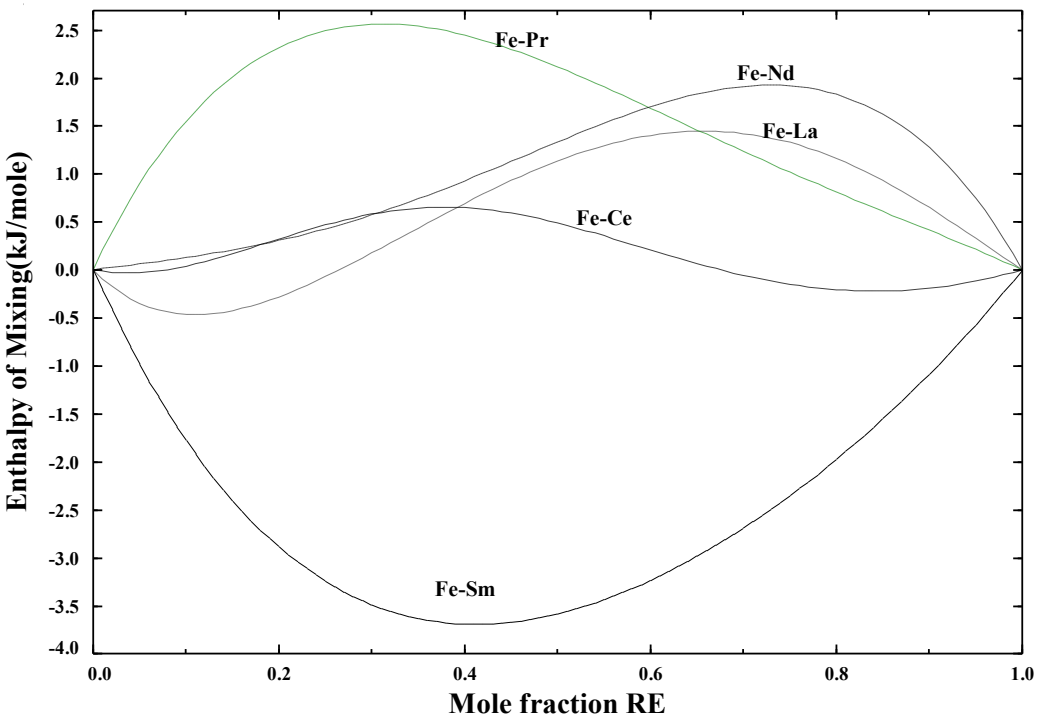

Fig. 4.6. Calculated enthalpy of mixing of liquid solution at 1973 K for the light RE – Fe system. RE = La, Ce, Pr, Nd and Sm.

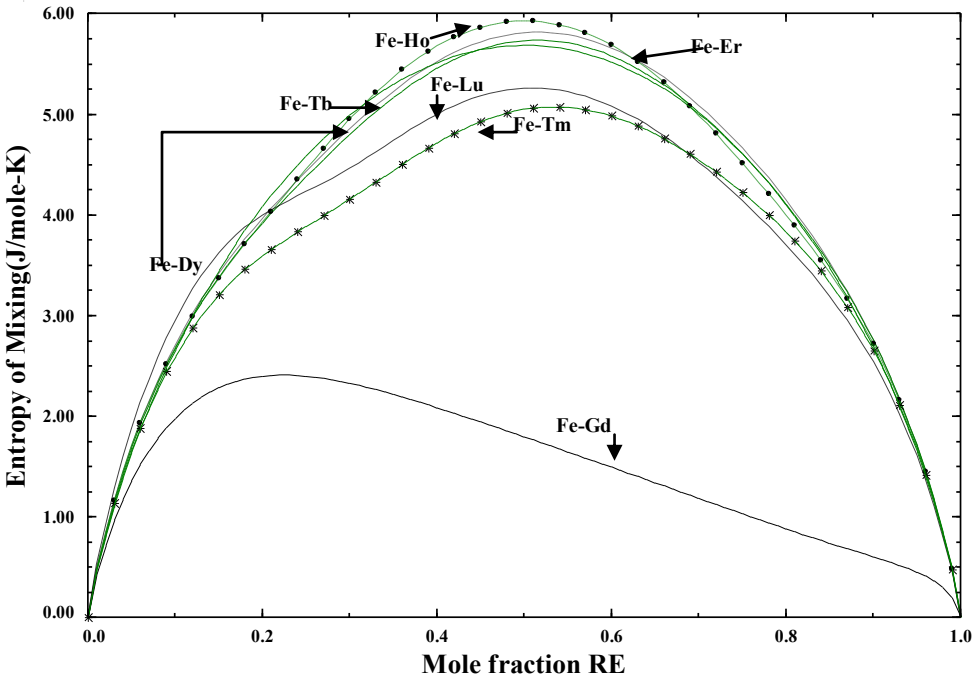

Fig. 4.7. Calculated entropy of mixing of liquid solution at 1973 K for the heavy RE – Fe system. RE = Gd, Tb, Dy, Ho, Er, Lu, and Tm.

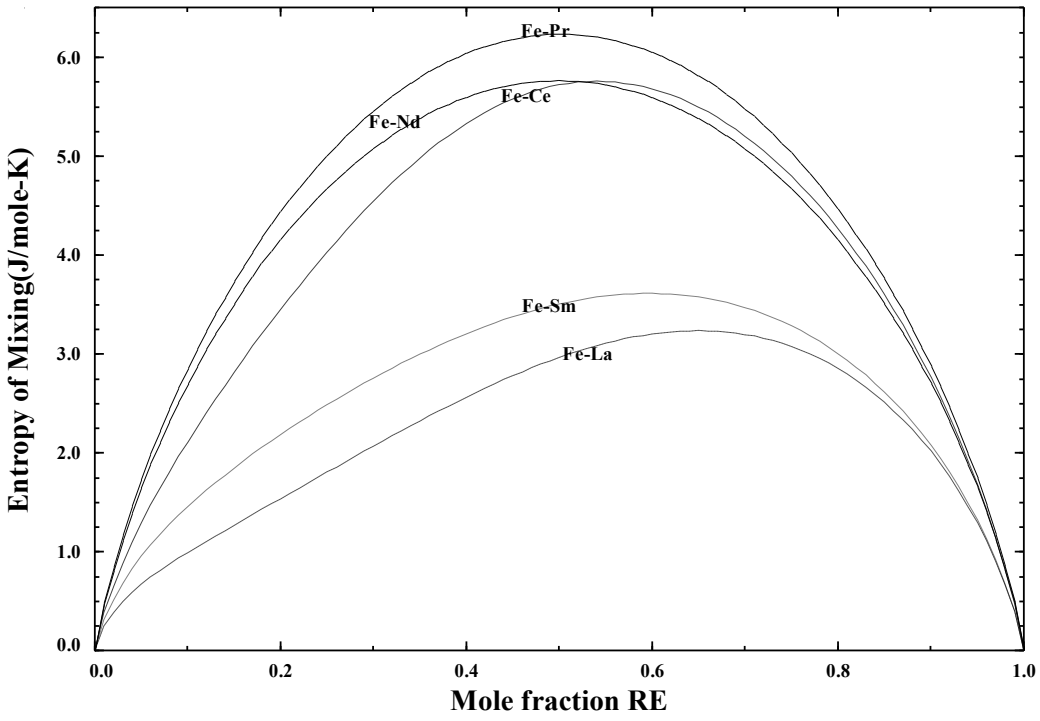

Fig 4.8. Calculated entropy of mixing of liquid solution at 1973 K for the light RE – Fe system. RE = La, Ce, Pr, Nd and Sm.

Chapter 5. Summary

The aim of the present work was to critically evaluate and optimize the binary systems Fe-La, Fe-Ce, Fe-Pr, Fe-Nd, Fe-Sm, Fe-Gd, Fe-Tb, Fe-Dy, Fe-Ho, Fe-Er, Fe-Tm, Fe-Lu, Fe-Sc and Fe-Y as a part of research project to develop the thermodynamic database for RE recycling process and Mg-RE alloy design.

The CALPHAD method and thermodynamic model used in the present study are introduced in Chapter 2. The Modified Quasi-chemical Model is used to describe the thermodynamics of liquid solution, and one sublattice Compound Energy Formalism is used for solid solutions. Magnetic contribution to the Gibbs energy of an intermetallic phase is also discussed. The Miedema's approach to theoretically calculate the enthalpy of formation for intermetallic phases is also elaborated. In Chapter 3, the thermodynamic assessments of all the fourteen binary Fe-RE systems are presented. All available experimental thermodynamic and phase diagram data on each system have been critically reviewed and discussed for each system. Optimization of all reliable experimental data has been carried out to obtain model parameters to describe the Gibbs Energy of all phases. Almost all of the intermetallic phases in Fe-RE systems have magnetic transition (Curie temperature), which is comprehensively taken account in the present study. RE elements can be divided into two groups: light RE group including La, Ce, Pr, Nd, Pm and Sm, and the heavy RE group including Eu, Gd, Tb, Dy, Ho, Er, Tm, Lu and Y. The phase diagram and thermodynamic data of Fe-RE system shows a periodic trend amongst each group of RE elements, and this trend could be used to resolve inconsistencies and lack of the thermodynamic and phase diagram data.

The present systematic thermodynamic study for Fe-RE systems shows some interesting results. It was found that the light RE elements do not form more than two compounds with Fe. For example, La forms no intermetallic compound, Pr forms one intermetallic compound, and Ce, Nd forms two and Sm form three intermetallic compounds, but all compounds show peritectic melting behaviour. On the other hand, the heavy RE elements form four intermetallic compounds. All intermetallic compounds in Fe with Gd, Tb and Dy show incongruent melting while $Fe_{17}RE_2$ in Ho, Eu, Tm, Lu and Y shows congruent melting behaviour. Sc shows a completely different behaviour from the other RE

elements. This is mostly probably attributed to the larger size of the light RE metals, which is due to their electronic configuration (less 4f-shell electrons). The atomic size of RE elements is decreasing as the RE elements move from left to right in the lanthanide series. With decreasing the atomic size of REs, the enthalpy of formation of the intermetallic compounds becomes more negative. Thus, the heavy RE group has more intermetallic compounds than the light RE group. Also, within the group, the elements with higher atomic number can form more stable intermetallic compounds. The enthalpy of mixing for liquid Fe-RE solutions shows similar trend.

The thermodynamic database obtained in the present study can be incorporated to a large multicomponent thermodynamic database available in FactSage in order to perform complex chemical reaction calculations and process design for RE recycling and phase diagram calculations for Mg alloy design.